AMERICAN UNIVERSITY OF BEIRUT

DEVELOPING A MULTIPLEXING PLATFORM FOR THE DETECTION OF SPECIFIC BIOMARKERS

by
SAMIR ABDALLAH ABOU SHAHEEN

A thesis
submitted in partial fulfillment of the requirements
for the degree of Master of Science
to the Department of Chemistry
of the Faculty of Arts and Sciences
at the American University of Beirut

Beirut, Lebanon
July 2016

AMERICAN UNIVERSITY OF BEIRUT

DEVELOPING A MULTIPLEXING PLATFORM FOR THE DETECTION OF SPECIFIC BIOMARKERS

by

SAMIR ABDALLAH ABOU SHAHEEN

Approved by:

Dr. Pierre Karam, Assistant Professor
Department of Chemistry — Advisor

Dr. Najat Saliba, Professor
Department of Chemistry — Member of Committee

Dr. Mohamad Hmadeh, Assistant Professor
Department of Chemistry — Member of Committee

Date of thesis defense: July 25, 2016

AMERICAN UNIVERSITY OF BEIRUT

THESIS, DISSERTATION, PROJECT RELEASE FORM

Student Name: _____
Last First Middle

○ Master's Thesis ○ Master's Project ○ Doctoral Dissertation

☐ I authorize the American University of Beirut to: (a) reproduce hard or electronic copies of my thesis, dissertation, or project; (b) include such copies in the archives and digital repositories of the University; and (c) make freely available such copies to third parties for research or educational purposes.

☐ I authorize the American University of Beirut, **three years after the date of submitting my thesis, dissertation, or project,** to: (a) reproduce hard or electronic copies of it; (b) include such copies in the archives and digital repositories of the University; and (c) make freely available such copies to third parties for research or educational purposes.

_____

Signature Date

ACKNOWLEDGMENTS

I am extremely thankful to my phenomenal advisor and brilliant mentor, Dr. Pierre Karam. The completion of this work couldn't have been possible without his valuable guidance and keen interest. He taught me a lot of competencies and boosted up my scientific reasoning. I was so lucky to work under his supervision during the previous two years as he has been always a source of inspiration and was always ready to assist and push me towards better performance and excellence.

I want to express my deep gratitude to all my professors and especially the committee members, Dr. Najat Saliba and Dr. Mohamad Hmadeh, for their continuous support and motivation.

I acknowledge with thanks the AUB librarians, chemistry department staff and KAS Central Research Science Laboratory team for their kind cooperation and efforts.

I address my sincere love and appreciation for my labmates in Dr. Karam's research group and would like to specially thank Mr. Hassan Fakih for his valued contribution to this work.

I also thank my colleagues at the chemistry department especially the precious Julie Nassar and Sarah Soussy for being always there for me through thick and thin. I was particularly fortunate and pleased that AUB granted me these two sisters with whom I shared a bunch of great and unforgettable memories.

At last, I owe a deep sense of gratitude to my family for their unconditional love, putting their faith in me and going out of their ways to share their support either morally, financially and physically.

AN ABSTRACT OF THE THESIS OF

Samir Abdallah Abou Shaheen for Master of Science
Major: Chemistry

Title: Developing a Multiplexing Platform for the Detection of Specific Biomarkers

The development of simple, sensitive and multiplexed detection system is highly desirable in the field of clinical diagnostics. This is mainly due to the fact that multiplexed systems can reduce labor, time and cost while maintaining a higher accuracy of detection. In view of that, herein we report on the preparation of different sensing platforms for the detection of trace amounts of protein and DNA biomarkers.

Using a chip-based electrochemical immunosensor, we were able to detect TBI biomarkers for lab purposes inside purified samples. The assay allowed us to investigate the microscale size regime of gold sensors and achieve sensitivity in the range of pg/mL. On the other hand, we described a fluorescent sandwich assay as an alternative method. The assay was built on gold coated polystyrene microspheres and visualized using flow cytometry with the aid of different labels. Out of three examined fluorescent tags, dye encapsulated liposomes gave the best enhanced sensitivity and allowed the detection of low biomarker levels that are clinically relevant.

Building upon our findings, we developed an ultrasensitive universal platform for the detection of oligonucleotide sequences. The basis of this scheme relied on immobilizing separately two DNA strands each complementary to a different portion of target analyte onto the surface of gold coated polystyrene microspheres and dye-encapsulated liposomes. The hybridization event was recognized by an enhancement of the fluorescent signal recorded by flow cytometry. The assay parameters were optimized so that the whole experiment can take less than 2 hours with a detection limit of 2.7 pM. Furthermore, the proposed scheme was shown to perform well in complex matrices such as serum making it promising platform for fast multiplexing diagnosis.

CONTENTS

ILLUSTRATIONS

Figure page

TABLES

CHAPTER I

INTRODUCTION

A. Biosensors

Despite the remarkable advances in the prevention of certain diseases, the call for reliable, rapid and real-time diagnostic tools is swiftly escalating.[1] Indeed, the interest in developing sensitive and specific point-of-care sensors has grown drastically due to their ability to outperform conventional methods in terms of speed, simplicity, portability, accuracy and cost.[2] The life expectancy of modern societies has increased with our ability to detect and diagnose diseases at early stages which allowed us in return to control diseases before they invade the body or turn into a serious epidemic.[3] A biosensor or a biological sensor is an analytical instrument composed of two main compartments, a bioreceptor that recognizes a specific target analyte and a transducer that converts and translates this recognition event into a readout signal (Figure I-1).[1-2] This combination facilitates the detection of molecules without the use of complex protocols and reagents. As such, biosensors are critical for decentralizing clinical applications, easy disease monitoring and moving the advanced research into the patient's bedside.[4] The glucose sensor and the home pregnancy test are the best examples of such devices.

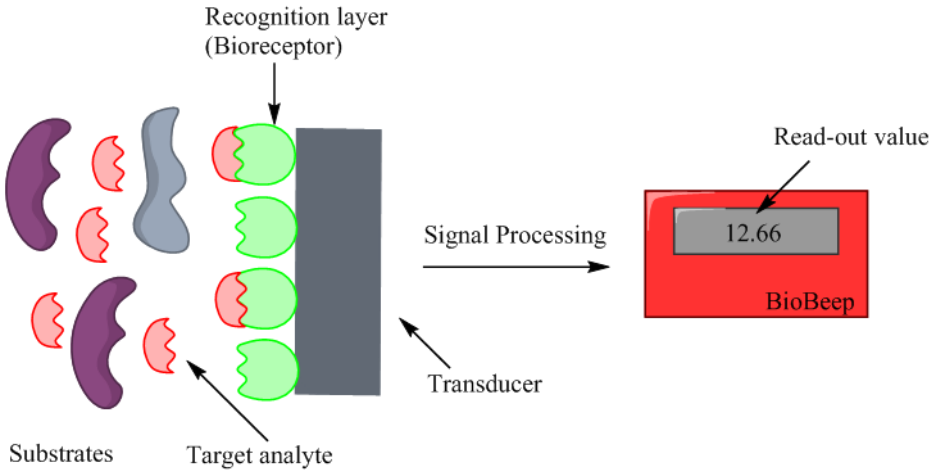

Figure I-1. Schematic diagram showing the components of a biosensor. The bioreceptor specifically recognizes the target analyte and induces an alteration in a physical parameter that can be impulsively detected by a transducer. The signal is then processed and displayed by a readout unit.

B. Biomarkers

A biomarker, as defined by the World Health Organization (WHO), is any substance that can be measured in the body and influence, characterize or predict a specific biological process.[5] A variety of biomarkers are commonly used today including proteins, carbohydrates, short circulating DNA and miRNAs.[5 6 7] The growing interest in studying these biomolecules in laboratory and clinical research is due to their significant ability to indicate the presence of a specific disease (eg. Diabetes, Cardiovascular, Alzheimer, Cancer etc…), distinguish and stage its severity.[8] For instance the presence of islet cell antibodies (ICA) and biochemical autoantibodies (BAA) in the blood of a person is used as a primary indication of type1 diabetes [9] and this risk increases when Zinc Transporter-8 Autoantibodies (ZnTA8) are found as well.[10] On the other hand, monitoring the level of biomarkers such as adiponectin, C-reactive protein (CRP), ferritin, interleukin-2 receptor A (IL2RA) and insulin allows predicting and preventing type 2 diabetes.[11]

1. Importance in Early Disease Detection

The detection of these biological indicators at an early stage of the disease is a very important signal for early warning of the damage which can stipulate a quick preventive action leading to a better outcome of treatment.[12] Moreover, it is critical for efficient diagnosis and clinical assessment to detect any infection at a low cost using rapid and highly accurate set of tools.[13] In fact, biomarkers have shown significant potentials for improving the accuracy of diagnosis and raising the rate of treatment in two of the most common and major diseases, Alzheimer and Cancer. [6]

a. Alzheimer Disease

Alzheimer disease (AD) is a chronic neurodegenerative disorder that affects aged people.[14] Initial symptoms of the disease are rarely distinguished from normal aging, yet AD proceeds by short term memory loss, language disorientation, loss of motivation and so on. Due to the lack of proper treatment, disease prevention remains the ultimate focus of ongoing research.[15] This essentially means that people at a high risk of the disease should be recognized before any of the early symptoms becomes certain and an effective intervention must be accompanied with to reduce the accumulation of neurofibrillary tangles, the hallmark of the disease.[16] In several studies, Uberti *et al.* showed that blood levels of conformationally distorted p53, a multifunction protein that functions as tumor suppressor and maintains genomic integrity, can be correlated to AD severity and even distinguish it from normal aging and other diseases (e.g,.Parkinson's disease).[17] Similarly, many studies demonstrated that elevated levels of cerebrospinal fluid tau (specifically p-thr231, p-ser199, and p-thr181) can provide sensitivity and specificity of AD of 81% and 91%, respectively.[15a,

[18] This leads several groups to conduct a tremendous amount of studies on putative disease-modifying drugs (e.g., curcumin) that showed potential for disease prevention and thus could be implemented in a proper treatment before the clinical manifestation of the disease.[19]

b. Cancer

Cancer, a large family of diseases involving the uncontrolled growth of a tumor cell that might invade other parts of the body, is considered as one of the most dangerous threats for human's lives.[20] More than 14 million of deaths caused by cancer cases were recorded in 2014 by the WHO, and what is worse is that this number is expected to escalate in the coming years.[21] Because of the critical role they play, biomarkers are currently used as part of the routine cancer diagnosis. Cancer biomarkers include a wide range of molecules such as DNA, RNA, microRNAs, sugars, proteins, lipids and others.[3, 20, 22] The application of these biomolecules allows early stage diagnosis, prognosis of patients at high risk and deciding on and monitoring of the proper treatment. One example is prostate specific antigen (PSA) , a commonly used biomarker to screen healthy patients for prostate cancer.[22] Furthermore, pre-symptomatic detection can greatly increase survival rates (Figure I-2). For instance according to Jemal *et al.* prostate cancer patients survival rates is 100% if detected at early stages but this rate drastically decreases to 30% when it becomes at a distant stages.[23] Likewise, biomarkers could be used to estimate the risk of developing a tumor for people with a strong family history of a specific sarcoma. As an example, Easton *et al.* and Hall *et al.* both demonstrated that women carrying germ line mutations such as BRCA1 have high potential of developing breast or ovarian cancer and so they need to

select a chemoprevention and a treatment method in order to decrease the risk of developing a malignancy.[24] Nevertheless, Paik *et al.* utilized gene expression signatures to determine prognosis of breast cancer while Bang *et al* .and Piccart-Gebhart *et al.* showed that over expression of HER2 gene biomarkers in breast cancer are very good at predicting response to anti HER2 therapy.[25] Also, biomarkers could be used to monitor for disease recurrence as in the case of serially screening alpha feto-protein (AFP), lactate dehydrogenase (LDH), and beta-HCG (bHCG) in germ cell tumor. [26]

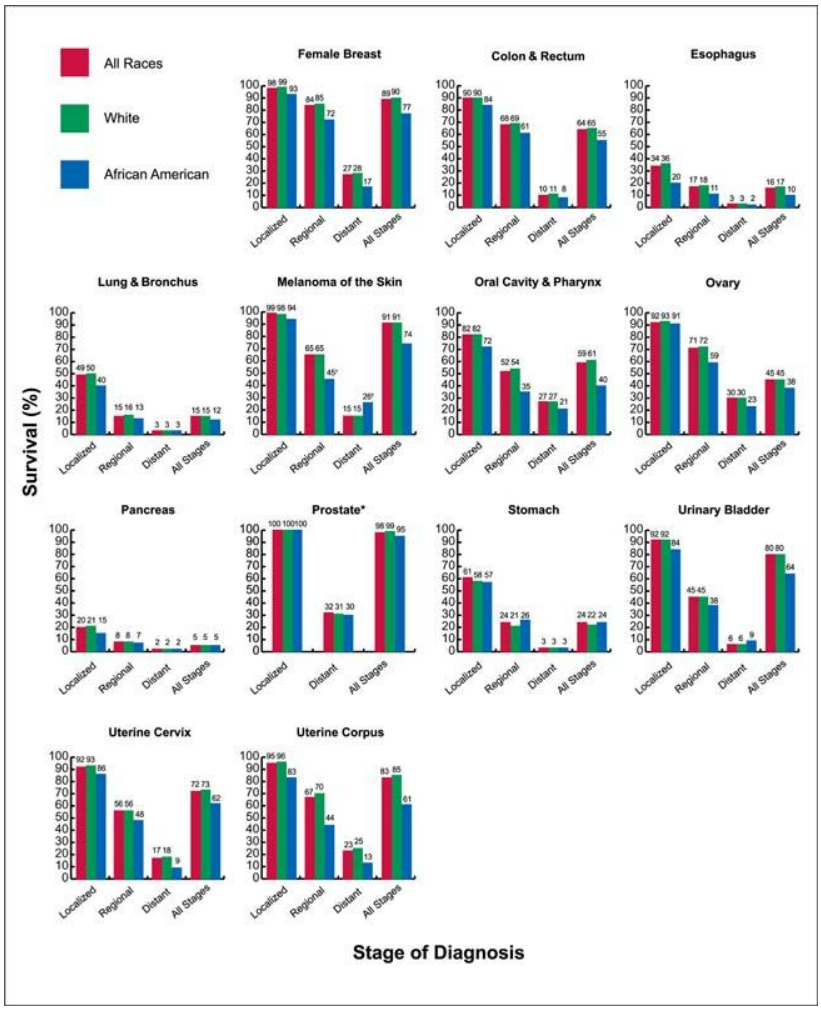

Figure I-2. Five-year relative survival rates among patients diagnosed with selected cancers by race and stage at diagnosis, united states, 1996 to 2003.* The rate for localized stage represents localized and regional stages combined. The standard error of the survival rate is between 5 and 10 percentage points. Note: Staging according to

Surveillance, Epidemiology, and End Results (SEER) historic stage categories rather than the American Joint Committee on Cancer (AJCC) staging system. Comparison of this data to that of previous years is discouraged due to the use of an expanded data set. Reprinted with permission from Jemal *et al.*[23]

C. DNA Biosensors

DNA biosensors showed a revolutionary tool in fundamental research, diagnosis and environmental sciences. [27] Recently, the interest in detecting oligonucleotides has expanded due to the specific and robust base pairing between DNA target and its complementary DNA probe which could be used to obtain a quantitative identification of specific diseases.

Oligonucleotide based assays are stable and have the potential to be designed into cheap, sensitive and specific assays while provide multiplexing capabilities.[28] Specifically, microRNAs are small non-coding oligonucleotides (22nt) endogenously expressed RNAs. They are frequently deregulated in tumors and are excreted into the serum.[29] Contrary to synthetic DNA which degrade rapidly once injected in plasma, these miRNAs were shown to be stable in blood.[29a, 30] They range at concentrations between 100 and 10 000 copies per microliter, highlighting them as great candidates for developing a novel and noninvasive diagnostic and prognostic tool for cancer in its early stages[29a] and they are regarded as tissue-specific markers for cancer classification[31] and detection.[32] Only 200 different miRNA sequences are needed to accurately classify 17 human cancers.[31] For instance, six specific miRNA biomarkers are over expressed in prostate cancer patients,[33] another five in gastric cancer,[34] and eleven in lung cancer.[30]

Conventional polymerase chain reaction (PCR) based methods which although offer ultimate sensitivities, [35] suffer from several drawbacks such as being very

expensive, labor demanding and requiring complex handling protocols. [36] Furthermore, these assays are subject to severe contamination, the involvement of time consuming thermal cycles and the lack of portability. [37] As such, researchers are putting an intensive focus on the development of reliable and ultrasensitive platforms that can perform PCR-free DNA analysis. The proposed biosensors are based on the detection of the hybridization between an immobilized oligonucleotides sequence and its complementary target probe and converting this event into an analytical signal. Hence, a tremendous amount of transducers has been established that are based on different techniques including colorimetric,[11] optical [38] or electronic-transduction ones. [39]

1. Colorimetric Methods

Mirkin *et al.*[40] pioneered the use of colorimetric techniques for ultrasensitive nucleic acid detection. The basis of this method is the ability of modified gold nanoparticles to aggregate and change their color upon the interaction with nucleic acids. In their sensing strategy, the gold nanoparticles were modified with 3' and 5' (alkanethiol)oligonucleotides in order to complex a target DNA probe. Upon hybridization these modified nanoparticles can arrange in head-to-tail (Figure I-3.A) or tail-to-tail (Figure I-3.B) resulting in a red shift that is correlated with the amount of detected target.

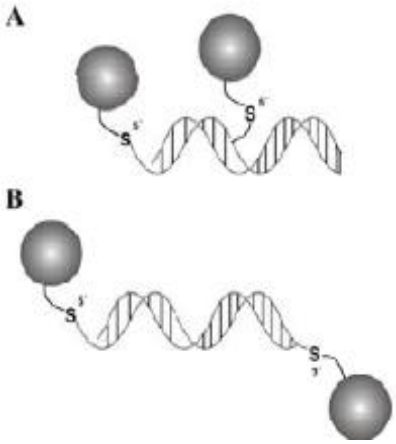

Figure I-3. Different alignments of alkanethiol modified oligonucleotides upon hybridization with a target DNA probe. A) Head-to-tail (B) Tail-to-tail. Reprinted with permission from HONG *et al.* [41]

In fact, gold nanoparticles have been exploited in DNA sensing schemes [42] due to their signal-enhancing power resulting from having high extinction coefficients and their fast and simple synthetic procedures. For example, Xia *et al.* developed a DNA sensing strategy employing unmodified colloidal gold nanoparticles and the different affinity between a cationic conjugated polyelectrolyte and single or double-stranded DNA probes (Figure I-4).[43] In this scheme, the conjugated polyelectrolyte only restrains the ability of single stranded DNA probes to stabilize gold nanoparticles against aggregation. This causes a characteristic color change and allows the visual differentiation of DNA strands at concentrations as low as 1.25pM, a 100 times lower detection limit than those reported by Mirkin *et al.* [40, 42a] However, a major limitation of this and other colorimetric methods is being not applicable for colored and opaque samples.[43]

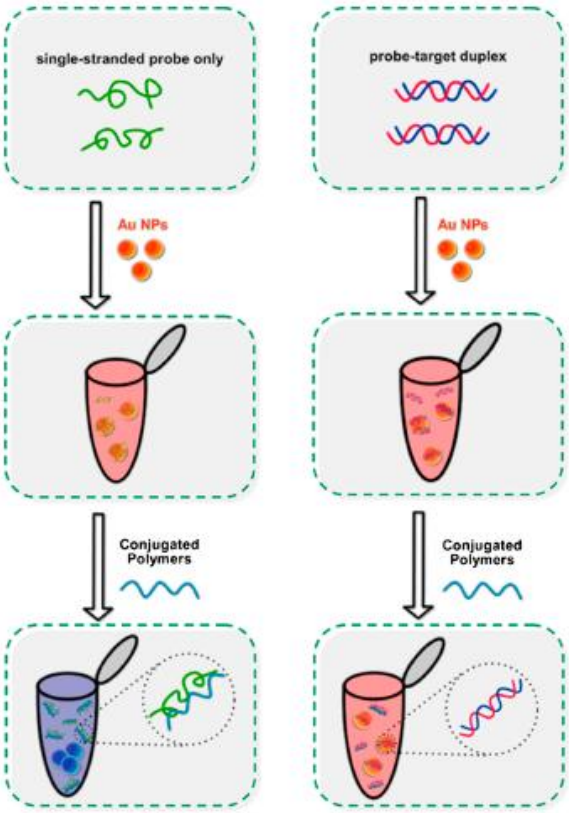

Figure I-4. Colorimetric assay for the detection of DNA. The color change is due to the ability of a conjugate polymer to interact with single stranded DNA rendering it incapable of preventing the aggregation of gold-nanoparticles while no such interaction and inhibition is observed with the double-stranded one. The assay is rapid and sensitive and even it requires less than 10 minutes to observe the color change with the naked eye. Reprinted with permission from Xia *et al.* [43]

2. Electrochemical Methods

Alternatively, electrochemical based methods offer several advantages such as being simple, highly sensitive and inexpensive.[28b] Indeed, they are much cheaper than conventional assays because they don't require labeling or the use of expensive enzymes. But, electrochemical methods may require time consuming cleaning procedure of electrodes and complicated surface chemistry. In addition, most of the electrical assays can't be implemented in a multiplex detection scheme.[44]

Kelly *et al.* reported the use of nanomicrostructured gold microelectrodes for rapid and ultrasensitive detection of oliogonucelotides (Figure I-5).[45] In this scheme,

gold was electroplated through apertures on the surface of the chip and the hybridization event was detected by differential pulse voltammetry (DPV) measured in solutions of hexaammineruthenium-(III) chloride. This approach allowed the achievement of an excellent detection limit of 2fM.

Meanwhile, there are other signal transduction methods that avoid analyte tagging such as surface plasmon resonance (SPR) [46] or ones that offer a high sensitivity such as surface-enhanced Raman scattering (SERS) [47], yet these techniques are very complex and expensive.

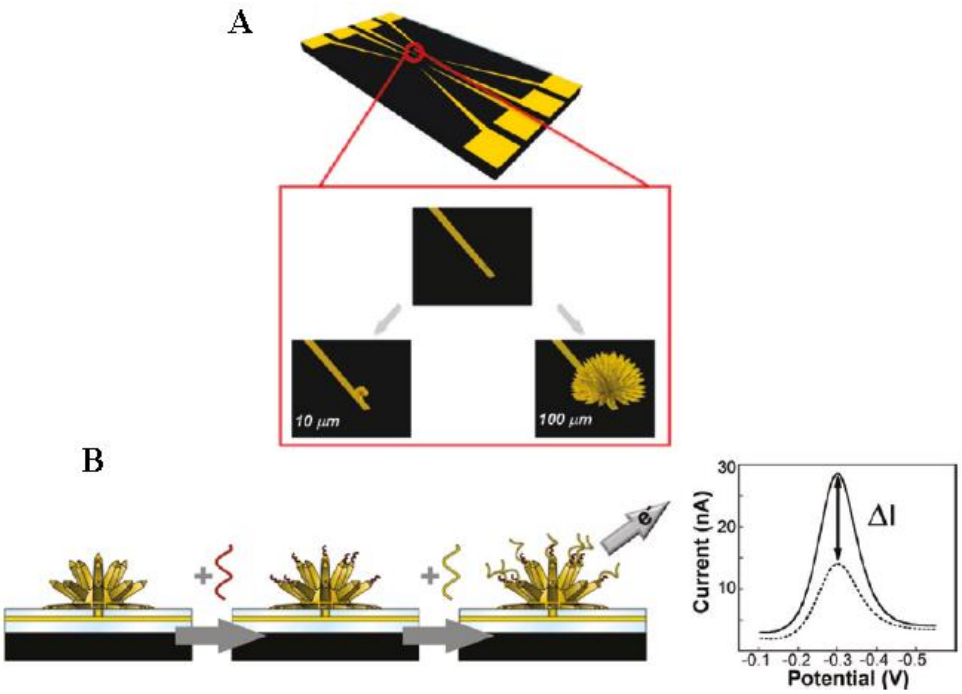

Figure I-5. Bacterial DNA sensing using hierarchical nanotextured microelectrodes. (A) Sensors of variable sizes. The sensors were electrodeposited on 5 μm apertures positioned at the ends of gold leads. (B) Functionalization and use of microsensors. the electrodeposited sensors were modified with probe molecules (red) complementary to a target bacterial gene (yellow). The current change corresponding to the hybridization event was assessed using differential pulse voltammograms and quantitating peak currents before (dotted line) and after (solid line) incubation. Reprinted with permission from Kelly *et al.*[45]

3. Fluorescent Methods

Essentially, methods of detection need to be fast, precise, cost-effective, highly selective and sensitive.[48] Also, it is admirable to implement an analytical device that requires a small amount of sample. Out of the various signal transduction methods, fluorescence seems to be the most reliable method that could satisfy these conditions. Indeed, the fluorescent signal is better for sensing than any other signal as it can often reveal hidden information about the material concentration, confirmation and composition.[49] Fluorescence due to its high sensitivity and versatility is widely used in olignucleotide detection schemes.[50] As well, it offers several advantages over PCR based techniques in terms of visualization and multiplexing.[38] In DNA detection, the signal is amplified by coupling the olignucleotide probe to a fluorphore such as organic dyes or quantum dots (QDs).[13b, 51] This step is the most critical in the ultratrace analysis. In one example, Pang *et al.* established a DNA-sensing platform on the basis of fluorescence resonance energy transfer (FRET) between blue-luminescent CdTe quantum dots and dye-labeled single-stranded DNA (Figure I-6).[52] In this scheme, a cationic polymer brings the donor into the proximity of the acceptor and the hybridization event is detected by the different FRET efficiencies resulting from different interactions between single or double stranded DNA and the polymer. This platform offered the advantage of solution based fluorescence detection of a specific DNA detection without the need of covalent immobilization. However, since a DNA probe is usually coupled to one fluorophore, it may result in low signal amplification in the case where target concentration is relatively low. Moreover, the sensitivity and consistency of the detection scheme is limited by the fluorescence probe used. For instance some organic dyes share several drawbacks such as having poor photostability,

small stokes shifts, short lifetimes and easy photobleaching.[38] On the other hand, quantum dots have high costs and high toxicity which makes them not suitable for biosensing applications.[53]

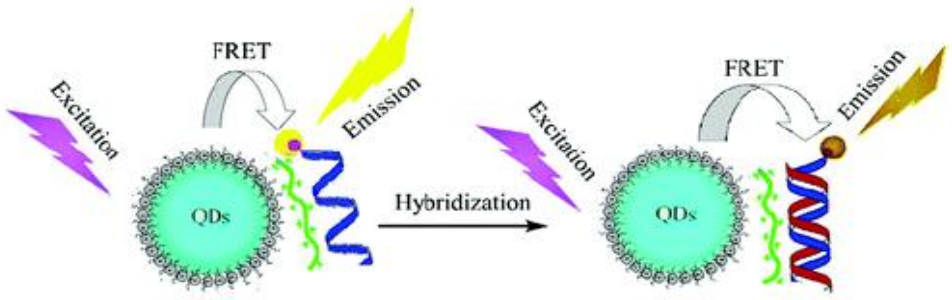

Figure I-6. A DNA sensing platform based on the fluorescence resonance energy transfer (FRET) between blue-luminescent CdTe QDs and dye-labeled ssDNA. aA cationic polymer brings the donor into proximity of the acceptor and the hybridization event is recognized by different FRET efficiencies resulting from different interaction abilities of single stranded (before hybridization) and double stranded DNA (after hybrdiziation) with the polymer. Reprinted with permission from Peng *et al.* [52]

a. Liposomes

A major enhancement of the fluorescent strategies could be the incorporation of many fluorophores together inside one larger molecule such as a liposome. Liposomes are spherical structures composed of amphipathic bilayers, usually phosophlipids, with an aqueous phase inside.[54] They have a large internal volume which allows molecules to be encapsulated within the aqueous cavity or trapped within the lipid tails.[55] Liposomes can be critical for signal amplification in the case of weak fluorescence signals as a large number of dyes can be trapped inside and then released under certain conditions. [55b, 56]

For instance, Kubo *et al.* proposed a novel method based on the use of dye-encapsulating liposomes to detect endocrine disrupting chemicals (EDC).[57] In this

platform, 1,2-dioleoyl-3-trimethylammonium propane (DOTAP) and 1,2-dioleoyl-sn-glycero-3-phosphocholine (DOPC) liposomes were encapsulated with a high concentration of carboxyfluorescein (CF) which would leak upon the penetration of EDCs inducing an enhancement of the fluorescence intensity proportional to the EDC concentration. Furthermore, this sensing strategy was done for four different EDCs allowing their detection at the 5ppm level, the required concentration for environmental measurements. This means that this liposomes' strategy offered the advantage of a high-throughput analysis system and an easy preparation and handling and hence it could be very practical as a universal platform to detect structurally diverse EDCs. Alternatively, the use of liposomes in various sensing platforms is possible because biomolecules such as oligonucelotides or proteins can be easily functionalized onto the surface of liposomes without any chemical modifications. [54a]

b. Flow cytometry

Recently, many hospitals have been using flow cytometry as a routine technique to carry the analysis of blood samples.[58] Indeed, flow cytometry is one of the most ultrasensitive fluorescent biophysical technologies techniques that provides rapid and simultaneous analysis of multiple quantitative and qualitative characteristics of single particles as they flow in a fluid stream past an excitation light source (Figure I-7).[59] Physical properties such as size and internal complexity are identified by the scattering of light at different angles. Light that is scattered axial to the laser beam (Forward scatter (FSC)) indicates the size of the population (0.5-120 µm range) whereas the perpendicularly scattered one (Side scatter (SSC) reveals the internal complexity or granularity. The flow cytometer consists of three main systems: fluidics, optics and

electronics. The fluidics stream transports and aligns the particles or cells so that they are individually interrogated through the laser beam. The optical system is made up of light sources (mainly lasers) to excite the particles in the sheath as well as filters and mirrors that isolate particular wavelengths and direct light to the appropriate detector (usually a photomultiplier tube). The electronic system converts the collected light signals into electronic ones that are digitized for computer analysis of the revealed physical and optical information.

Flow cytometry does not only utilize signal per particle measurements to acquire multiple characteristics of the system but also it allows several analytes to be quantified and distinguished simultaneously using different labels. This makes it of higher sensitivity and versatility when compared to a regular spectrometer that bases its measurements on a bulk volume of sample and has no ability to multiplex.[60] Moreover, the ability of flow cytometry to generate rapid clinical information from complex media such as human blood and to provide real time monitoring makes it a very interesting and powerful research tool that is frequently employed in hospitals and clinics. For instance it is now routinely used for immunophenotyping of a variety of specimens, diagnosis of health disorders such as blood cancer, DNA content analysis, quantification of soluble analytes and many more applications. [50, 59a, 60] Flow cytometry is becoming smaller, user -friendly and less expensive which makes it a promising device to be implemented in the point of care settings.[50 60]

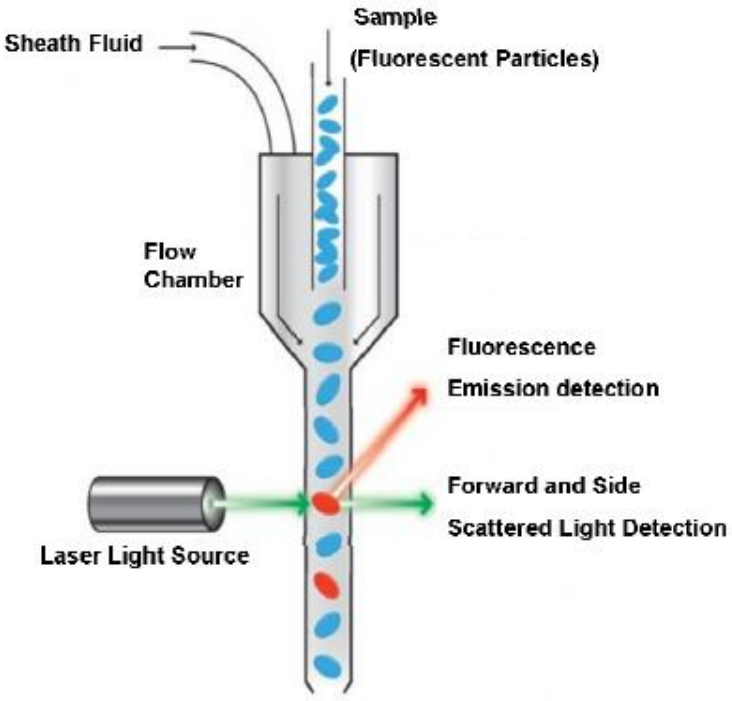

Figure I-7.Schematic representation of the key features in a flow cytometer.Adapted from http://www.abcam.com/index.html?pageconfig=resource&rid=12405

D. Multiplexing

The current focus is to develop a universal sensor that can multiplex which means that it is capable of detecting a broad range of different target sequences simultaneously. [42b, 61] This is because a multiplexed detection of correlated multiple biomarkers of the same disease increases the accuracy and reliability of the detection. [62]

In addition, a multiplex detection would save time, labor and materials it allows the detection and analysis of all the targets of interest in a single run rather than doing each in a separate experiment. As a matter of fact, many techniques have been utilized in a multiplex detection of oligonucleotides. For instance, Wang *et al.* proposed the use of quantum dots nanocrystals for sensing different targets using stripping voltammetry measurements (Figure I-8).[63] This sensing strategy incorporates the

sensitivity and selectivity of nanoparticles along with the advantage of inherently amplified signal that results from pre-concentrating the target analyte. In this platform, multiple target DNA can be simultaneously detected by coupling each to a different inorganic colloidal tag.[63] The high selectivity and remarkable sensitivity of the assay make it a promising candidate that could be adapted to other biological assays, especially immunoassays. However, most electrochemical methods, including stripping voltammetery, are not well devised for multiplex detection since they have a poor reproducibility and require an intensive experimental optimization. On the other hand, fluorescent techniques have higher versatility and thus they are exploited more in multiplexing detection. These techniques are usually based on the use of organic dyes [64] or quantum dots.[65] Nevertheless, they are still limited by multiple factors such as the degree of amplification and expensiveness.

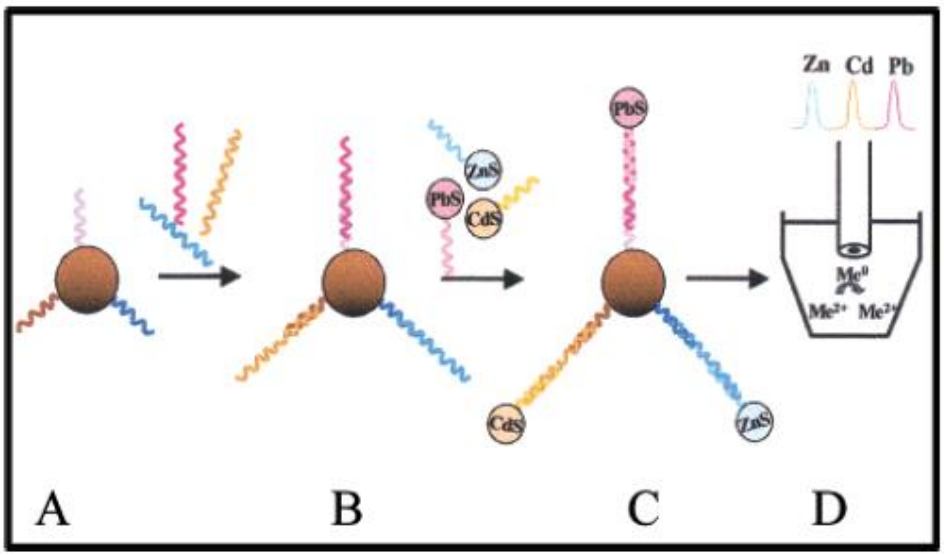

Figure I-8. Multi-target electrical DNA detection protocol based on different inorganic tags. (A) Introduction of probe-modified magnetic beads. (B) Hybridization with the DNA targets. (C) Second hybridization with the QD-labeled probes. (D) Dissolution of QDs and electrochemical detection. Reprinted with permission from Wang *et al* .[63]

E. Traumatic Brain Injury

Traumatic brain injury (TBI), an alteration to the brain caused by an external mechanical force, is considered as one of the foremost causes of deaths and disabilities among young adults and children.[66] The symptoms of mild traumatic brain injury as determined by the American Congress of Rehabilitation Medicine can range from immediate loss of consciousness or memory to concussion and confusion.[67] However, these symptoms might not directly appear after the injury and so TBI is usually described as an invisible wound and a silent killer.[68] The global health impact of the "silent epidemic", Centers for Disease Control and Prevention (CDC) description of TBI, is escalating as the number of victims induced mainly by motor vehicle use and military or blast activities is dramatically increasing.[69] For instance, more than 500000 cases sustaining permanent disability are reported each year associated with 300000 deaths.[66b, 70] Nevertheless, these numbers don't include those who don't seek medical treatments or are seen in private clinics and thus the danger of TBI seems to be underestimated.

1. Diagnosis and Clinical Assessment

Because the risk of a traumatic brain injury could get worse swiftly without treatment, it is vital for doctors to assess the situation and to grade its severity rapidly.

a. Glasgow Coma Scale (GCS)

Classically, assessing the situation has been done using the Glasgow Coma Scale (GCS) described in 1974 by Teasdale and Jennett.[71] This 15 point-test (Table I-1) is a quick and simple tool to diagnose TBI and stage its severity based on the evaluation

of the eye opening, motor and verbal responses to stimulation.[69b] The interpretation of the overall scores result in classifying TBI into 3 categories: mild (GCS 14-15) moderate (GCS 9-13) and severe (GCS <9). [70b] However, GCS scores are not always reliable as they depend on the user and the time of assessment as well as some symptoms might be confounded with other trauma and drug use.[70a, 72]

Table I-1. Glasgow Coma Score (GCS). Reprinted with permission from Barlow.[69b]

Eye opening	
Spontaneous	E4
To speech	3
To pain	2
Nil	1
Best motor response	
Obeys	M6
Localizes	5
Withdraws	4
Abnormal flexion	3
Extensor response	2
Nil	1
Verbal response	
Orientated	V5
Confused conversation	4
Inappropriate words	3
Incomprehensible sounds	2
Nil	1
Total E + M + V	3–15

b. Image Testing

Alternatively, image testing using conventional imaging techniques such as Computerized Tomography (CT) scan and Magnetic Resonance Imaging (MRI) is informative and can provide a detailed view of the brain.[73] For instance, CT scan uses X-rays to quickly produce cross sectional images of the brain that could detect bleeding,

blood clots and battered brain tissues whereas MRI utilizes magnets and radio waves to image the anatomy of the brain. But, the expensiveness of these techniques and being not available in all medical centers, as well as its incapability to always detect mild brain injuries and provide information about the mechanism make them not practical for routine and clinical assessment.[66b]

c. TBI biomarkers

Interestingly, the use of biomarkers could circumvent the pitfalls of the available assessment tools and offer a great gain to specifically and sensitively diagnose TBI and evaluate neurological deficit.[67] While the Cerebospinal Fluid (CSF), the fluid that bathes the central nervous system, serves as an excellent source of biomarkers, its acquisition is a relatively invasive one.[70a] Hence, researchers focus on identifying biomarkers in the blood rather the CSF because acquiring a blood sample is much easier and clinically accepted.[67b, 70a] As such, several blood biomarkers have been evaluated on their capability to provide substantial information and reveal the severity of the injury.[68] For instance, elevations in serum level of neuron specific enolase (NSE), a neuronal damage marker, have been correlated with severe TBI.[70a, 74] However, it was found that this marker is not specific only for TBI as it is released into the blood stream as a result of hemolysis too and thus its accuracy in predicting the injury decreases.[75] Likewise, Glial Fibrillary Acidic Protein (GFAP), a protein found in the astroglial skeleton, seems to be a promising biomarker because its serum levels increase within few hours of injury and are correlated with severe cases but still its lack of high specificity has limited its clinical uses.[74, 76] On the other hand, Myelin Basic Protein (MBP) which is

released upon the injury of white matter offers high specificity for TBI but its delayed introduction intothe serum (2-3 days) makes it unfavorable. [75, 77]

i S100B

Out of the various TBI biomarkers used, S100B, a calcium binding protein, remains the most studied one. S100B normal serum levels in a healthy individual is around 0.2 ng/mL, but an increased concentration in the CSF and serum can be detected within 6h of a mild traumatic brain injury.[78] In one study, Korfias *et al.* stated that a cut-off value of 0.5 ng/mL and higher is correlated to a severe trauma while values between 0.2 and 0.5 ng/mL indicate the prescence of a mild TBI.[79] Nevertheless, serum S100B levels were predictive of deaths at a cut-off value of 1.13 ng/mL. In fact, S100B is a highly sensitive protein and its level in the CSF were shown to be the foremost accurate evidence of an injury yet its specificity decreases when detected in serum as it can be released by cells outside the central nervous system.[70a, 78c] This means that it can't be used as a stand-alone biomarker for an accurate diagnosis and so a combination with other markers is necessary to be specifically and sensitively more informative about the injury. [70a, 80]

F. Infectious diseases:

Infectious or transmissible diseases are the result of the invasion of one's immune system by pathogenic organisms e.g., viruses, fungi, bacteria, parasites, etc...[81] Indeed, life-threatening infections have been the principal cause of deaths and disabilities in developing countries. [82] According to the WHO reports on infectious disease and poverty, more than 4.5 million people die each year from acute infections of

which 95% are caused by the absence of proper diagnostic and treatment tools.[7, 83] Nevertheless, these numbers are significantly boosted by the increased viral outbreaks (Zika, Ebola, H1N1 flu, SARS and others) and the capability of viruses to rapidly spread, multiply and turn into fatal diseases. As such there is a vast necessity for having reliable point of care devices that could quickly and accurately diagnose the disease at an early stage of infection and hence stimulating a higher rate of successful treatment.

1. Hepatitis B Virus

Hepatitis B virus (HBV) is considered as one of the most severe life-threatening viruses that causes a serious global problem.[84] It infects the liver leading to cirrhosis, heptocellular carcinoma and other decompensated liver diseases.[85] According to the world health organization (WHO), it is estimated that more than 2 billion people has experienced past or current HBV infections and around 240 millions are chronically infected. Moreover more than 800000 die each year due to liver diseases caused by this infection. Despite that HBV vaccines are 95% effective in preventing infections, there is no specific treatment for acute HBV.[85b] As such, the diagnosis of HBV at an early stage is vital since HBV is capable of escaping immune surveillance by mutating its structural genes as well as patients are at high risk of chronic development when their serum viral load is more than 10^5copies/ml.[84] Furthermore the detection needs to be confirmed inside laboratories so that hepatitis B can be differentiated from other hepatitis caused by different types of viral agents.[86]

2. Bacillus Anthracis

Bacillus Anthracis (BA) is a rodshaped, gram-positive ,spore forming bacterium that causes anthrax, a lethal and acute infectious disease mainly for grazing and herbivore animals and potentially for humans.[87] Despite that anthrax has been well known since the nineteenth century, the interest in studying it was renewed as of September 27, 2001, the date of the first USA anthrax attack.[88] The toxins responsible for the disease symptoms are germinated by the spores formed when exposed to a nutrient-rich environment though these spores are inactive and persistent under extreme environmental conditions.[87b] Besides, these spores could be resilenced by heat or radiation which makes BA suitable for the use as a biological warfare agent.[89] In fact, during the fall of 2001, BA spores were sent to US organizations via public mail resulting in 19 infections and 5 fatalities and more than 10000 people to take antibiotics following their agent exposure possibility.[87c] This experience raised the urgency of developing reliable methods that could detect this pathogen with high sensitivity and specificity. As such various detection techniques were developed ranging from culture based ones to DNA amplification devices.[87c] However, the specificity of these methods remains tricky as other Bacillus species share similar phenotypic and genotypic characteristics.[87b]

G. Thesis Layout and Objectives

This thesis work aims at developing potential biosensing platforms for the detection of trace amounts of specific biomarkers (proteins and DNA) using electrochemical and fluorescent approaches. Towards reaching our ultimate objective, we will test our sensing strategies using TBI protein biomarker (S100B) and then using

short oligonucleotide sequences specific for HBV and BA. In the electrochemical approach, we will utilize differential pulse voltammetery to monitor the faradaic current of fabricated gold microelectrodes whereas in the fluorescent approach we will use flow cytometry to visualize the fluorescence intensity of synthesized gold coated polystyrene microspheres. The thesis layout consists of 5 chapters. In chapter 1, we presented an overview of biosensors, biomarkers of the diseases of interest and the common detection methods. In chapter 2, we will detail the experimental procedures and all sensing protocols used in chapter 3 and 4. As such, two strategies for the sensing of S100B biomarker will be presented (electrochemical immunoassay and fluorescent sandwich assay) as well as a multiplexing fluorescent platform for the detection of trace amount of DNA. In chapter 3, we will display the results of our proposed detection methods of TBI and discuss them. Likewise in chapter 4, we will show the results and a detailed discussion for the detection of DNA along with all different optimizations. Finally in chapter 5, we will compile the concluding remarks of all chapters and give future directions and implications.

CHAPTER II

EXPERIMENTAL

This chapter includes the synthesis and characterization procedures of all composites and materials used in the thesis as well as the different sensing protocols.

A. Contribution to This Work

Mr. Hassan Fakih performed the synthesis, optimization and characterization of the monodispersed micropolystyrene gold coated beads (PS-Au).

B. Materials

3,3′-Dithiodipropionic acid di(N-hydroxysuccinimide ester) (DSP), $C_{14}H_{16}N_2O_8S_2$; Ethanolamine (C_2H_7NO); Potassium chloride (KCl); Gold(III) chloride trihydrate ($HAuCl_4.3H_2O$); Potassium ferricyanide ($K_3[Fe(CN)_6]$); Potassium ferrocyanide trihydrade ($K_2[Fe(CN)_6 .3H_2O$); Potassium phosphate monobasic ($KH_2 PO_4$); Potassium phosphate dibasic (K_2HPO_4); Styrene **(**St**),** $C_6H_5CHCH_2$; Polyvinylpyrrolidone powder (PVP , MW 55K); Sodium citrate dehydrate ≥ 99%, $HOC(COONa)(CH_2COONa)_2.2H_2O$; Dithiothreitol (DTT); Tetraethyl orthosilicate reagent grade (TEOS), 98%,$Si(OC_2H_5)_4$; 3-Aminopropyltrimethoxysilane97% (APTES),$H_2N(CH_2)_3Si(OCH_3)_3$; Serum replacement (50x), Biotin; 4, 4′-Azobis (4-cyanovaleric acid) (ACVA); 2-Methoxyethanol (Mtx); Ethanol (C_2H_5OH); Hydrochloric acid(HCl) and Nitric acid(HNO_3) were purchased from Sigma-Aldrich. EDC (1-ethyl-3-(3 dimethylaminopropyl)carbodiimide hydrochloride) and Ammonium hydroxide, ACS reagent, 28-30% solution in water (NH_4OH) were purchased from ACROS Organics. All buffers were

prepared using deionized water (18μΩ-cm, Nanopure Diamond, CRSL, AUB). Gold coated polystyrene beads (PS-Au) were synthesized in our lab according to the protocol described in CHAPTER IIG.

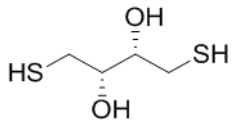

Figure II-1.Chemical Structure of Dithiothreitol (DTT)

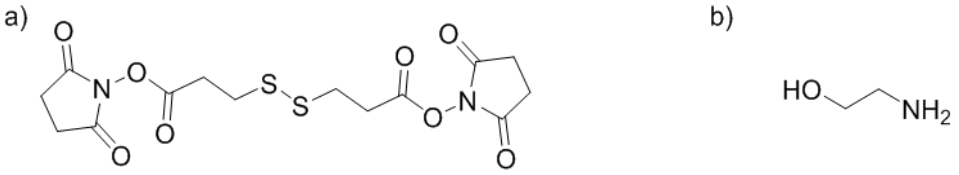

Figure II-2.Chemical structures of a) dithiobis(succinimidyl propionate) (DSP).b) Ethanolamine (C_2H_7NO).

Streptavidin, Alexa Fluor® 647 conjugate , $DiIC_{18}$ (5) solid (1,1'-dioctadecyl-3,3,3',3'-tetramethylindodicarbocyanine, 4-chlorobenzenesulfonate salt)(DiD) and 4-Di-16-ASP (4-(4-(dihexadecylamino)styryl)-N-methylpyridinium iodide) (DiA) were purchased from Molecular Probes,USA. 1-2dioleoyl-sn-glycero-3-phosphocholine (DOPC) ,1,2-dioleoyl-sn-glycero-3-phosphoethanolamine-n-[methoxy(polyethylene glycol)-1000] (ammonium salt) (18:1 PEG1000 PE) and 1,2-dioleoyl-*sn*-glycero-3-phosphoethanolamine-N-(biotinyl) (sodium salt) (18:1 Biotinyl PE) were purchased from Avanti polar (France).

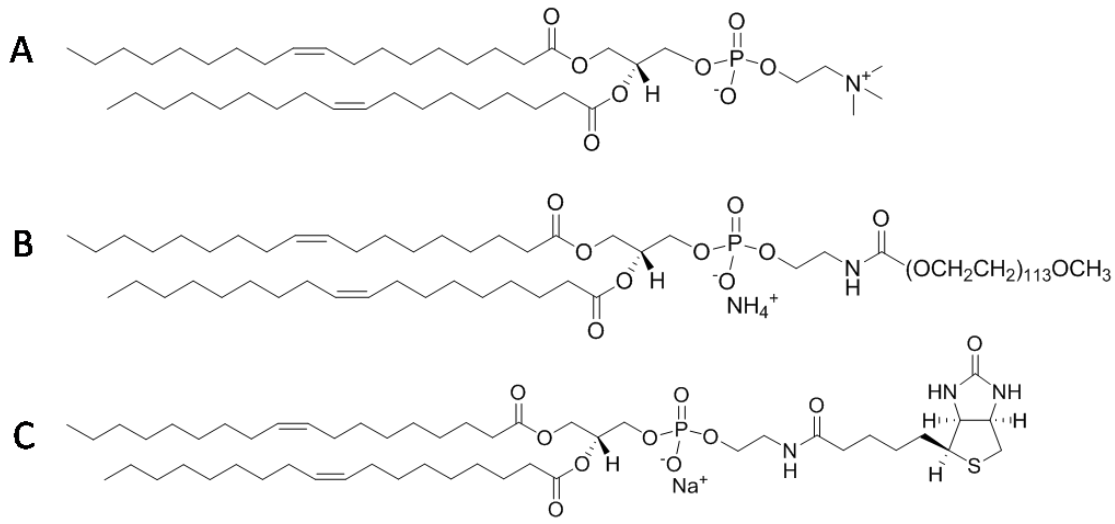

Figure II-3. Chemical Structure of A) 1-2dioleoyl-sn-glycero-3-phosphocholine (DOPC). B) 1,2-dioleoyl-sn-glycero-3-phosphoethanolamine-n-[methoxy(polyethylene glycol)-1000] (ammonium salt)(PEG-PE).C) 1,2-dioleoyl-*sn*-glycero-3-phosphoethanolamine-N-(biotinyl) (sodium salt) (18:1 Biotinyl PE)

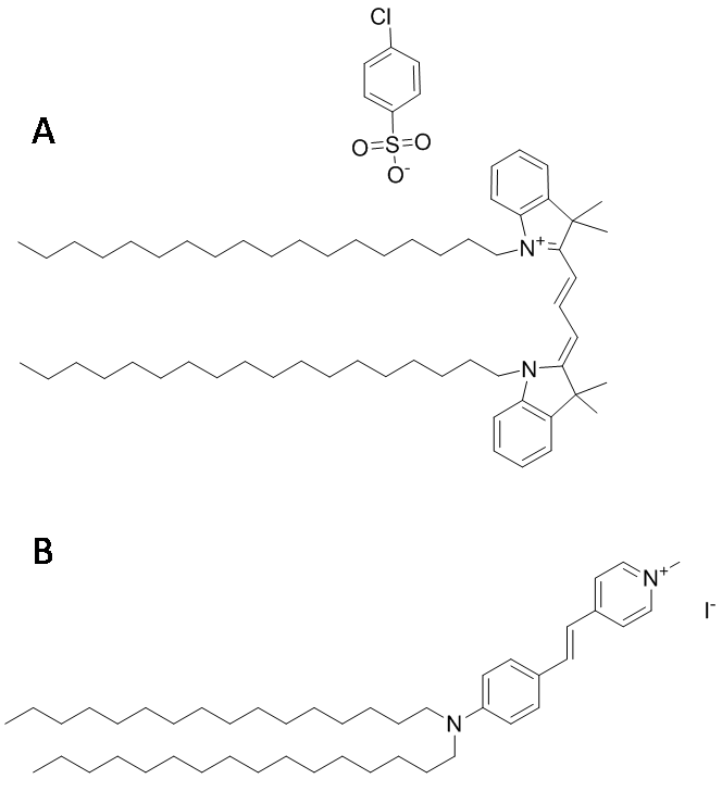

Figure II-4. Chemical structure of A) DiIC18 (5) solid (1,1'-dioctadecyl-3,3,3',3' tetramethylindodicarbocyanine, 4-chlorobenzenesulfonate salt) (DiD). B) 4-Di-16-ASP (4-(4-(dihexadecylamino)styryl)-N-methylpyridinium iodide) (DiA)

2 mm diameter gold working electrode; Platinum wire counter electrode; Ag/AgCl reference electrode with porous teflon tip and Electrode polishing kit were purchased from CHI instruments. Anti-S-100(beta-subunit) antibody (monoclonal) detecting antibody was purchased from mybiosource. Rabbit Anti-Human S100B capturing antibody was purchased from DAKO. Anti-Mouse IgG (whole molecule) −Biotin antibody produced in goat secondary antibody and S-100B Protein from bovine brain, ≥70% (HPLC) were purchased from Sigma-Aldrich.

Illustra MicroSpin G-25 Columns were purchased from GE Healthcare. DNA sequences listed in Table II-1 were purchased from IDT DNA

Table II-1.Oligonucelotides Sequences

Name	**Sequence**
HVB-T	5'-TGG CTT TCA GTT ATA TGG ATG ATG TGG TA-3'
HVB-P1	5'-/5ThioMC6-D/AA AAA AAA AAT ACC ACA TCA TCC AT-3'
HVB-P2	5'-ATA ACT GAA AGC CAA AAA AAA AA/3CholTEG/-3'
BA-T	5'-GAG GGA TTA TTG TTA AAT ATT GAT AAG GAT-3'
BA-P1	5'-/5ThioMC6-D/AA AAA AAAAAA TCC TTA TCA ATA TT-3'
BA-P2	5'-TAA CAA TAA TCC CTC AAA AAAAAA /3CholTEG/-3'

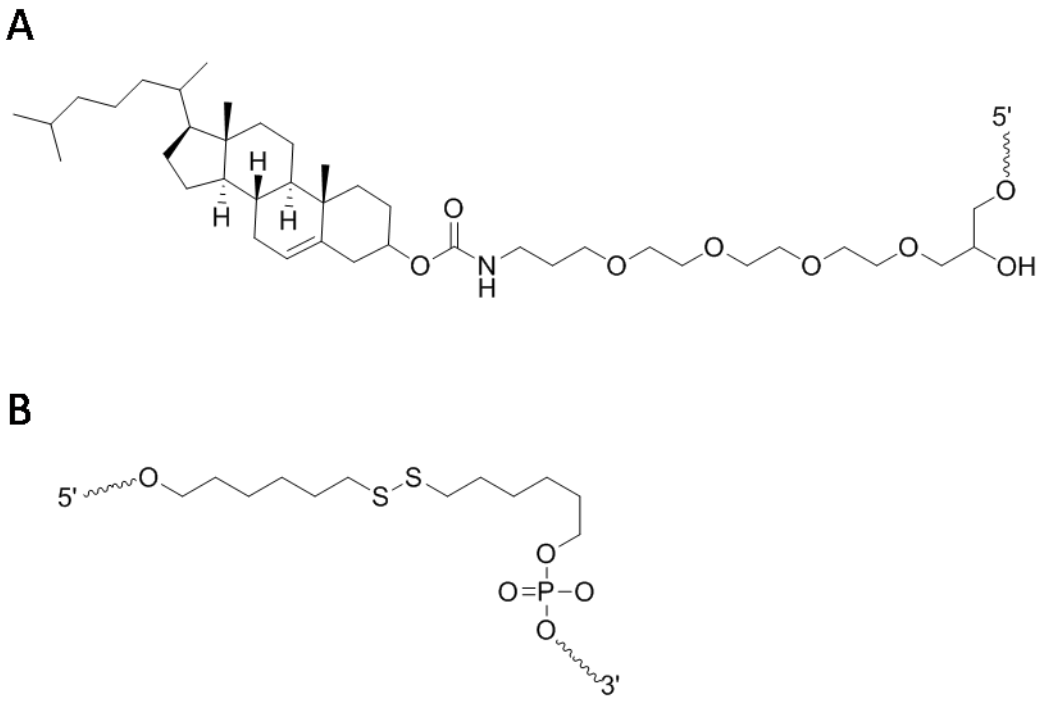

Figure II-5.Chemical structure of A) Cholesteryl-triethyleneglycol (CholTEG). B) 5' Thiol Modifier C6 S-S (5ThioMC6-D)

C. Instrumantation

The scanning electron microscopy (SEM) images were obtained using TESCAN MIRA3 LM SEM. The samples were prepared on a carbon conductive tape and dried overnight in a desiccator. The voltage used for acquiring all images was 15 kV. Infrared Spectra were obtained using Nicolet 4700 FT-IR spectrometer.Dynamic Light Scattering (DLS) measurements were done using Brookhaven particle size analyzer.

Electrochemical analysis: All electrochemical measurments were carried out using a CHI630E potentiostat with a three-electrode system consisting of an Ag/AgCl reference electrode, a platinum wire auxiliary electrode and standard gold substrate or fabricated gold microsensor as working electrode. Electrodeposition of the microsensors

was done using DC potential amperometry at varying voltages and durations in a solution containing 20 mM $HAuCl_4$ in 0.5M HCl. Differential pulse voltammetry (DPV) signals were measured in a 10 mM phosphate buffer solution (pH = 7) containing 2.5 mM $K_3[Fe(CN)_6]$, 2.5 mM $K_2[Fe(CN)_6]$, and 0.1 M KCl. The signals were obtained from a range of 0 mV to 600 mV with a potential step of 5 mV, pulse amplitude of 50 mV, pulse width of 50 ms, and a pulse period of 100 ms.

Flow cytometry measurements were collected using BD SORP Aria II 5B-3R Flow cytometer; DiA and FITC-silica were excited at 488 nm whereas Streptavidin Alexa Fluor® 647 or DiD liposomes were excited at 633 nm. The emissions intensities were collected using 530/30 filter for FITC, 585/42 filter for DiA and 660/20 filter for DiD or Streptavidin, Alexa Fluor® 647. The size of the nozzle used was 70µm with a 1.0 filter and the number of the recorded events was fixed at 10000. The voltages used were adjusted so that the blank sample had its peak at 10^2 and then kept constant throughout the experiment. Steady state fluorescent measurements were collected using LUMINA Fluorescence Spectrometer. The samples were excited at 644 nm and the emission spectra were collected between 655 and 750 nm.

D. Synthesis of Colloidal Silica Nanoparticles

Monodispersed silica nanoparticles were prepared by a hydrolysis and condensation mechanism of TEOS in ethanol with the presence of ammonium hydroxide (Figure II-6). [90] Briefly, 140 mL of ethanol, 40 mL deionized water and 2.5 mL ammonium hydroxide (30%) were mixed together and sonicated for 5 minutes. After that 5 mL of TEOS (99%) was added dropwise for an hour and a gradually opaque color started to appear indicating the formation of silica suspension. The reaction

mixture was left under stirring for 24 hours and then the obtained silica nanoparticles were stored at 4 °C for further use.

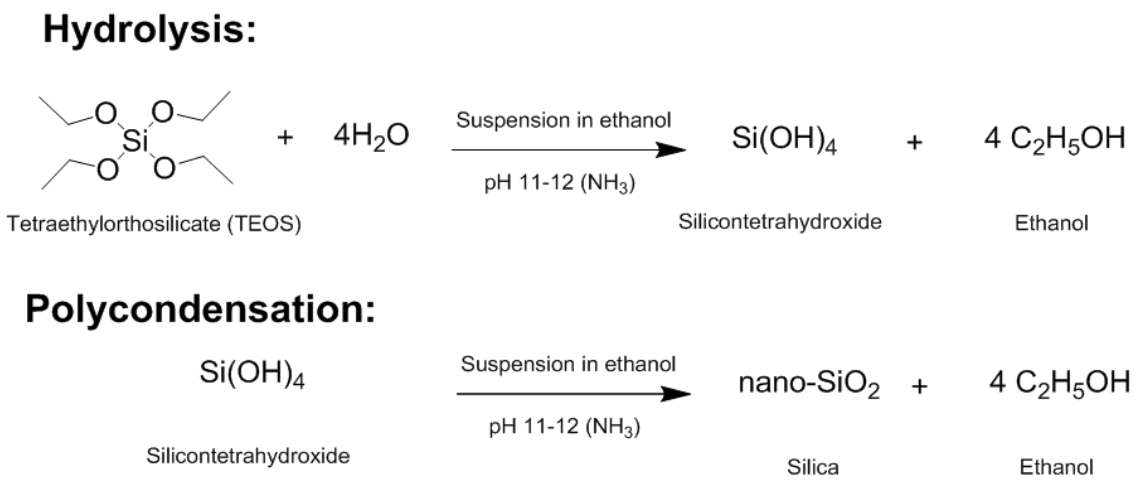

Figure II-6.Schematic representation of the reaction of synthesis of colloidal silica nanoparticles

E. Synthesis of FITC-doped Silica Nanoparticles (FITC-SNP)

Colloidal fluorescent silica nanoparticles were prepared according to a previously reported two step method. [91] First a bright yellow precursor solution was prepared by dissolving FITC (39 mg, 0.10 mmol) and APTES (23 µL, 0.10 mmol) in 100 mL ethanol and allowing them to react for 24 hours at 42 °C. In the next step, 8 mL of the precursor solution and 4.5 mL of TEOS were dissolved in 150 mL mixture solution (14.7 mL DIW, 134 mL ethanol and 1.3 mL ammonium hydroxide (30%)) and then left under stirring (500 rpm) for 6 hours at room temperature. The SEM image (Figure II-7) confirms that the synthesized nanoparticles are colloidal with an average size of 40 nm whereas DLS measurements (Table II-2) shows that the particles are monodispersed.

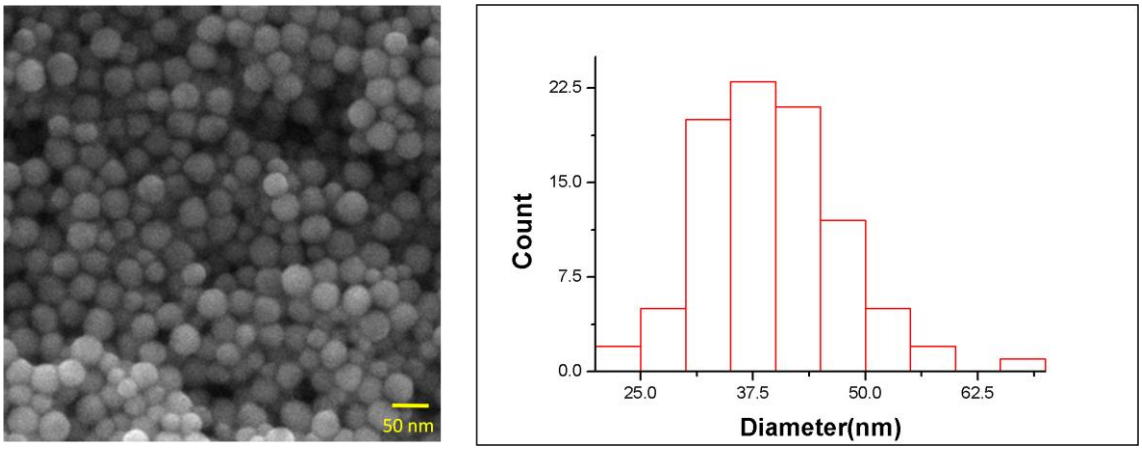

Figure II-7. Left, SEM image of FITC-doped silica nanoparticles. Right, Image analysis of the FITC-doped silica nanoparticles using ImageJ software. Average diameter = 39.77 nm with standard deviation = 4.03 (N = 255).

Table II-2.particle size identified by DLS measurements

Sample	Eff.Diameter(nm)	Half-width(nm)	Polydispersity
Silica nanoparticles	118.5	21.4	0.031

1. Calculating Number of FITC Molecules per Silica Particle

Density of silica is

$$D_{\mathrm{SiO}_2} = 2.65 \frac{g}{cm^3}$$

Density of TEOS is

$$D_{TEOS} = 0.933 \frac{g}{cm^3}$$

Radius of a silica particle as determined from SEM image is

$$R = 20\ nm$$

$$= 20 \times 10^{-7} cm$$

Volume of a silica particle is

$$V = \frac{4}{3}\,\pi\,R^3$$

$$= \frac{4}{3}\,\pi\,(20 \times 10^{-7} cm)^3$$

$$= 3.35\ \times\ 10^{-17}\ cm^3$$

Mass of a silica particle is

$$=\ V \times\ D_{\mathrm{SiO}_2}$$

$$= 3.35\ \times\ 10^{-17}\ cm^3\ \times\ 2.65 \frac{\mathrm{g}}{\mathrm{cm}^3}$$

$$= 8.88\ \times 10^{-17}\ g$$

Mass of TEOS is

$$= D_{TEOS} \times Volume\ of\ TEOS\ added$$

$$= 0.933 \frac{g}{cm^3} \times 4.5\ mL$$

$$= 4.199\ g$$

According to stoichiometry of the reaction: $n_{TEOS} = n_{SiO_2}$

So total mass of SiO_2 is

$$= \frac{mass\ of\ TEOS}{Molar\ mass\ of\ TEOS} \times Molar\ mass\ of\ SiO_2$$

$$= \frac{4.1985\ g}{208.33\ g/mol} \times 60.08\ g/mol$$

$$= 1.211\ g$$

$$Number\ of\ silica\ particles = \frac{\text{total mass of } SiO_2}{\text{mass of a silica particle}}$$

$$= \frac{1.211\ g}{8.88\ \times\ 10^{-17} g}$$

$$= 1.364\ \times 10^{16}$$

In order to know how much the concentration of FITC inside the silica nanoparticles, a calibration curve (Figure II-8) was generated from triplicate measurements of FITC concentrations between 0.08 and 0.6 mM, Then 2 mL of the prepared FITC-SNP solution was centrifuged at 7000 rpm for 5 min in order to remove the excess FITC molecules and then redispersed in ethanol. This sample response was obtained using UV-Vis spectrophotometry and the concentration was then calculated at λ_{max} from the equation of the calibration curve.

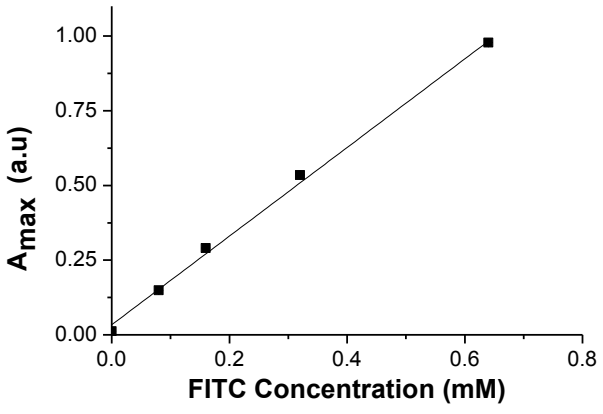

Figure II-8. Calibration curve of the FITC concentration measured between 0.08 and 0.64 mM at $\boldsymbol{\lambda_{max}} = 488$ nm. The equation of the line is $y = 1.483x + 0.033$ with an r^2 value of 0.999.

$Equation\ of\ the\ calibration\ curve\ is\ y = 1.483x + 0.033$

$Concentration\ of\ FITC = C_{FITC}$

$$= \frac{Sample\ Response - y_{intercept}}{Slope}$$

$$= \frac{0.8532 - 0.033}{1.483}$$

$$= 0.55\ mM$$

Number of FTIC moles $= n_{FITC}$

$$= C_{FITC} \times V_{solution}$$

$$= 0.55\ mM \times 162.5\ mL$$

$$= 8.94 \times 10^{-5} mol$$

Number of FITC molecules $= number\ of\ FITC\ moles \times Avogadro's\ number$

$$= 8.94 \times 10^{-3} mol \times 6.022 \times 10^{23} mol^{-1}$$

$= 5.38 \times 10^{19}$ FITC molecules

Number of FITC molecules per silica particle $= \frac{5.38 \times 10^{19}}{1.364 \times 10^{16}}$

$= 3946$ FITC molecules/ silica particle

2. Grafting of NH_2 Group onto Silica Nanoparticles

This procedure was used for functionalization of both silica and FITC-silica nanoparticles with amine groups (Figure II-9).[92] In a typical experiment, 1.5mL of APTES (97%) and 8.5mL DIW were added to 10 mL of the synthesized silica nanoparticles. The reaction mixture was vortexed for a couple of seconds and left for 5 minutes at room temperature. 5 mL of HCl (37%) was added to protonate the amine groups and the mixture was again vortexed for 1 minute. The beads mixture was then isolated and purified by repeated centrifuge and washing cycles (8000 rpm for 5 minutes, rinse with DIW (3x)) and the obtained pellet was freeze dried overnight. The functional groups on the silica nanoparticles were identified by FT-IR spectra shown in Figure II-10.The peaks observed at 1100 and 950 cm^{-1} revealed the SiO–H and Si–O–Si groups respectively while the hydrogen bonded silonol groups have peaks at around 3300 and 500 cm^{-1}. The amine functionalization was verified by the appearance of the broad band at 3400 cm^{-1}corresponding to the N–H stretching vibration and the two bands at 1630 and 1430 cm^{-1} representing the N–H bending of the free NH_2 group. Furthermore, the absorption bands at 2972 and 2852 cm^{-1} correspond to the asymmetric and symmetric stretching vibrations of the CH_2 group respectively and hence are attributed to the anchored propyl group of APTES .[93]

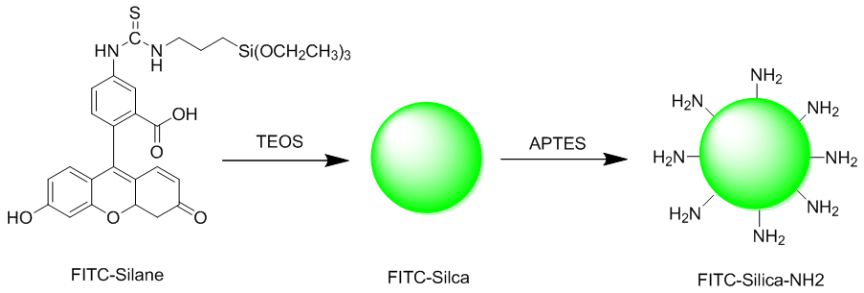

Figure II-9.Schematic representation of the synthesis of FITC-doped silica nanoparticles and its functionalization with primary amine using APTES

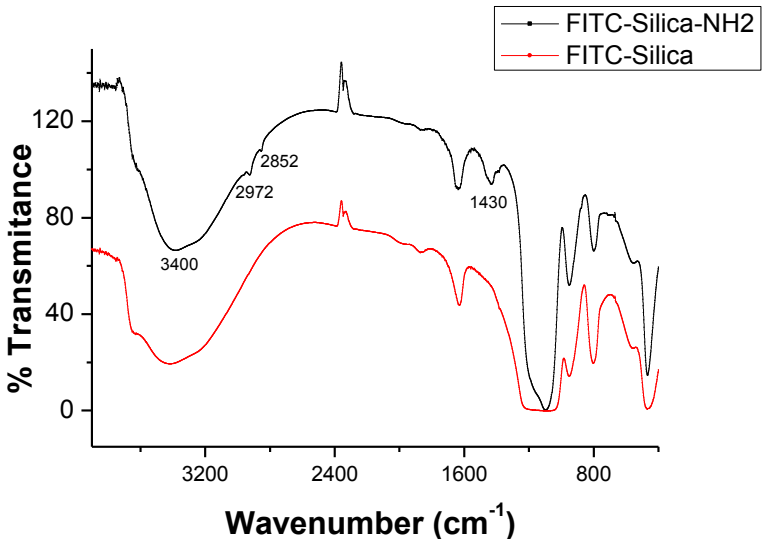

Figure II-10.FTIR spectra recorded between 4000 and 400 cm^{-1} of FITC-silica and FITC-silica-NH_2. The presence of peaks at 2972 and 2852 and 1430 cm^{-1}confirms the amine functionalization. The peak at 3400 cm^{-1} corresponds to the N-H stretching vibration however it overlaps with the peak corresponding to the hydrogen bonded silonol group.

3. Functionalization of Silica Nanoparticles with Biotin

Silica nanoparticles were conjugated to biotin via EDC crosslinking mechanism shown in Figure II-11.[94] In the first step, EDC reacts with the carboxylic group on the biotin to form an active ester. Next, the amine-functionalized silica nanoparticles display the ester by a nucleophilic attack and form an amide bond with the biotin and an EDC-by-product is released as soluble urea derivative. In a typical experiment, 7.5 mg of biotin and 1.8 mg EDC were dissolved in 7.5 mL of DIW and reacted for 4 hours at room temperature. To this solution, 0.016 g of amine functionalized silica nanoparticles dissolved in 2.5 mL of DIW was added and reacted with vigorous stirring at room temperature for 24 hours. The functionalization was confirmed by carrying a fluorescence biotin-streptavidin affinity test described below.

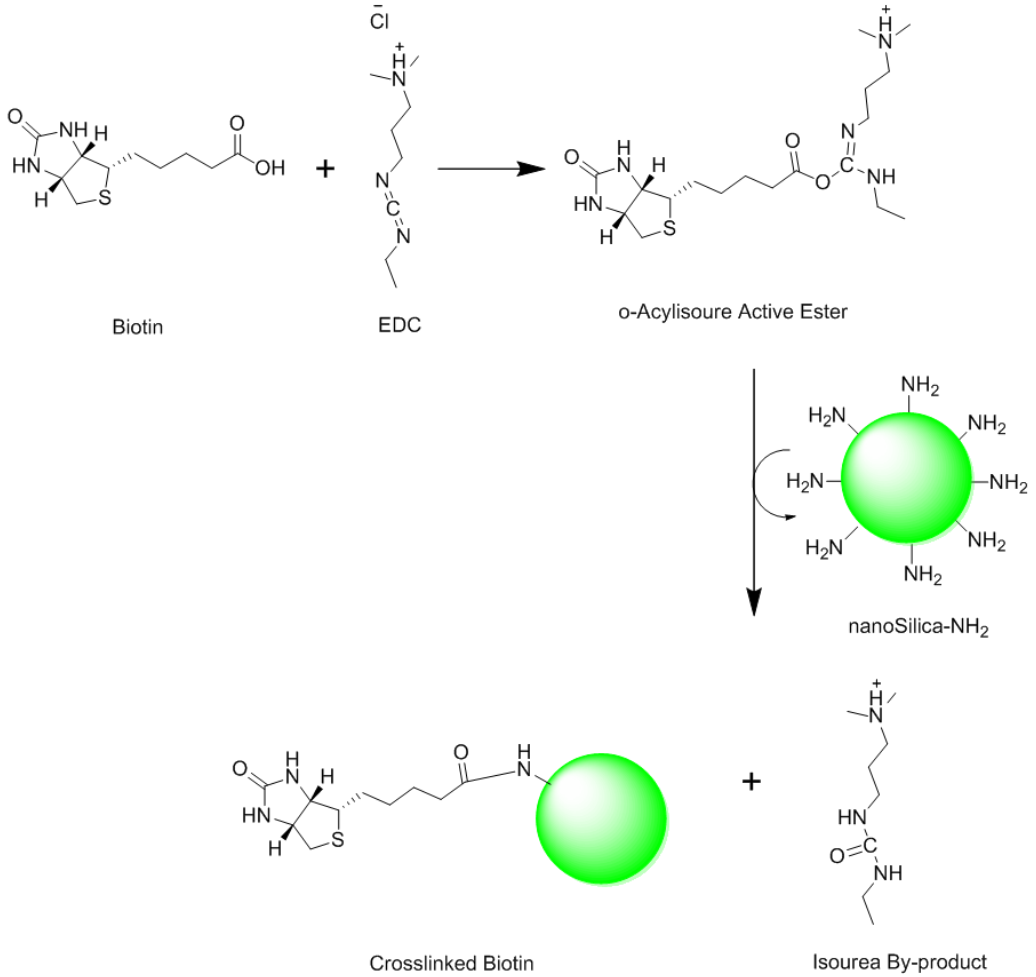

Figure II-11.EDC (carbodiimide) crosslinking reaction scheme.This mechanism involves two steps: the formation of an active ester of EDC and biotin followed by an amide bond formation between amine functionalized nanoparticles and biotin via a nucleophilic attack.

a. Biotin- Streptavidin Affinity Test

0.5 µL of alexa 546 fluoro (37.8 µM) was added to 1 mL of biotinlayted silica nanoparticles and left for 20 min at room temperature. The beads were then isolated by centrifugation at 7000 rpm for 6 min and the supernatant was replaced with DIW. The steady state fluorescence measurements shown in Figure II-12 showed that there is a fluorescence enhancement of the sample after the addition of labeled streptavidin confirming that the silica beads are functionalized with biotin.

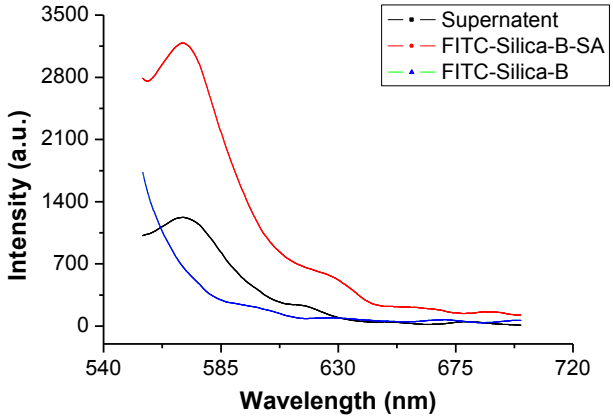

Figure II-12.Emission spectra for biotinylated silica, supernatant and tested beads. Excitation was done at 546 nm and the emission was collected between 573 and 650 nm.

F. TBI Electrochemical Scheme:

Electrochemical based techniques are widely applied in biosensor development due to its undisputable advantages.[95] Contrary to ELISA methods [96], electrochemical-based sensing methods are cheap, fast, user friendly and could be readily developed into small portable point of care (POC) device to perform electrochemical based sensing experiments for a price tag of as little as 500$. [97] As such, we are interested in this part of the chapter in developing an electrochemical immunosensor that allows direct and simple detection of clinically relevant concentrations (1 ng/mL) of the S100B biomarker with high sensitivity and specificity. The underlying principles of our sensing strategy include:

1. Macro-electrode Preparation

To ensure having a clean and uniform electrode surface, a standard 2 mm gold electrode was electrochemically pretreated by cycling between -1 and 2 V vs. Ag/AgCl reference electrode in 0.5 M sulfuric acid for 50 times and then mechanically cleaned by abrasive polishing using 0.05 micron Gamma alumina powder for couple of minutes.

The electrode was rinsed thoroughly with DIW and ethanol and then dried under nitrogen stream.

2. Fabrication of Nanostructured Gold Microelectrodes

The chips were first cleaned by rinsing with acetone, ethanol and DIW and then dried under a nitrogen stream. Electrodeposition was performed at room temperature. The apertures on the fabricated electrodes were used as the working electrorde, Ag/AgCl as a reference electrode and a platinum wire as an auxiliary electrode. Gold nanostructured microsensors of different sizes (10, 30, 60 μm) were formed by DC potential amperometry at 0 mV for 30 s, 150 mV for 200 s and 0 mV for 200 s respectively and using a deposition solution containing 20 mM $HAuCl_4$ in 0.5 M HCl .[98] The fabricated sensors were very reproducible with minor morphological differences (Figure II-14).

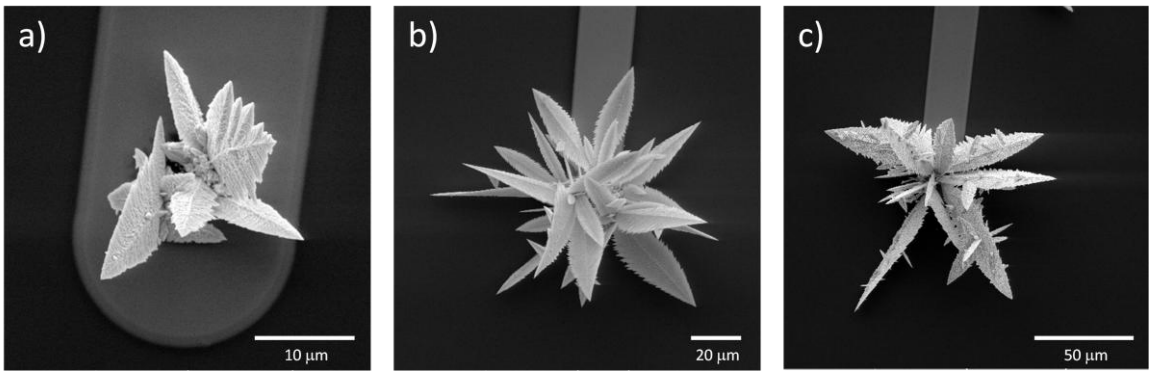

Figure II-13. SEM images of three differently sized gold microsensors. All the sensors were fabricated using DC potential amperometry and a deposition solution containing 20 mM $HAuCl_4$ in 0.5M HCl. a) SEM image of 10 μm sensor; this structure was fabricated at 0 mV for 30s b) SEM image of 30 μm sensor; this structure was fabricated at 150 mV for 200s. c) SEM image of 60 μm sensor; this structure was fabricated at 0 mV for 200 s.

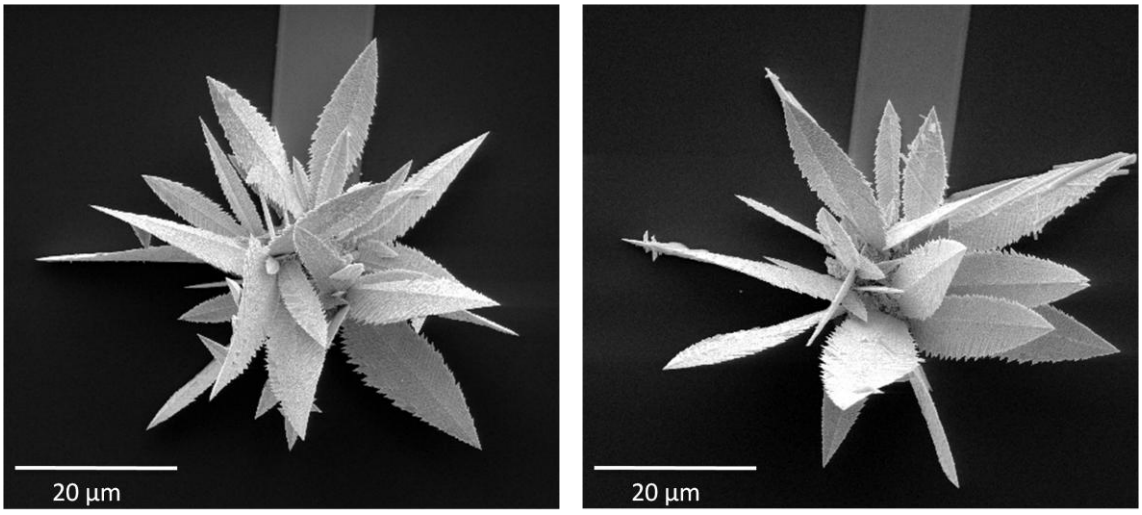

Figure II-14.SEM images showing an example of similar morphology and reproducibility of 30 µm gold sensors.

3. Formation of Immunosensor:

This was done in two steps:

a. DSP Modification and Formation of a Reactive Self Assembeled Monolayer (SAM):

Gold electrode was immersed in 1mM DSP in DMF for 30 minutes at room temperature followed by rinsing with DIW and PBS to remove the unreacted and weakly adsorbed DSP molecules (Figure II-15.a).

b. Immobilization of Antibodies

After the removal of non-bonded thiols, antibodies were directly coupled to the DSP SAM via amide bond formation (Figure II-15.b). As such, 10µg/ml of anti-S100B antibodies was dropped onto the gold surface for 30 minutes at room temperature. Next the electrode was immersed in ethanolamine solution (1M, pH 8.1) for 15 minutes to

block the residual reacting sites. Finally, the immunosensor was washed 3 times with PBS prior to electrochemical readout.

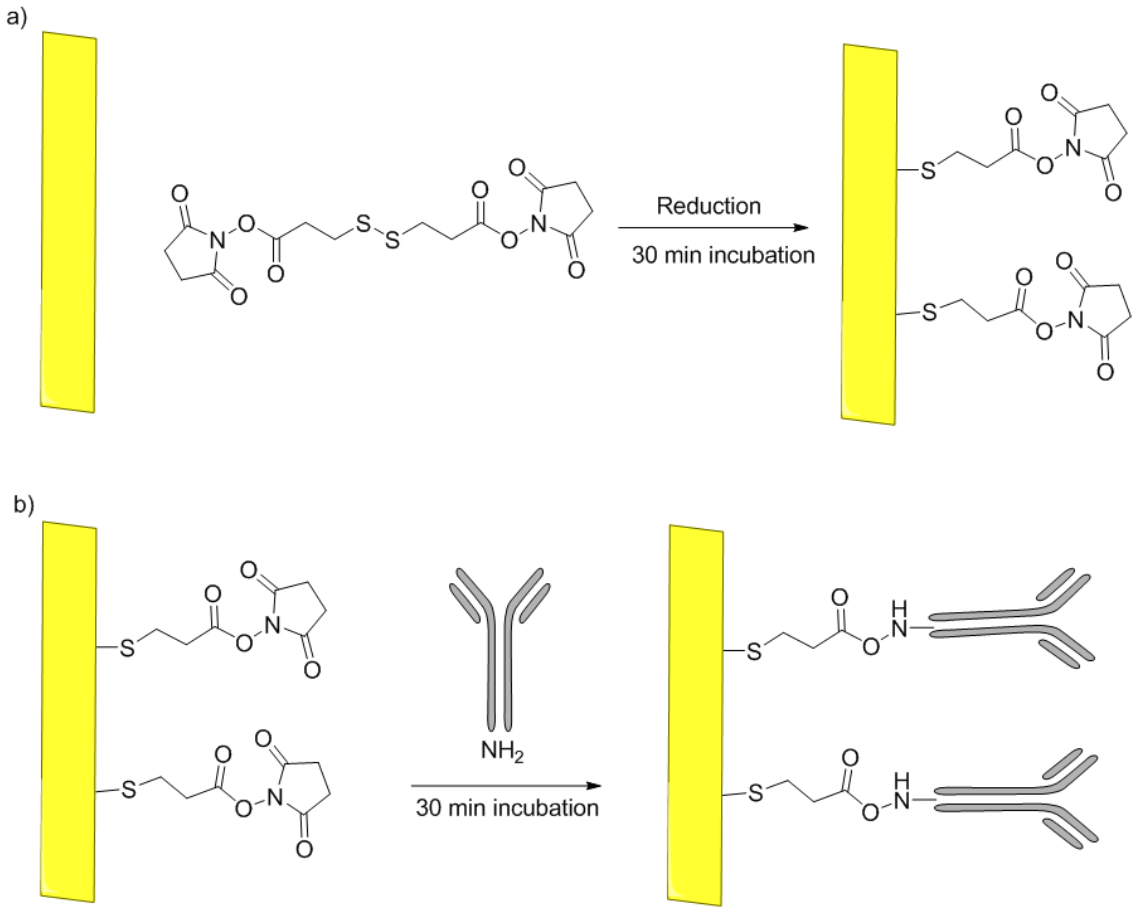

Figure II-15. Schematic illustration of the sensor functionalization with antibodies. a) Formation of self-assembled monolayer of DSP. b) Reaction mechanism of antibodies on DSP coated gold electrode.

c. Detection of Antigen

S100B antigen of desired target concentration was dropped onto the surface of the antibody-modified sensor for 1 hour at room temperature and the electrode was then rinsed thoroughly with PBS prior to DPV measurements. The detailed procedure for the detection scheme is illustrated in Figure II-16. The detection is based on the DPV

current change before and after the antigen–antibody interaction whereby the signal change corresponding to target protein binding to the antibody is calculated as follows

$$\Delta I\% = \frac{\text{Current Antibody}(I_I) - \text{Current Antigen}(I_A)}{\text{Current Antibody } (I_I)} \times 100$$

In fact, electrochemical blocking assays have been used for sensitive label free detection of a wide range of biomolecules including oligonucleotides and proteins. [98-99] Kelley *et al.* have reported the detection of the cancer biomarker CA-125 using electrochemical blocking assays with low detection limit of 0.1 U/mL, a concentration that is 150 times better than the commercially available test. [98] Its simple working scheme relies on the steady diffusion of small electroactive molecules to a metal electrode where upon oxidation or reduction gives a detectable current. When the diffusion of the small molecules is hindered by the binding the specific biomarker, the current dramatically decreases.

A- Fabrication of Nanostructured Gold Micro-electrodes

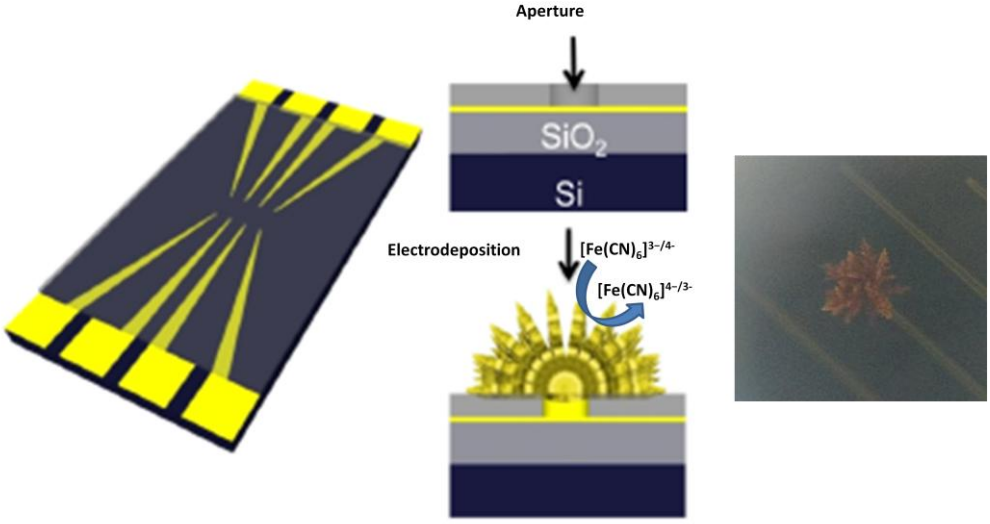

B- DSP SAM Formation and Attachment of Proteins

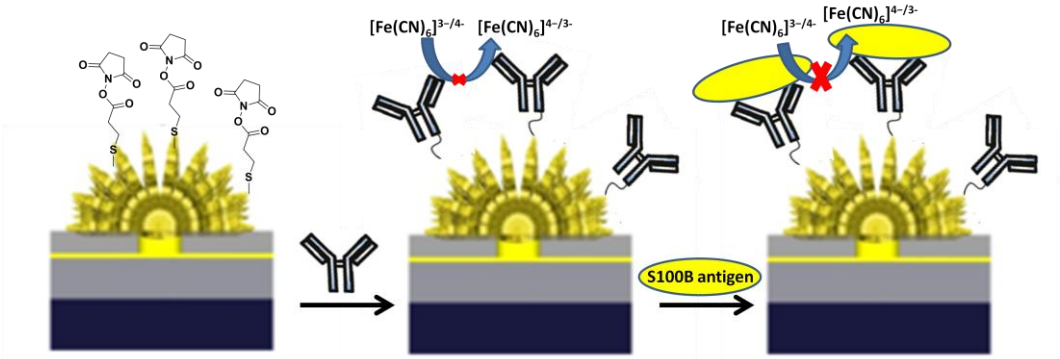

C- Electrochemical Readout

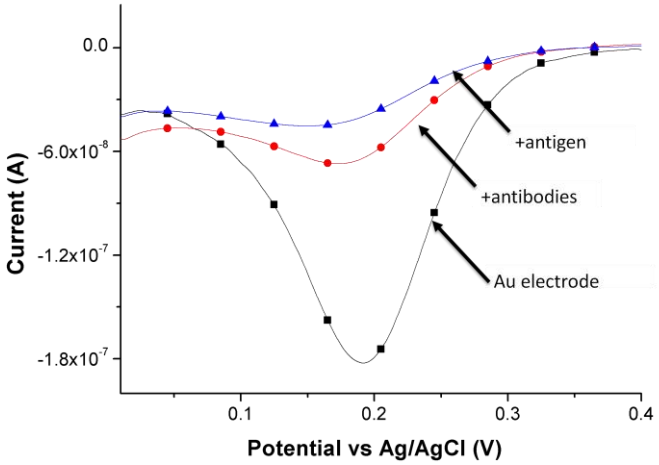

Figure II-16. Overview of the chip-based biomarker detection. DPV measurments were taken after each modification step. A- generation of the Au sensors. Left, a schematic illustration of the sensor chip. Middle, fabrication of the Au nanostructured microelectrodes by Au electrodeposition on the apertures. Right, a photograph of a 10µm fabricated gold microelectrode. B- Schematic of sensor functionalization. Left, a DSP SAM is formed on the Au structure . Middle, addition of the anti-S100B antibodies to prepare antibody-modified surface. Right, illustration of the detection of S100B antigen. C-Differential Pulse voltammetry demonstrating the electrochemical detection of biomarkers. The signal decrease is attributed to the hindrance of the interfacial electron transfer reaction of $[Fe(CN)6]^{3-/4-}$.

G. Polystyrene Microspheres Synthesis

Monodisperesed micro-polystyrene beads were synthesized by a slight modification of a previously reported dispersion polymerization procedure.[100] The reaction that governs the polymerization process is shown in Figure II-17 whereby the azo initiator 4,4'-azobis(cyanovaleric acid) (ACVA) was used to conduct the polymerization process. To obtain the desired size, we varied the quantities of the starting materials (monomer concentration, initiator concentration, stabilizer concentration and solvent). Briefly, as optimized, 0.5 g PVP stabilizer (Mw ~ 55 KDa) and 0.1 g ACVA initiator (Mw 280.27 g/mol), 1:39 molar ratio, were mixed in 24mL of the solvent mixture (65%Mtx, 27 % Ethanol, and 8% DIW) with vigorous stirring under nitrogen for 15 minutes. This is done to deprive the medium from oxygen and thus eliminating its inhibiting effect that might interfere in the polymerization. To the above mixture, styrene monomer (20mL, 3.95M) is added and the whole mixture is then allowed to react with 80rpm stirring at70 ^{o}C for 24 hrs. The obtained beads were isolated and purified from the small sized beads by repeated centrifugation (800rpm for 8mins) and redispersion cycles. Finally they were diluted with DIW to 10wt% solid before use. Figure II-18 and Figure II-19 show a mono dispersed polystyrene population

with an average size of 4.72µm. This size is very well suited for consistent flow cytometry measurements.

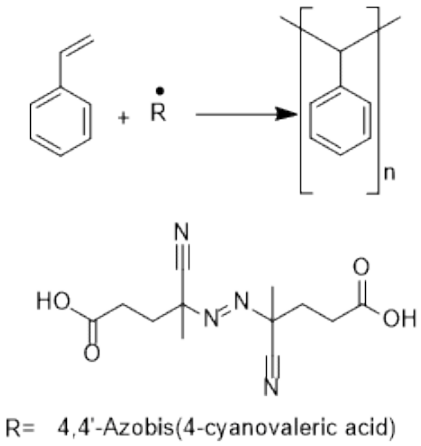

Figure II-17. Schematic representation of the reaction of polystyrene polymerization. The reaction starts from styrene monomer and 4, 4′-Azobis (4-cyanovaleric acid) (ACVA) as a free radical initiator and is performed at 70 °C under inert atmosphere and constant stirring (80 rpm).

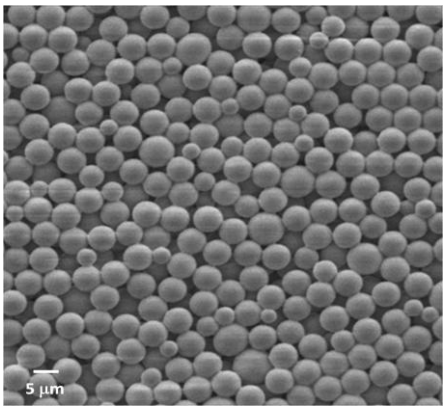

Figure II-18.SEM image of polystyrene beads obtained using 500:1 monomer: initator mole ratio.

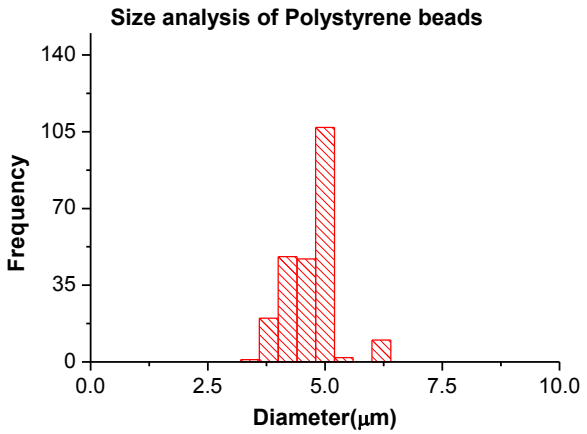

Figure II-19.Image analysis of polystyrene beads using ImageJ software. Average diameter = 4.72μm with standard deviation = 0.48 (N = 235)

1. Grafting of Gold Nanoparticles onto Polystyrene Beads (PS-Au)

Gold nanoparticles coated polystyrene composite beads were synthesized by a redox mechanism using trisodium citrate as a reductant (Figure II-20). First, the polystyrene beads were washed with a mixture of ethanol and deionized water (2:1 volume ratio) to make the PVP coated surface metastable for coating. Then 100mL of $4.92x10^{-4}$ M $HAuCL_4$ aqueous solution was heated to boiling in a silicon oil bath after which 1.2:1 volume ratio of PS beads:sodium citrate ($8x10^{-2}$ M) suspension was added to the mixture and left for 30 minutes with vigorous stirring. After cooling down, the residual free gold nanoparticles were eliminated from the sample via repeated centrifugation and redispersion cycles. Finally, the PS-Au (1x) concentration used in all of our experiments was prepared by four times washing of 4 mL functionalized beads solution resuspended in 4 mL of DIW. The figures below show size and particle analysis of the obtained composite beads. The size of the grafted gold nanoparticles is equal to 24.74 nm which is admirable for a good packing of material (DNA strands, antibodies etc...).

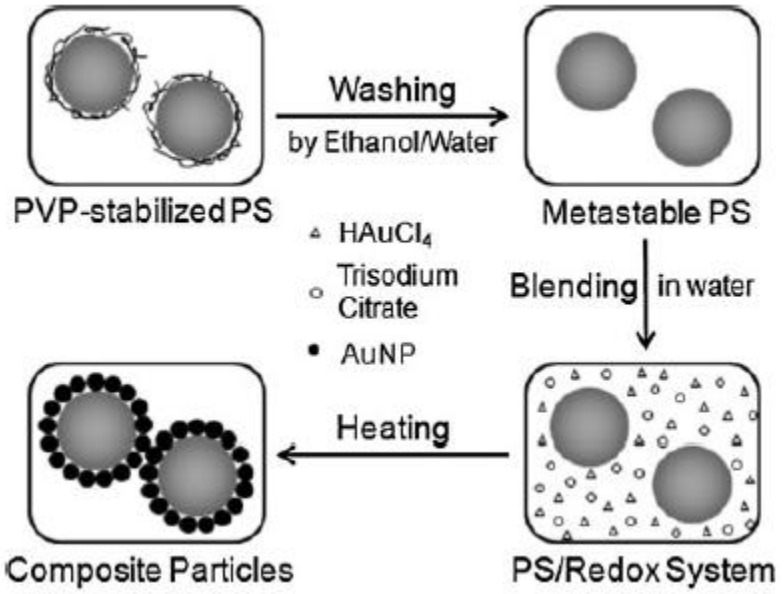

Figure II-20. Schematic procedure for the formation of AuNPs-coated (Reprinted with permission from Wang et al. [101]

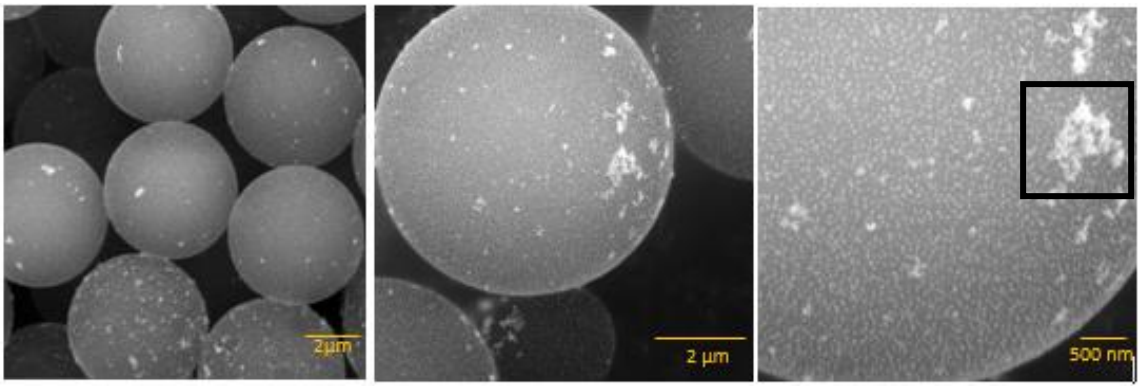

Figure II-21.SEM images of gold coated polystyrene beads (PS-Au). The highlighted area in the right image is where the elemental analysis was performed.

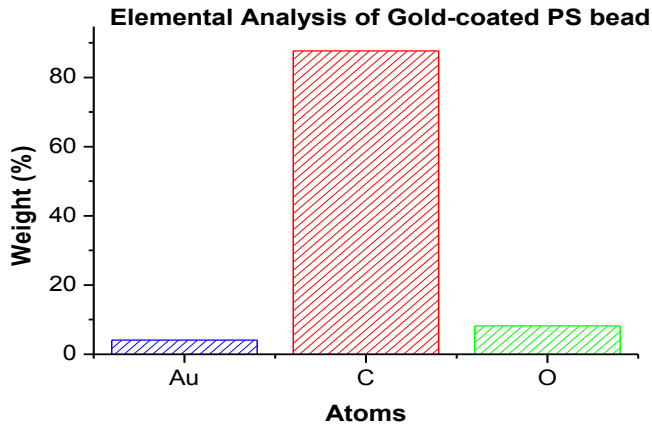

Figure II-22. Elemental analysis of a gold coated polystyrene bead to confirm the coverage with gold nano-particles. Weight percentages are: 87.69 for Carbon, 8.21 for Oxygen, and 4.09 for Gold.

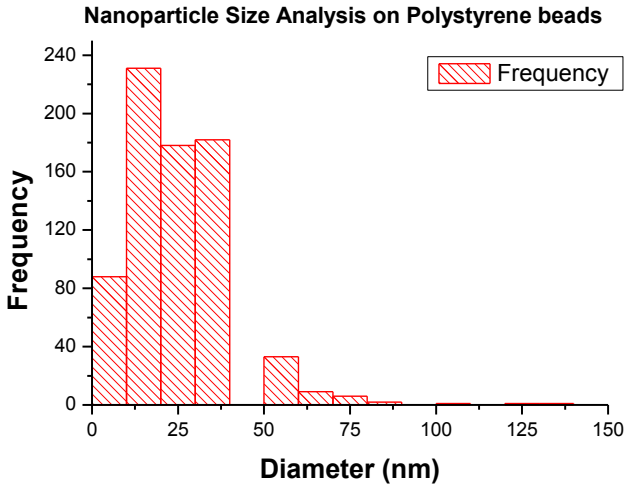

Figure II-23.Particle size analysis of gold nanoparticles on the surface of a PS bead. The average diameter was calculated to be 24.74 nm with a standard deviation of 14.36 nm (N = 729)

H. Preparation of Fluorescent Liposomes

Unilamellar liposomes were prepared by thin layer evaporation followed by polycarbonate membrane extrusion.[102] DOPC powder prepared in chloroform (25 mg/ml) was mixed in a vial with aliquots of DiD in ethanol and PEG-PE (200 mg/ml) to get a final molar ratio of 1:1592:270 DiD: DOPC: PEG-PE. The sample vial was then

rotated and dried under nitrogen to form a thin film layer. After that the lipid film was hydrated to a final concentration of 20mM lipids using PBS (0.01 M, pH = 7.01) .The obtained lipid suspension was vortexed for 1 minute and then extruded 20 times through 100nm pore size polycarbonate membrane, using an Avanti's mini-extruder.

1. Number of DOPC Lipid Molecules per Liposome [103]

The surface area is defined as $4\pi r^2$, so for a typical liposome of 1 lipid layer with a radius of 50nm it will be $4\pi(50\ nm)^2 = 31416\ nm^2$. Considering that a DOPC lipid headgroup has an area of 0.82 nm^2 and that two lipid layers would form a liposome,[104] then the number of lipid molecules per liposome should be

$$= \left(\frac{2\ \times\ surface\ area\ of\ liposome}{area\ of\ DOPC\ lipid\ headgroup}\right)$$

$$= \left(\frac{2\ \times\ 31416\ nm^2}{0.82\ nm^2}\right)$$

$= 76624$ DOPC lipid molecule/ liposome

2. Number of DiD Dyes per Liposome

The molar ratio of DiD:DOPC as prepared is 1:1592 therefore the number of DiD dyes per liposome is equal

$$(total\ number\ of\ lipid\ molecules\ per\ liposome)\ \times (ratio\ of\ DiD{:}\ DOPC)$$

$$= 76624\ \times \left(\frac{1}{1592}\right)$$

$= 48$ DiD molecule/ liposome

The distance between two DiD dyes on a liposome is

$$= 2 \times Radius\ of\ a\ DiD\ sphere$$

$$= 2 \times \sqrt{\frac{surface\ area\ of\ liposome}{number\ of\ Dyes \times \pi}}$$

$$= 2 \times \sqrt{\frac{2 \times 31416\ nm^2}{48 \times \pi}}$$

$$= 40.8\ nm$$

3. Number of PEG-PE per Liposome

The molar ratio of PEG-PE: DOPC is 1:6.1, thus the number of PEG-PE per liposome is:

$$= (total\ number\ of\ lipid\ molecules\ per\ liposome) \times (ratio\ of\ PEGPE{:}DOPC)$$

$$= 76624 \times \left(\frac{1}{6.1}\right)$$

$= 12561$ PEG-PE molecule/ liposome

I. Preparation of Biotinylated Fluorescent Liposome

Unilamellar biotinylated liposomes were prepared using a slight modification of the protocol described above. Briefly DOPC powder prepared in chloroform (25 mg/ml) was mixed in a vial with aliquots of DiD in ethanol and biotinyl-PE (50 mg/ml) to get a final molar ratio of 1:3180:252 DiD: DOPC: Biotinyl-PE. The rest of the preparation is exactly the same as before.

1. Number of DOPC Lipid Molecules per Biotinylated Liposome

This number is 76624, calculated as in sectionCHAPTER IIH.1.

2. Number of DiD Dyes per Biotinylated Liposome

The molar ratio of DiD:DOPC as prepared is 1:3180 therefore using the same calculations as before, the number of DiD dyes per liposome is equal 24 and the distance between two DiD dyes on a liposome is 58 nm.

3. Number of Boitinyl-PE per Liposome

The molar ratio of Biotinyl-PE: DOPC is 1:12.6, thus the number of Biotinyl-PE per liposome is

$$= (total\ number\ of\ lipid\ molecules\ per\ liposome) \times (ratio\ of\ BiotinylPE{:}DOPC)$$

$$= 76624 \times \left(\frac{1}{12.6}\right)$$

$= 6080$ Biotinyl-PE molecule/ liposome

J. TBI Fluorescent Scheme:

Inspired by the use of ELISA, we aimed at developing a sandwich assay that allows us to detect clinically relevant concentrations of the biomarker (1 ng/mL). In this sensing scheme, we tried three approaches on the basis of the use of different fluorescent tags.

The general scheme includes:

1. Preparation of DSP SAM

Gold coated polystyrene beads (PS-Au) were incubated with DSP (1 mM) for 30 min at room temperature to allow for the formation of a SAM. Next, the beads were freed from excess DSP by centrifugation at 900 rpm for 9 min and then re-dispersed in PBS buffer.

2. Attachment of Capturing Antibodies

The DSP modified PS-Au beads were incubated with primary 1 anti-S100B antibodies (10 µg/mL) for 30 min at room temperature to prepare the capturing antibody layer (Figure III-9.1).

3. Blocking Any Non-specific Binding Site

Ethanolamine (1M, pH 8.1) was added to the beads mixture for 15 min followed by the addition of BSA (1 mg/mL) for another 15 min to ensure all the residual reacting sites are blocked. The beads were then purified from the unbounded antibodies, BSA and ethanolamine by repeated centrifugation and redispersion cycles.

4. Attachment of the Antigen

S100B antigen of desired concentration was added to the antibody modified beads (Figure III-9.2) for 1 hour at room temperature and then the unbound antigen was removed by centrifugation again.

5. Attachment of Detecting Antibodies

The antigen modified beads were incubated for 1 hour at room temperature with primary 2 anti-S100B antibodies (10 µg/mL) that bind different S100B epitope (Figure III-9.3). Hence the sandwich is formed; that is the antigen is stuck between two antibodies. The unbounded antibodies were then removed by centrifugation.

6. Attachment of Biotin Labeled Secondary Antibodies

Biotinylated secondary antibodies (10 µg/mL) that can specifically bind to the antibody's Fc region (non-specific) of the detecting anti-S100B antibodies (Figure III-9.4) were applied to the beads mixture for 30 minutes followed by a centrifugation step to remove the unbound conjugates from the system.

7. Coupling of the Fluorphore

The difference in the schemes corresponds to the use of 3 different fluorescent tags that will be discussed later. However, in all of them we used the streptavidin-biotin interaction illustrated below (Figure II-24) to couple the fluorophore to the sandwich assay. Streptavidin can bind up to four biotin molecules and thus serves as a bridge to combine several biotinylated parts in the surface layer.

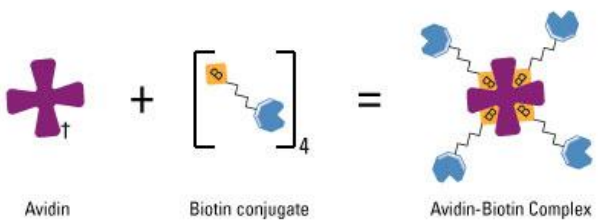

Figure II-24.Schematic of the avidin-biotin interaction. Avidin, streptavidin or NeutrAvidin Protein can bind up to four biotin molecules, which are normally

conjugated to an enzyme, antibody or target protein to form an avidin-biotin complex. Adapted from https://www.thermofisher.com/lb/en/home/life-science/protein-biology/protein-biology-learning-center/protein-biology-resource-library/pierce-protein-methods/avidin-biotin-interaction.html

K. DNA sensing Protocol

1. DNA Assembly Onto the Fluorescent Liposomes

Labeled liposomes were incubated with cholesterol-functionalized DNA probes as optimized in CHAPTER IVB.3 in a 1:1000 DNA: DOPC molar ratio for 30 minutes at room temperature.

a. Number of HVB-P2 DNA per liposome:

The molar ratio of DNA: DOPC is 1:1000 therefore the number of DNA probes per liposome is

$= (total\ number\ of\ lipid\ molecules\ per\ liposome) \times\ (ratio\ of\ DNA{:}DOPC)$

$= 76624\ \times \left(\frac{1}{1000}\right)$

$=$ 77 HVB-P2 / liposome

2. DNA-cleaving

To avoid lowering the efficiency of immobilization induced by the formation of DNA dimers, disulfide functionality on the oligonucleotides was cleaved by incubation with DTT (1:33 DNA: DTT mole ratio) for one hour. The mechanism of the reduction of the disulfide bond by DTT is illustrated in Figure II-25 whereby it involves two sequential thiol-disulfide exchange reactions with the formation of a DTT ring (oxidized form). The cleaved oligonucleotides were then purified and separated from

DTT and small thiolated alkanes by size exclusion chromatography using Microspin G-25 columns and centrifugation at 2360 rpm for 2 minutes.

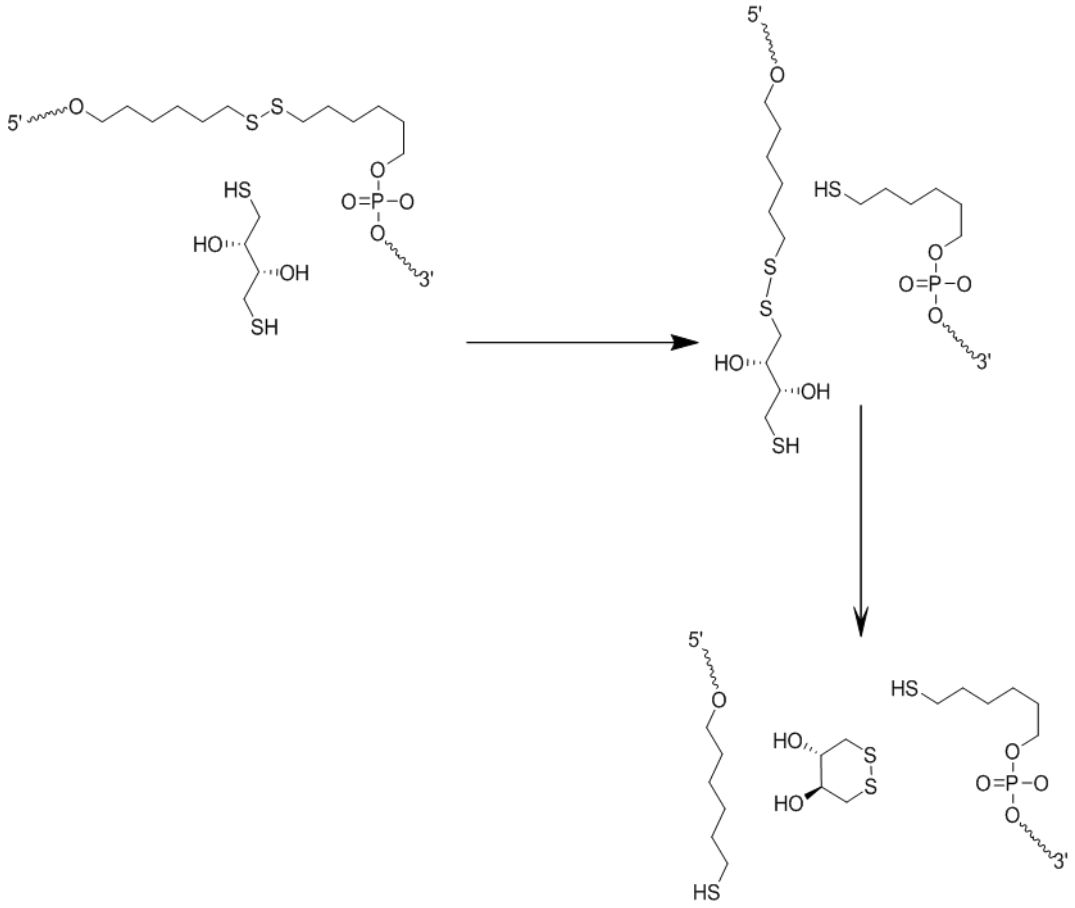

Figure II-25.DNA cleavage by DTT via two sequential thiol-disulfide exchange reactions.

3. DNA Assembly Onto Gold-coated Polystyrene Beads (PS-Au)

Cleaved DNA probes were directly immobilized onto the surface of PS-Au beads by a slight modification of a previously reported salting procedure. [105] Mirkin *et al.* used incremental additions of NaCl (2M) to increase the salt concentration of the mixture of gold nanoparticles and oligonucleotides to 1 M followed by an overnight incubation. However, in our case the salting time was reduced to less than 2 hours

whereby the desired probe concentration was mixed with PS-Au bead solution in PBS (0.01M, pH=7.01) followed by incremental additions of NaCl (4M) every 15 minutes for one hour to reach a final concentration of 0.6M . This was done to prevent the electrostatic repulsions between DNA strands and thus ensuring the stability of oligonucleotides on the beads' surface. Afterwards, the beads mixture was incubated at room temperature for around 15 minutes to assure that assembly took place .Excess oligonucleotides were then removed by centrifugation at 900 rpm for 9 minutes and the supernatantwas replaced by TEbuffer (5 mM Tris-HCl, pH 7.5, 1 mMethylenediaminetetraacetic acid (EDTA), and 0.5 M NaCl, pH=7.01) to enhance the hybridization efficiency.[106]

4. DNA Hybridization

Functionalized liposomes and desired target concentrations were added to the functionalized beads mixture and left for 30 minutes. After that the beads mixture was centrifuged at 900 rpm for 9 minutes, isolated and redispersed in 500 µL PBS(0.01 M, pH = 7).

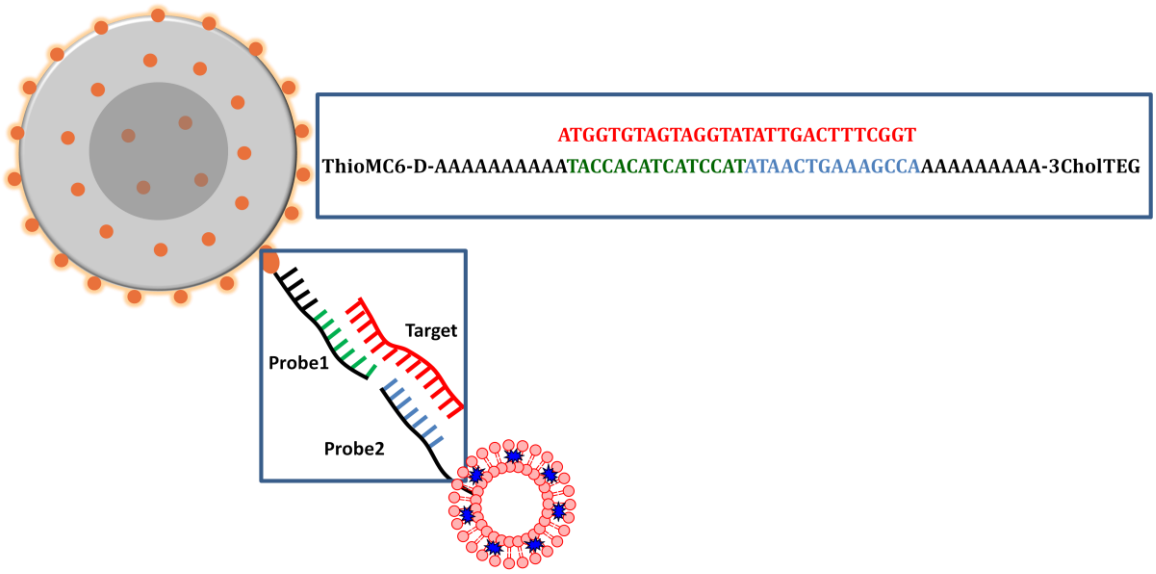

Figure II-26.The hybridization scheme between HVB-P2 functionalizedDiD liposomes, HVB-P1 and HVB-T

5. Flow Cytometry Sample Preparation

To avoid clogging of the used nozzle, the mixture was diluted to a ratio of 0.2 (200/1000 µL) with PBS (0.01 M, pH = 7).

CHAPTER III

TRAUMATIC BRAIN INJURY

A. Introduction

TBI represents a global health concern affecting both civilians and military personnel during times of peace or war. Statistically, around 2 million cases of TBI are reported annually in USA costing directly and indirectly a total of $ 76.3 billion per year. [107] Of these, more than 50,000 patients die and 80,000 sustain permanent disabilities. Nevertheless, it is estimated that TBI will be the leading cause of death and disability by year 2020 with over than 10 million cases. [108] The majority of TBIs result in diffuse and complex pathologies that progress over time causing neural damage that might not be reversible, yet the ability to accurately diagnose and monitor TBI is still lacking. This creates a need for identifying biomarkers capable of reflecting core elements of the severity, pathophysiology and pathotrajectory process of TBI. [109] Depending on the type and severity of the injury, different cellular pathways are activated releasing hundreds of characteristic molecular products. [110] The current diagnostic immunoassay platforms such as enzyme linked immunosorbent assay (ELISA), under best performance, have an average detection limit of few nanograms (ng/mL). [111] As such, developing a robust, simple to use and sensitive platform to accurately diagnose and monitor TBIs is highly admirable in brain injury studies. Furthermore, there is no existing point-of-care (POC) device that can detect TBI biomarkers in human biofluid such as CSF and blood.

In response to the needs presented above, the objective of this chapter is to build up an ultrasensitive and specific sensing scheme to detect a well characterized TBI

biomarker (S100B). The assay will be based on two different methods, electrochemical and fluorescence. However, in both cases we are only interested in qualitative and not quantitative testing of the S100B biomarker. The experimental procedures were all detailed in the previous chapter and so this chapter will only include the results and discussion of the proposed strategies.

B. Results and Discussion

1. Electrochemical Scheme

a. Self-Assembled Monolayers (SAMs)

In order to obtain a highly sensitive sensing surface of an immunosensor, the immobilized binding partner must be necessarily presented to its corresponding ligand so that they can bind without any steric hindrances. [112] This becomes more important particularly when antibodies are the ones attached to the solid support. Antibodies usually lose a part of their binding capability if they are randomly oriented on the surface (Figure III-1) .[113] [114] As such, the anchoring of the biocomponent should be constructed in a convenient way. Self assembled monolayers (SAMs) that spontaneously form from thiolated amphiphilic compounds in contact with gold offer several advantages over other approaches in terms of high reproducibility, accurate positioning of the bioreceptor on the surface of the transducer and proximity to its surface and thereby can be used in a miniaturized biosensor with a comparable size of a microelectronic device.[115] [116] In this work, we used DSP to crosslink the gold and antibodies as it is a homobifunctional N-hydroxysuccinimide (NHS) ester that can form a SAM on the gold electrode surface due to its disulphide group.[117] The NHS group tends to couple primary amines as principle targets and hence it is widely used for

linking proteins through their terminal amines to gold surface.[118] [119] Under a suitable pH range (7-9), the succinimidyl ester of DSP, a very good leaving group, is replaced by the electron donating primary amines so that an amide bond is formed between DSP and the antibodies. Indeed, building a DSP SAM is much more advantageous over other conventional methods. It allows the covalent attachment of antibodies to the gold surface without requiring any chemical activation step. In addition, its short height (12 or 8 atoms) makes the binding antibody-antigen pair in proximity to the sensing electrode which allows the direct electron/charge transfer from redox centers resulting in a more sensitive detection of the binding event.[120] [121]

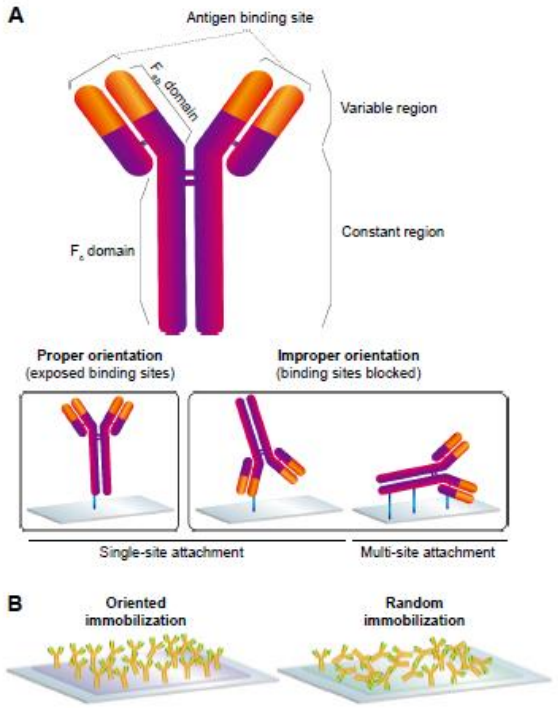

Figure III-1. Schematic illustration of IgG different surface orientations (A) Typical structure of an antibody and its oriented positions that can affect binding affinity .(B) Scheme of the different types of immobilization of antibodies. Abbreviations: IgG, immunoglobulin G; Fab, fragment antigen-binding; Fc, fragment crystallizable. Reprinted with permission from Jeong *et al.* [122]

i Cross Linker Time Optimization

Crosslinking time is a critical issue in the preparation of the SAM. Extensive cross linking leads to the formation of large protein aggregates that will decrease the detection sensitivity. To determine the minimum time required to get a consistent DSP monolayer, an optimization experiment was performed initially. The experiment was conducted spectroscopically rather than electrochemically given the nature of DSP which makes it difficult to detect using electrochemical methods. Gold nanoparticles were incubated with 1mM DSP solution in DMF at room temperature and the absorption spectrum was then monitored using UV-Vis spectroscopy. As shown in Figure III-2, the gold nanoparticles absorbance spectrum shifts from having its maximum at 522 nm to a longer wavelength in the first 30 min of incubation whereby it becomes stable at 528 nm no matter how long the time of incubation increases. This indicates that only half an hour is needed to ensure an optimal and unvarying DSP SAM formation prior to any antibody functionalization setup. The 6 nm red shift is by the increased refractive index near the nanoparticle surface due to the presence of DSP molecules. [123]

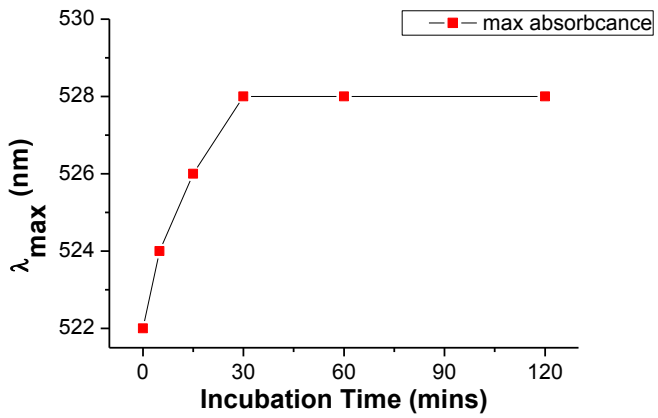

Figure III-2. Kinetics of the DSP SAM formation. Colloidal gold nanoparticles were incubated with 1mM DSP in DMF at room temperature. As the incubation time

increases, the nanoparticle aborbance spectrum shifts to a longer wavelength until it reaches a steady state at 528 nm after 30 minutes indicating the formation of an unvarying DSP SAM.

b. Electrochemical Characteristic of Different Electrodes

In our study, we aimed at developing a direct electrochemical immunoassay to detect S100B antigen on the basis of monitoring the faradaic current generated by a small redox active group before and after the antigen–antibody interaction. Among the various electrochemical techniques, we elected to utilize differential pulse voltammetry (DPV) due to its ability to minimize the charging current and extract only the faradaic one and thus ensuring the analysis of electrode reactions with high precision and sensitivity. DPV uses a series of increasing small amplitude potential pulses whereby the current is measured just before and near the end of each pulse allowing time for the decay of the non-faradaic current. [124]

In fact, when we monitored the currents generated by $Fe(CN_6)^{4-}$ at each time point, we noticed a clear correlation between the presence of analytes and the decrease of the peak current. In other words, the current of the bare electrode is attenuated more and more after each modification step (Figure II-16). This attenuation is attributed to the obstruction of the access of the molecular reporter to the gold surface efficiently and thus hindering its electron transfer reaction.

At first, we tested our sensing scheme using the regular gold electrodes. As shown in Figure III-3, the achieved sensitivity was a low one (21%) even when using the highest concentration of antigens (10 µg/mL). Therefore, in the rest of the experiments only gold micro-electrodes will be utilized because we want to decrease the background current which decreases as we decrease the electrode size.

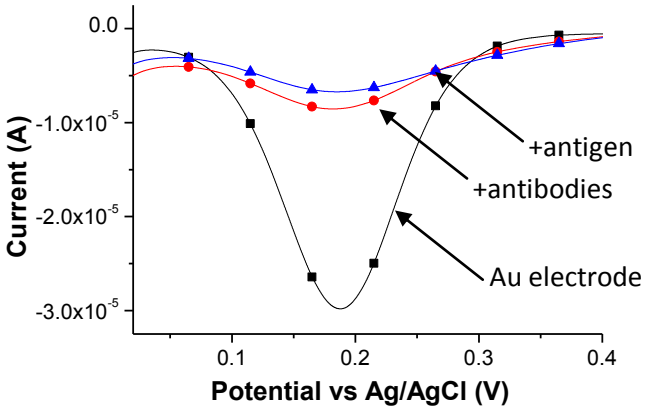

Figure III-3. DPV showing signal attenuation after each modification of a standard 2mm gold electrode. 10µg/mL of anti-S100B antibodies was applied to the surface of the gold electrode for 30minutes. 10µg/mL of S100B antigen was applied to the antibody modified gold electrode for 1 hour. The signal change corresponding to the antigen-antibody interaction is$\Delta I\% = 21\%$.

Next, we wanted to examine how the sensor footprint affects the sensitivity of the antigen detection. As such, three different structures were made by manipulating the electrodeposition conditions (Figure II-13) and their responses to the 1µg/mL S100B concentration were evaluated (Figure III-4). We observed that the sensitivity increased as the size of the sensor decreased. Indeed, the smallest sensor allowed the detection of around 10 times lower signal changes than the largest sensor and 5 times than the intermediate one. As the analyte concentration decreases, we would expect fewer antibody binding sites to be filled. These binding sites represent a larger fraction of the total sensor area and therefore a larger signal change is observed with the smallest sensor. This reflects that the smallest sensor has the best signal-to-noise ratio which allows for an improved sensitivity. Henceforth, all sensing experiments will be conducted using the smallest microelectrode size.

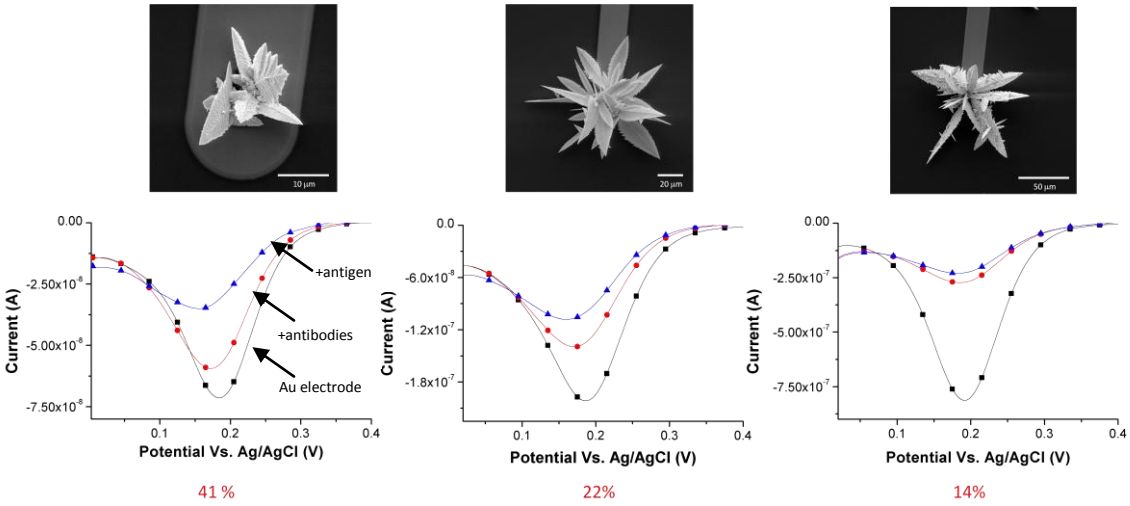

Figure III-4. Electrochemical behavior of three differently sized sensors showing signal attenuation after each modification step, small (left), intermediate (middle) large (right). In all cases, 10µg/mL of anti-S100B antibodies was applied to the surface of the gold electrode for 30minutes after which 1µg/mL of S100B antigen was applied to the antibody modified gold electrode for 1 hour. The best sensitivity was achieved using the smallest sensor .The signal changes corresponding to the antigen-antibody interactions are$\Delta I\% = 41\%$,$\Delta I\% = 22\%$ and $\Delta I\% = 14\%$ for the small, intermediate and large sized sensors respectively.

c. Antibody Concentration Optimization

While we were trying to detect decreased concentrations of the antigen, the signal change started to diminish at 10 ng/mL and below. Given that the antibodies are in much excess at these antigen concentrations, we decreased the antibodies concentration from 10 µg/mL to 1 µg/mL to allow for a more exposed gold surface and therefore we can observe a clearer signal change for the antigen-antibody interaction. Figure III-5 shows that the sensitivity at analyte concentration of 10 ng/mL increases considerably from only 6% in the case of 10 µg/mL antibodies concentration to 52% in the case of 1 µg/mL. Therefore we decided to stick to the 1 µg/mL in further electrochemical experiments.

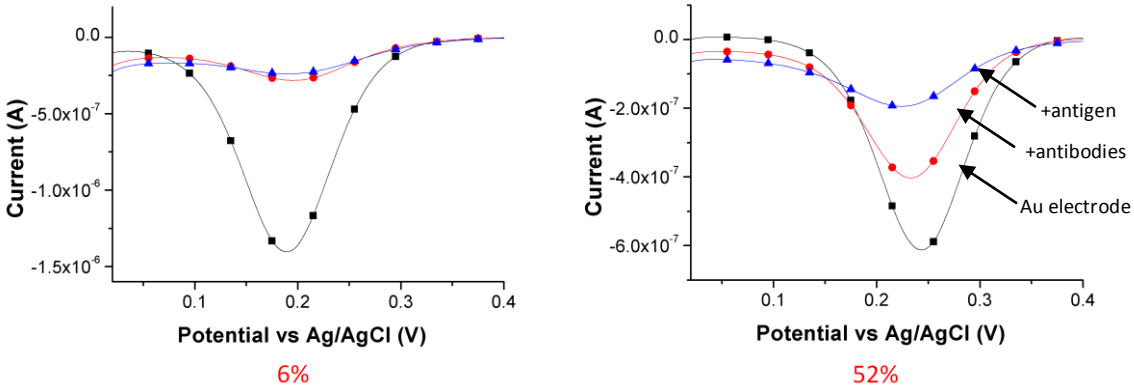

Figure III-5.DPV showing signal attenuation after each modification of a 10µm gold microelectrode. In both cases 10 ng/mL of S100B antigen was applied to the antibody modified gold electrode for 1 hour. Left, using 10 µg/mL of anti-S100B antibodies concentration ΔI% obtained was 6%. Right, using 1µg/mL of anti-S100B antibodies concentration ΔI% obtained was 52%.

d. S100B Detection

Using the immunosensor with 1 µg/mL antibodies concentration, detection of 1ng/mL, 100 pg/mL and 10 pg/mL was attempted. As Figure III-6 illustrates, even the lowest antigen concentration (10 pg/mL) was detectable with a sensitivity of 27%. This is already 100 times lower than the concentration that we wanted to detect (1 ng/mL). Therefore, we decided to stop at this limit and challenge our system with different fluids to check if it could be utilized in clinical applications.

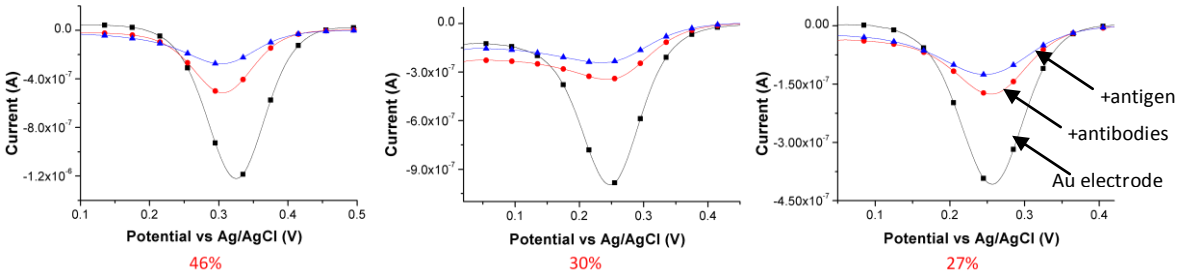

Figure III-6. DPV showing signal attenuation after each modification of a 10µm gold microelectrode with different antigen concentrations. For each case, 1µg/mL of anti-

S100B antibodies was applied to the surface of the gold electrode for 30 min. The antigen concentration used was 1ng/mL (left); $\Delta I\% = 46\%$, 100 pg/mL (middle); $\Delta I\% = 30\%$, 10pg/mL (right); $\Delta I\% = 27\%$.

e. Negative Control

Despite that "signal-off" approaches are sometimes problematic due to the risk of false positives, our chip-based scheme mitigates this risk because it allows the simultaneous measurements of a negative control and the designated samples. As shown in Figure III-7, the addition of buffer instead of antigen doesn't induce any change in the peak current of antibody modified electrode. This confirms that any signal-change is specific for the antigen-antibody binding event only.

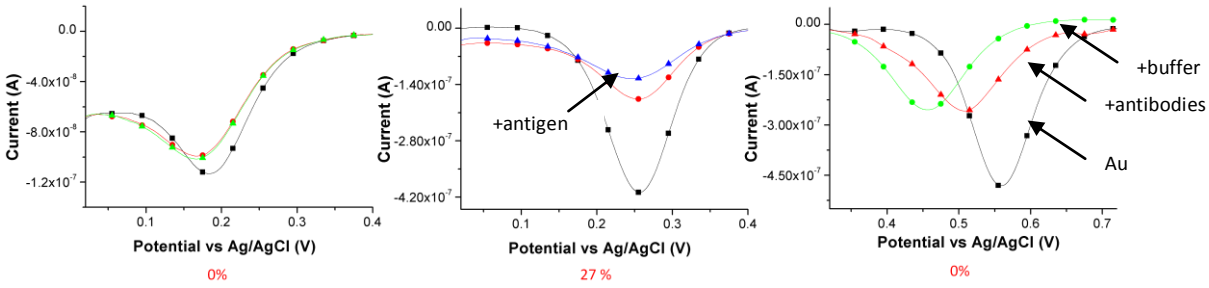

Figure III-7. DPV showing the electrochemical behavior of a 10µm gold microsensor. Left , negative control showing no signal changes. Right, another negative control with no signal change but with a shift caused by the reference electrode. Middle, positive control (10ng/mL) showing $\Delta I\% = 27\%$.

f. Serum Testing

To examine if the detection system is applicable with biological fluids, a standard gold electrode was incubated with serum replacement (1x) for half an hour after which a DPV measurement was taken. Serum is an extremely complex biological fluid containing enormous amount of proteins and other interfering molecules. Unfortunately this complex fluid gave a false positive attenuation of the peak current

caused by the nonspecific attachment of its proteins to the gold surface (Figure III-8). This means that our proposed system performance is clinically-irrelevant and hence is only applicable for lab testing with clean buffers or on a purified serum sample which defies the main objective of this work.

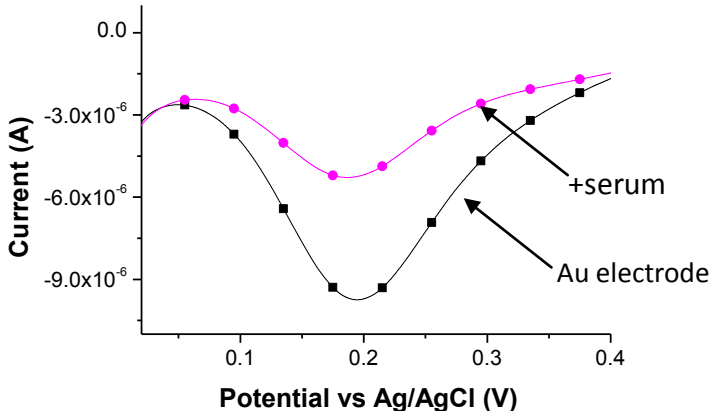

Figure III-8.DPV showing the change of current with serum. $\Delta I\% = 14\%$

g. Inferences

Herein we have described an electrochemical immunosensor for label-free detection of low levels of S100B, a well characterized TBI biomarker. Using sensors of different sizes, we showed that small surface area sensors are better for ultrasensitive protein detection and achieving high sensitivities. This chip-based scheme allowed the determination of targets in the pg/mL range. This sensitivity is better than that of common detection methods for S100B such as ELISA(5ng/mL), Immunoluminometric (110 pg/mL) and Immunoradiometric assays (20pg/mL) .[125] However this method was shown to be effective only with purified samples. This means that it couldn't be implemented in a POC device and hence we shifted our aim towards developing an alternative method capable of detecting TBI biomarkers with higher specificity. In the

next parts of this chapter, we will be describing a fluorescent approach using gold modified polystyrene microbeads so that we can utilize the same modification procedures.

2. Fluorescent Scheme

The use of a sandwich assay offers the advantage of a high specificity because two antibodies are binding to the same antigen ensuring that it is specifically captured and detected. Nevertheless, the immobilization of the capturing antibody lessens the effect of nonspecific adsorption of any protein to the surface. Without this layer, any protein found in the system might competitively adsorb to the surface decreasing the amount of immobilized antigen.[126] Moreover using purified antibodies to detect a specific antigen eliminates the need for further purification steps and thus ensuring a high sensitivity with a simplified assay.[127] On the other hand, the visualization depends on the ability of the fluorophore used to reflect the amount of captured antigen.

a. Use of Alexa Fluor 647 Tag

Because Streptavidin-based detection techniques are commonly used in flow cytometry, we first tested our sensing scheme using Alexa Fluor 647 (AF 647) as a fluorphore (Figure III-9). In a typical experiment, steps 1-6 were done as described above for 3 samples of different antigen concentrations (10 µg/mL, 1 µg/mL and 0.1 µg/mL) and a blank (no antigen) and then 0.5 µl of AF 647 (2 mg/ml) was added to each mixture for 15minutes followed by multiple centrifugation and redispersion cycles. The relative fluorescent intensities were then recorded using flowcytometry and compared to the blank. Results (Figure III-10) showed that the sensitivity (fluorescence

shift) decreases as the target concentration decreases whereby the shift appears to be statistically irrelevant at a concentration of 0.1 µg/mL. This means that the proposed system is still far away from our targeted limit of detection. In fact, AF 647 contains 6 to 9 dye molecules per one streptavidin [128] so we speculated that if we use an alternative fluorescent tag that contains a greater number of dye molecules, we can improve the detection limit up to our prospects.

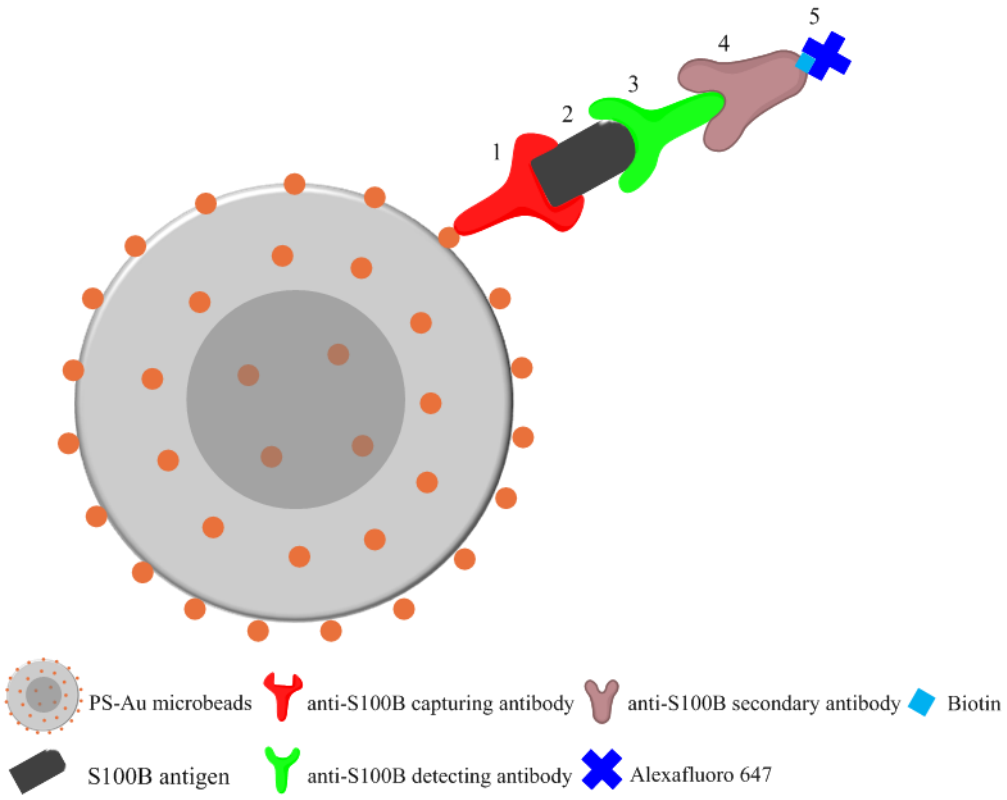

Figure III-9. Schematic illustration showing the sandwich assay with the use of AF 647 tag.

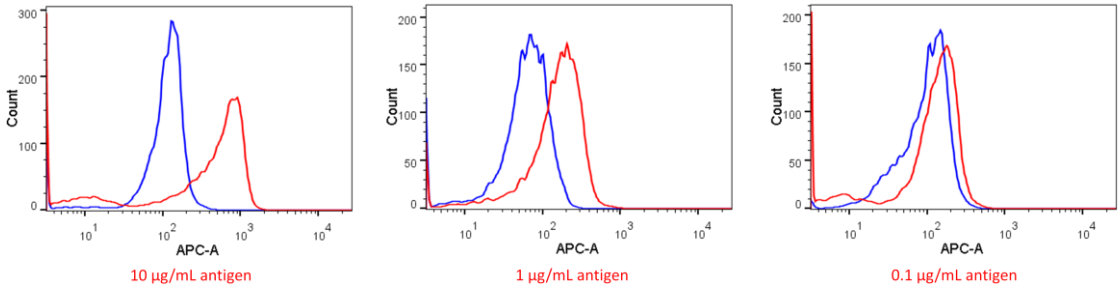

Figure III-10. Flow cytometry measurements for different S100B concentrations. The blue and red lines represent the blank and sample responses respectively. The experiment was done at room temperature with 10µg/mL anti-S100B capturing antibodies, 10µg/mL anti-S100B detecting antibodies, 10µg/mL anti-S100B secondary antibodies and 0.5µL of AF 647 (2mg/ml).

b. Use of FITC-SNP

Fluorescein derivatives are the most used fluorescent labels in biological applications due to their high extinction coefficients and excellent fluorescence quantum yield.[129 130] As such, in an attempt to enhance the sensitivity, we decided on coupling biotinylated FITC-SNP to the sandwich assay as we can incorporate a huge number of FITC dyes per silica particle.[91] In this experiment, a sample of 100 ng/mL antigen concentration and a blank were prepared by following the protocol described above with a slight modification in step 7 corresponding to the use of unlabeled streptavidin for bridging the biotinylated FITC-SNP and the sandwich assay (Figure III-11). 0.5 µl of unlabeled streptavidin was added to the beads for 15 min followed by multiple centrifugation and redispersion cycles and then biotinylated FITC-SNP were added for another 15 min after which the beads were washed again prior to the flowcytometric measurements. Unfortunately as can be shown from Figure III-12, the use of FITC-SNP didn't enhance the sensitivity as the signal change is very similar to that in the case of labeled streptavidin. Therefore, this was statistically unsatisfying too. We argued that

the antigen might be adsorbing on the SiO_2 nonspecifically which might account for the low sensitivity of the assay. Hence we opted to use fluorescent liposomes as another substitute.

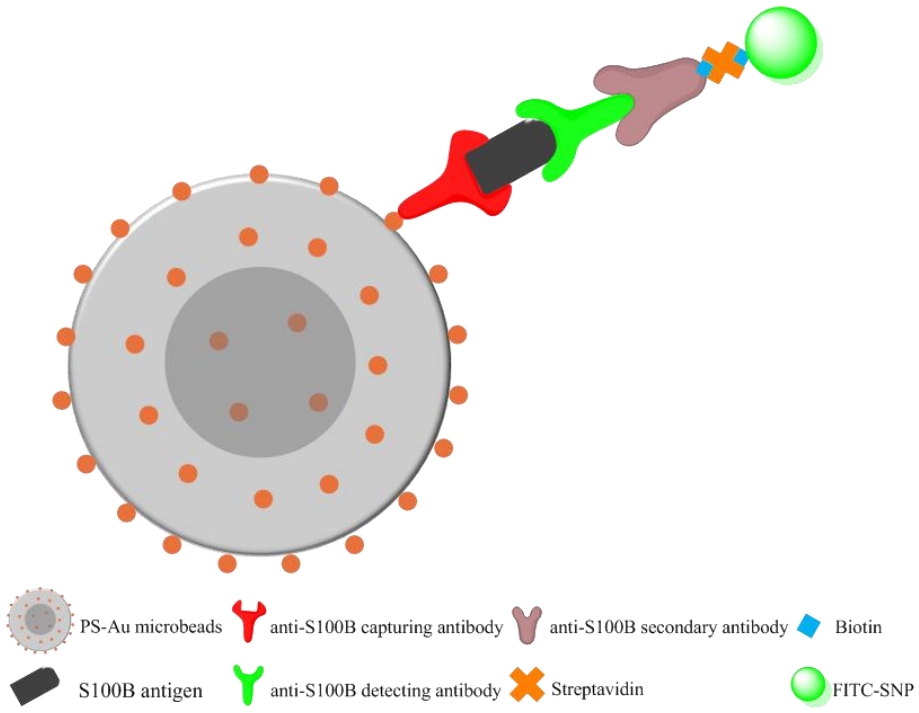

Figure III-11.Schematic illustration showing the sandwich assay with the use of FITC-SNP tag.

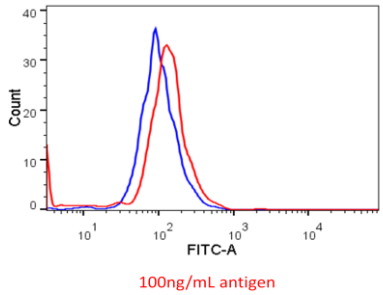

Figure III-12. Flow cytometry measurement for 100 ng/mL S100B concentration. The blue and red lines represent the blank and sample responses respectively. The experiment was done at room temperature with 10 µg/mL anti-S100B capturing

antibodies, 10 µg/mL anti-S100B detecting antibodies and 10 µg/mL anti-S100B secondary antibodies.

c. Use of Biotinylated DiD Liposomes

Liposomes offer the advantage of incorporating many fluorophores together. This means that fluorescent intensity could be significantly enhanced. As such, we decided on embedding DiD dyes inside the hydrophobic membrane of biotin functionalized DOPC liposomes and test whether coupling these liposomes to the sandwich assay would improve the system's sensitivity (Figure III-13). Again unlabeled streptavidin was used to bridge the sandwich assay and the fluorescent liposomes with the same incubation and washing steps that were done to the FITC-SNP case. Here, samples of decreasing concentrations (100 ng/mL, 10 ng/mL and 1 ng/mL) were tested and compared to a blank. As can be seen from Figure III-14, our system was able to get to the 1 ng/mL limit and significantly detect higher concentrations. In fact if we compare the sensitivities of the three approaches (Figure III-15), we see that liposomes allowed signal amplification with respect to other methods resulting in a huge improvement of sensitivity and hence the detection of lower concentrations.

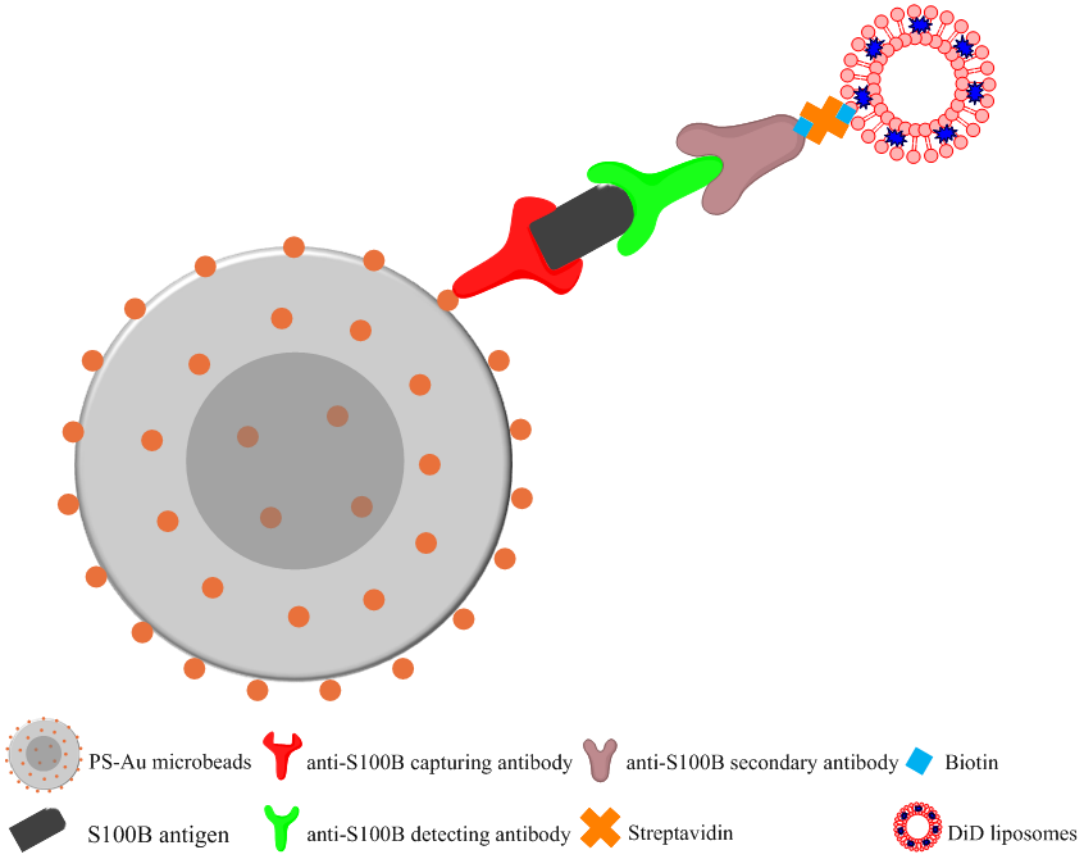

Figure III-13.Schematic illustration showing the sandwich assay with the use of DiD encapsulated liposomes.

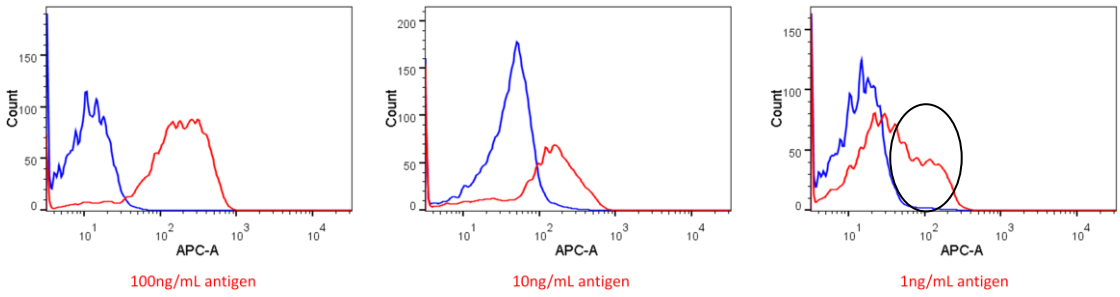

Figure III-14. Flow cytometry measurments for different S100B concentrations. The blue and red lines represent the blank and sample responses respectively. The exeperiment was done at room temperature with 10 µg/mL anti-S100B capturing antibodies, 10 µg/mL anti-S100B detecting antibodies, 10 µg/mL anti-S100B secondary antibodies and 5 µL DiD liposomes(1x).The highlighted area in the right graph corresponds to the fraction that is higher than the background.

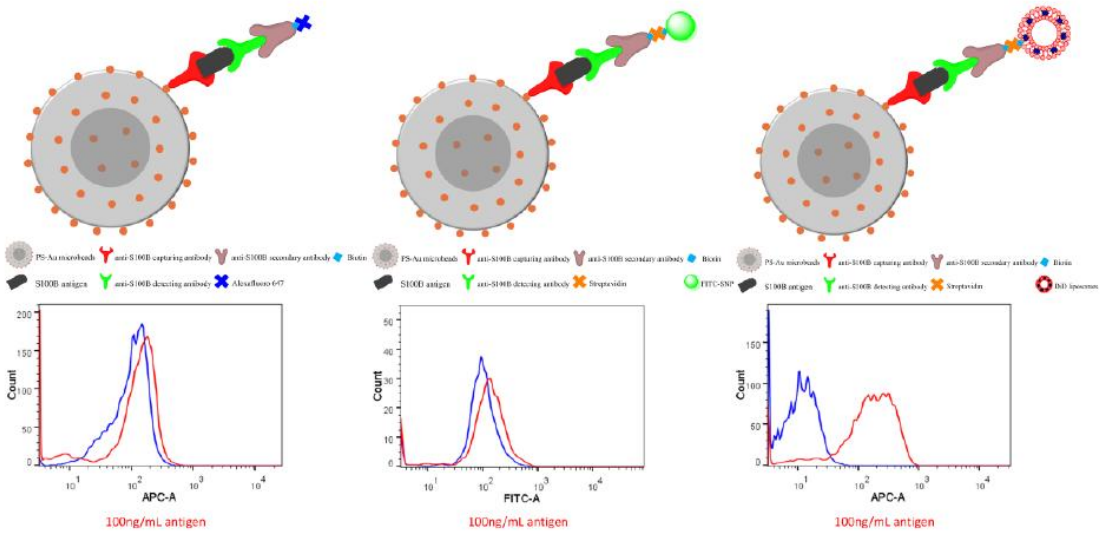

Figure III-15.Flow cytometry measurements for 100 ng/mL antigen concentration showing the different sensitivities using the three sensing schemes. The blue and red lines represent the blank and sample responses respectively.

d. Inferences:

In this fluorescent approach, the use of AF 647 or FITC-SNP didn't ensure a good sensitivity whereas the use of liposomes enhanced the intensities because it allowed the coupling of many fluorophores rather than just one.

Unfortunately, the project faced a major setback when the company producing the specific antibodies for the S100B discontinued the product. Producing the antibody in house is very expensive. This prevented us from further optimizing the sensitivity and tests the probe in serum samples.

C. Conclusion

In the electrochemical scheme, we developed an immunosensor on the surface of gold microelctrodes for simple and direct detection of S100B biomarkers based on

monitoring the peak current using differential pulse voltammetry (DPV). The use of succinimide ester as a crosslinker rather than glutaraldehyde, carbodiimide, Protein A etc... [9–11] offered the advantage of having a robust attachment of protein and easy surface modification. We examined the effect of different electrode sizes on the sensitivity as well as the application of complex biological fluids and we were able to detect very low concentrations (pg/mL range). Whereas in the fluorescent scheme, a sandwich assay coupled to a fluorphore was built on polystyrene gold coated microbeads (PS-Au) and visualized using flow cytometry. We tried to optimize our sensing scheme by using three different fluorescence tags. Combining the advantages of flow cytometry (very sensitive fluorescent-based method), nanostructured gold nanoparticles (easy surface modification) and fluorescently labeled liposomes (bright fluorescent tags), we succeeded in getting to the limit of a clinically relevant concentration (1ng/mL). This is comparable to those obtained without the use of expensive intensification protocols such as the rolling cycle amplification or polymerase chain reactions. Gervais *et al.* developed a fluorescent sandwiched immunoassay using capillary-driven microfluidics and PDMS substrates to detect protein biomarkers with a detection limit of 1ng/mL .[131] Sojka *et al.* also developed an immunoradiometric assay for the detection of S100B biomarkers with a detection limit of 1.8ng/mL.[132] Therefore, our sensing strategy, although not optimized yet, has a clear advantage regarding the low detection limit.

CHAPTER IV

DNA SENSING

A. Introduction

Building on the previous sensing, we aimed in this chapter at developing a multiplex sensing platform to detect trace amounts of short unique oligonucleotide sequences specific for *Bacillus Anthrax (*BA) and *Hepatitis B Virus* (HBV) using fluorescent methods. The assay was built on polystyrene-gold microbeads whereby a thiol modified DNA strand along with a cholesterol modified one were used to capture a target DNA sequence. The visualization was performed using flowcytometry with the aid of dye labeled liposomes. To improve the efficiency of our system, the different parameters were optimized separately before carrying statistical analysis and determining the limit of detection. Finally, we tested our sensing scheme for the ability to detect multiple DNA targets simultaneously. Accordingly this chapter includes the results and a detailed discussion of the DNA sensing protocol, statistical analysis and multiplexing experiment.

B. Results and Discussion

In order to get the best detection of our sensing system and carry out the statistical analysis and multiplexing, we first conducted optimization experiments for:

1- Surface probe concentration on the PS-Au microspheres

2- DNA probe- liposome composite concentration

3- DNA to DOPC ratio

4- Dye Concentration inside the liposomes

5- Hybridization buffer

6- Hybridization time

As well we tested the performance of our sensing scheme in a serum matrix.

1. Optimization of Surface Probe Concentration on the Gold-Coated Polystyrene Beads

Immobilization of the oligonucleotide probe is one of the most important aspects towards the development of a DNA biosensor. [27] The detection sensitivity is marked by the efficacy of capturing the target sequence by the surface oligonucleotides. This largely depends on the degree of DNA packing; high surface concentration renders the access to the target difficult due to steric hindrance while lower surface concentration result in collapsing of DNA probes and thus a lower chance of target catchment. To test for the best probe density at the surface of gold-coated polystyrene beads, we prepared five samples (10, 50, 100, 200 and 500 nM in probe solution concentrations) by mixing different amounts of HVB-P1 with the PS-Au beads. The five samples were then allowed to hybridize with a 1 nM HVB-T concentration and HVB-P2 functionalized DiD liposomes (1x dye concentration – 100 nM probe concentration) for 30 minutes after which flow cytometric measurements were carried out and compared to the blank sample. The later was prepared in the same manner but with no addition of targeted DNA. As shown in Figure IV-1, the fluorescent intensity increases as the concentration ofHVB-P1 decreases. This is attributed to having the oligonucleotides strands well separated on the surface of the PS-Au beads at a lower concentration which causes a lower degree of steric hindrance and therefore an improved sensitivity. Here we can see that in the case of 10, 50 and 100 nM

concentrations, the fluorescence enhancement is very similar. However, the 10nM concentration is optimal because oligonucleotides have a larger space between each strand resulting in a better packing of probes. This is in agreement with other reports such as those done by Georgiadis*et al.*[133]and Zhou *et al.* [134]who showed that a high probe concentration assembled onto the surface is needed to enhance sensitivity as it increases the chance of capturing target DNA but highly packed surfaces result in higher degree of steric hindrance and electrostatic repulsions and thus limiting the probe-target association (Figure IV-2). Hence, the 10nM probe concentration was adopted for the rest of experiments.

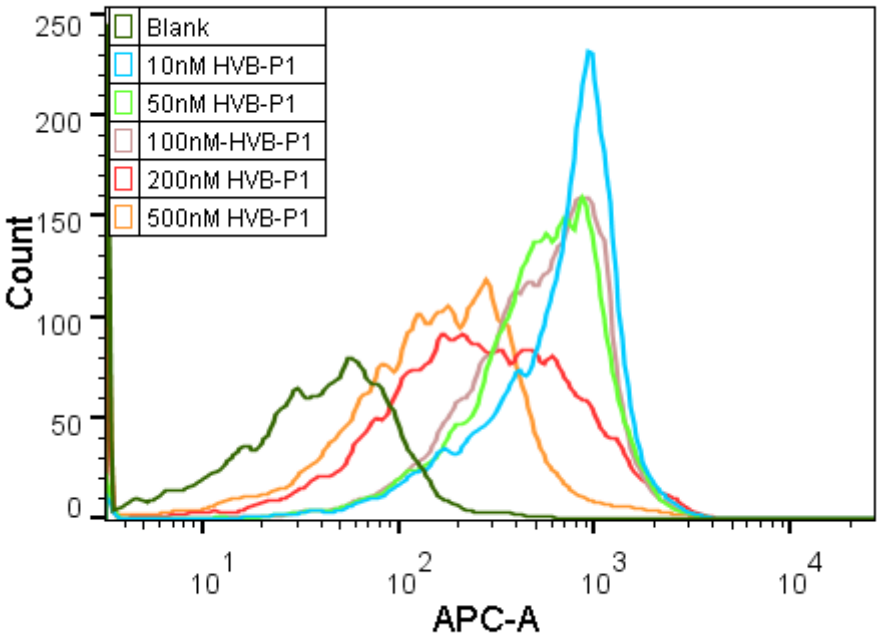

Figure IV-1. Flow cytometry measurements for 1nM HVB target with variations in HVB-P1 concentration. The experiment was done at room temperature with DiD liposomes (1x) functionalized by 100 nM HVB-P2, 10 mM PBS buffer (pH = 7.01), 0.6M NaCl, 3 mM Tris-HCl and 0.6 mM EDTA

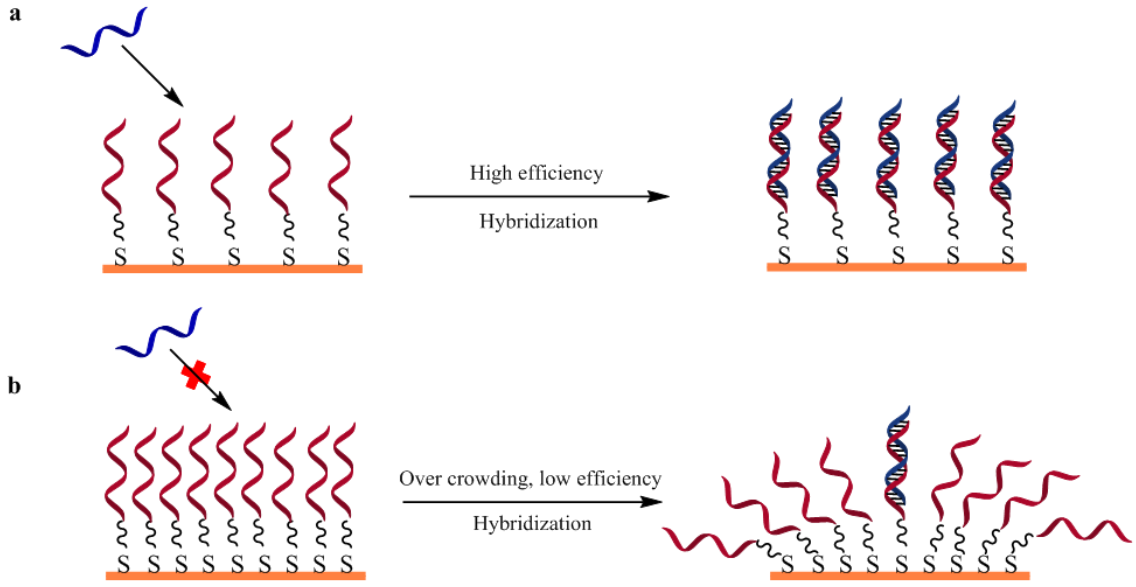

Figure IV-2. Schematic illustration of an upright conformation of DNA probes on a gold surface. a) Ideally packed DNA probes;the large interprobe distance allows for complete hybridization. b) Densely packed DNA recognition layer; the steric hindrance and electrostatic repulsion of probes result in poor hybridization efficiency.

2. Optimization of Solution Concentration of the Probe-Liposome Composite

Likewise to examine the best DNA probe solution concentration assembled onto the fluorescent liposomes, different aliquots of HVB-P2 functionalized DiD liposomes (1x) (1:1000 DNA: DOPC molar ratio) were added to different beads mixture to yield probe solution concentrations of (10, 50, 100, 200 and 500 nM) respectively and a blank (100 nM). After that, each sample was allowed to hybridize for 30 minutes with the 10 nM HVB-P1 functionalized PS-Au beads and 1 nM HVB-T concentration. Flow cytometric measurements were carried out then and compared to the blank sample. As shown in Figure IV-3, although we can still detect the 1nM HVB-T while using a low (10 nM) or a high (500 nM) HVB-P2 concentration, the use of 100 nM HVB-p2 concentration showed the best sensitivity with around 6 times greater fluorescence enhancement and thus it was chosen to be optimal. This could be attributed

to having over-crowding of the surface of PS-Au with higher composite number rendering a low efficiency of hybridization. Accordingly, the 100nM HVB-P2 solution concentration was used for the remaining sensing experiments.

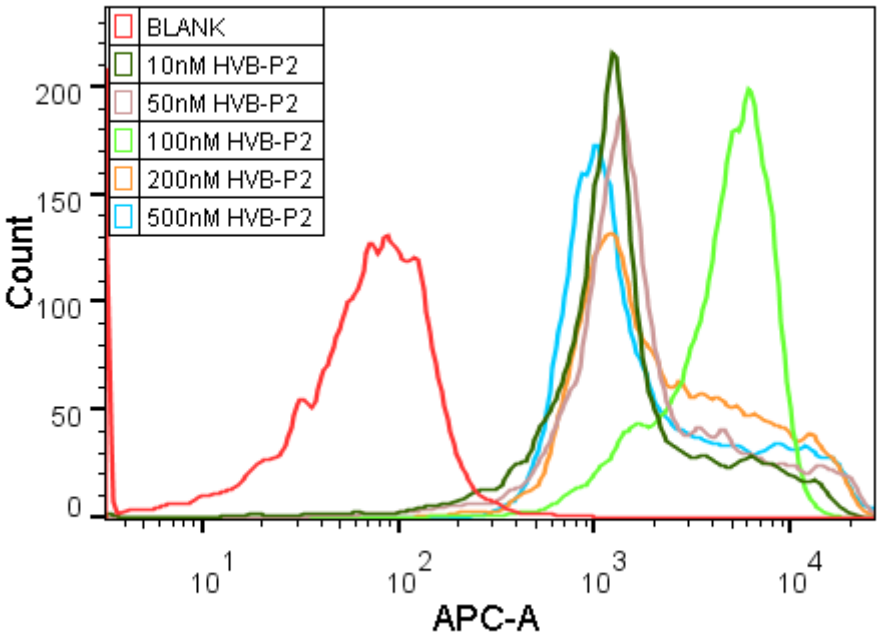

Figure IV-3.Flow cytometry measurements for 1nM HVB target with variations in HVB-P2 concentration. The experiment was done at room temperature with DiD liposomes (1x), 10 nM HVB-P1, 10 mM PBS buffer (pH = 7.01), 0.6 M NaCl, 3 mM Tris-HCl and 0.6 mMM EDTA

3. Optimization of DNA to DOPC Ratio

Moreover, to investigate the DNA to DOPC optimal molar ratio, samples of ratios (1:200, 1:400, 1:1000, 1:2000 and 1:14000) and a blank (1:1000) were prepared by mixing different amounts of DiD liposomes and HVB-P2 DNA and then the same amount of the five samples were allowed to hybridize with 10 nM HVB-P1 functionalized DiD liposomes and 1nM HVB-T concentration for 30 minutes. Results (Figure IV-4) showed that the sensitivity increases as the ratio of DNA to DOPC

decreases until reaching 1:1000 ratio whereby the sensitivity starts to decrease as the ratio decreases too. As a matter of fact, excess DNA results in having bulky surface of the lipid membrane and thus an increase in electrostatic repulsions among oligonucleotides while excess DOPC results in having an insufficient amount of immobilized DNA strands/ liposome and hence in both cases we observed a decrease in sensitivity. Nevertheless these two parameters are best balanced in the case of 1:1000 DNA: DOPC molar ratio which was chosen to be optimal.

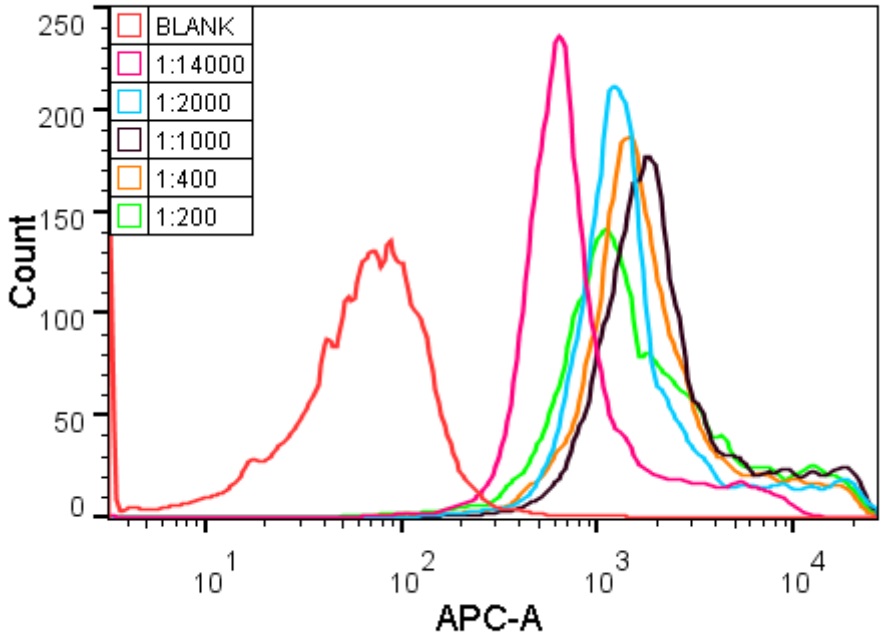

Figure IV-4.Flow cytometry measurements for 1nM HVB target with variations of DNA:DOPC ratio. The experiment was done at room temperature with DiD liposomes (1x), 10 nM HVB-P1, 10mM PBS buffer (pH = 7.01), 0.6 M NaCl, 3mM Tris-HCl and 0.6 mM EDTA

4. Optimization of Dye Concentration inside the Liposomes

The number of dye molecules which are incorporated inside liposomes is critical for the purpose of visualization. In order to test for the best signal amplification

and thus having the ultimate sensitivity, we examined the effect of dye concentration inside the liposomes on DNA detection. Three DiD liposomes (0.1x, 1x, 100x) with 1:15920, 1:1592 and 1:159 DiD to DOPC molar ratio respectively were prepared and mixed with 10µM HVB-P2 DNA each. Then they were allowed to hybridize with 100nM HVB-P1 functionalized PS-Au beads and 1nM HVB-T concentration. Flow cytometric results (Figure IV-5) showed that the sensitivity increases as the dye concentration inside the liposomes increases and thus the number of fluorescent molecules per probes-target association becomes higher. However, we need to avoid non-radiative decay such as Förster resonance energy transfer (FRET) which occurs at a certain distance (Förster radius) between dyes. The FRET efficiency is inversely proportional to the 6^{th} power of the radius; this means that it highly depends on the distance between the donor and acceptor.[135] Nonetheless, most of fluorophore pairs have their Förster radii within the range of 1-10nm. [136] Therefore in order to have the best fluorescence enhancement and to prevent self-quenching, the distance between the dyes needs to be greater than the Förster radius. In our case we aimed at having a reliable and cheap detection scheme knowing that the Förster distance of DiD is around 5nm. Thus we chose to work with the 1x concentration because we wanted to decrease the cost of the setup by using less amount of the dye yet having a very good fluorescent enhancement. Nevertheless after we did the calculations we found that the distance between DiD dyes using 1:1592 DiD: DOPC molar ratio was 20.4nm. Hence, we still have a margin to increase the sensitivity if we want by increasing the DiD:DOPC molar ratio.

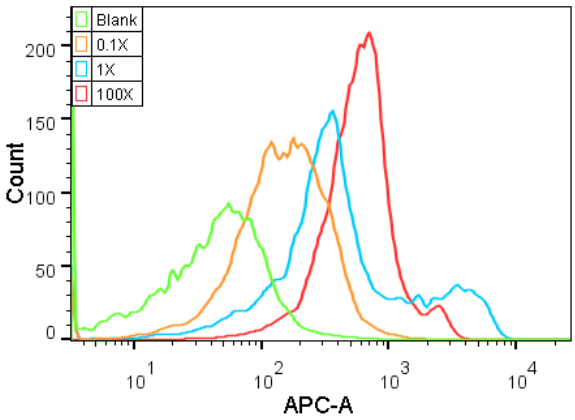

Figure IV-5.Flow cytometry measurements for 1nM HVB target with variations of DiD concentration inside the liposome. The experiment was done at room temperature for 30minutes with 100nm HVB-P2 and 10nM HVB-P1 in 10mM PBS buffer (pH=7.01), 0.6M NaCl, 3mM Tris-HCl and 0.6mMM EDTA

In a similar experiment, we tested the signal amplification of another fluorescent dye (DiA) using the BA sequences and the same conclusions were drawn (Figure IV-6).

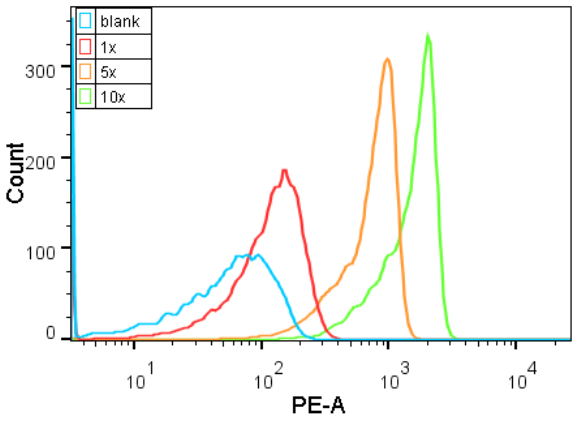

Figure IV-6.Flow cytometry measurements for 1 nM BA target with variations of DiA concentration inside the liposome.The experiment was done at room temperature for 30minutes with 100 nm BA-P2 and 10nM BA-P1 in 10 mM PBS buffer (pH = 7.01), 0.6 M NaCl, 3 mM Tris-HCl and 0.6 mM EDTA

5. Optimization of Hybridization Buffer

Without the use of proper buffer solution for DNA resuspension, the risk of damaging the oligonucleotides becomes high due to chemical processes such as depurination and deamination.[137] Moreover, the interaction of nucleic acids with divalent or monovalent cations affects its physical properties.[138] For instance, divalent cations such as Cu^{2+}, Fe^{2+}or Mg^{2+} strongly stabilize the nucleic acids duplexes but it can serve as cofactors for enzymatic reactions that involves DNA degradation.[138-139] On the other hand, it was shown by Peterson *et al*. that the yield of probe immobilization on the surface is enhanced by the use of monovalent cations in the hybridization buffer.[133] Actually, the concentration of these cations is critical while performing DNA detection as it affects both the efficiency and specificity.[138] As such researchers tend to use hybridization buffers containing monovalent cations (eg. sodium) to minimize the electrostatic repulsion between the DNA strands and chelating agents to complex the divalent metal ions and thus suppressing the DNA degradation process they induce.[140, 138, 139] Herein we tested three previously reported buffers, EDTA-Tris-NaCl buffer (TE) [106], citric acid buffer (SSC) [139] and magnesium buffer (Mg^{2+}) [138, 140] to determine the optimal medium that we should use in order to maintain the best interaction between oligonucleotide sequences and that will allow an enhanced sensitivity. In a typical experiment, we measured the fluorescent intensity of three samples with different hybridization buffers but all containing 1nM HVB-T, 100 nM HVB-P2 functionalized DiD liposomes and 10nM HVB-P1 functionalized PS-Au. Results (Figure IV-7) showed that TE buffer allowed the detection with a slightly improved fluorescent signal when compared to either SSC or Mg^{2+} buffers. Indeed, TE buffer is optimal because it contains monovalent ions (Na^{+}) that interact with DNA at the phosphate group leading

to a decrease in electrostatic repulsion between DNA strands and therefore an increase in the yield of DNA immobilization and EDTA which is known to be an efficient chelating agent for excess divalent ions that are cofactors for DNA degradation enzymes. Consequently, the TE buffer reagents are both contributing to a higher efficiency of hybridization and thus TE buffer was adopted for all the sensing experiments.

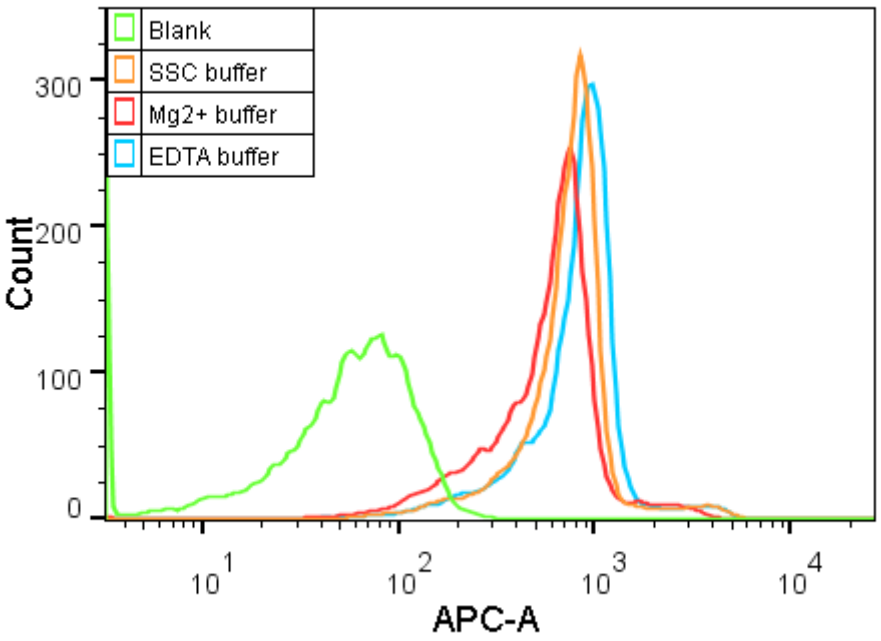

Figure IV-7.Flow cytometry measurements for 1 nM HVB target with variations of the hybridization buffer. The experiment was done at room temperature with 10 nM HVB-P1 and DiD liposomes (1x) functionalized with 100nm HVB-P2 in 10 mM PBS buffer (pH =7 .01) and 0.6 M NaCl

6. Hybridization Time Optimization

Furthermore, it is vital in any sensing scheme to reduce the experimental time without losing the accuracy of your system. Time is a critical issue in determining the usefulness of any sensing system. Short time schemes are much appreciated as they

facilitate fast onsite screening and real time monitoring and easier routine assessment. While several researchers reported DNA hybridization processes that required an overnight incubation [106a,106b, 133] our sensing strategy allowed minimizing the hybridization time into half an hour only and even a 2 hours for the whole experiment. In fact, to investigate the minimum time required to get a decent detectable signal, sample 1-4 containing same components (100 nM HVB-P1, 100 nM HVB-P2 and 1 nM HVB-T) were allowed to hybridize for 5, 15, 30 and 60 minutes respectively and then compared to a blank. Results (Figure IV-8) showed that even a 5 minutes hybridization time was sufficient for getting a clear fluorescent signal increase that is way more than three standard deviations of the blank, and thus could be used to report 1nM detection with high confidence. However, the shift increased as hybridization time increased until it approached its maximum at 30 minutes after which there was no significant change in the signal and therefore 30 minutes was chosen to be the optimal hybridization time.

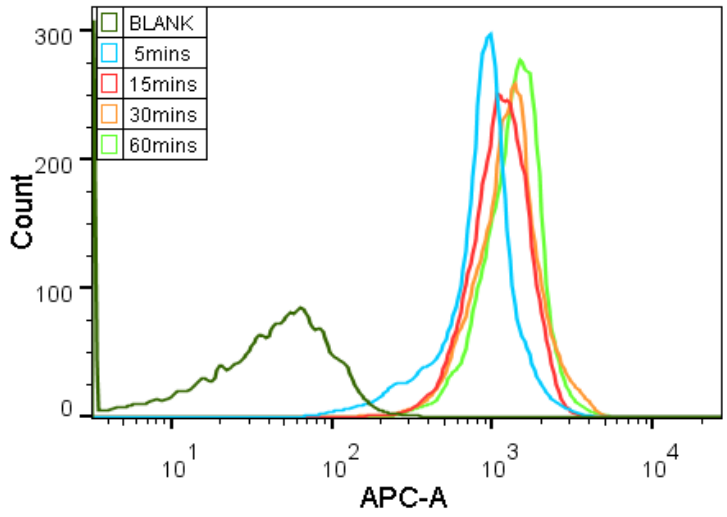

Figure IV-8.Kinetics of fluorescence enhancement using flow cytometry measurements for 1 nM HVB target. The experiment was done with10 nM HVB-P1 and DiD

liposomes (1x) functionalized with 100nm HVB-P2 in 10mM PBS buffer (pH = 7.01), 0.6 M NaCl, 3 mM Tris-HCl and 0.6 mM EDTA

7. Serum Effect

The detection of biomarkers in their native environment has gained a lot of interest in the last decades. Following the advent of molecular biology and glucose biosensor breakthrough ,the development of blood biosensors for clinical assessment has expanded as it facilitates the real time monitoring of biomarkers level of specific diseases in the serum without complex purifying procedures .[141,142] For instance, Lee *et al.* [85a]and Iloeje *et al.*[85b] showed that elevated levels of HVB biomarkers inside the serum directly correlates with increasing risk of cirrhosis whereby patients showed potential high risk of developing the diseases when their serum viral load was greater than 10^5copies/ml. However bioanalyis in complex fluids still presents a critical and a challenging task because of the high background signals coming from the probe itself and proteins inside the fluids. Therefore, having a set of tools to detect serum DNA level with high performance is crucial for easy diagnosis and risk monitoring. As a proof of concept, we investigated the sensitivity of our sensing scheme by carrying tests in an artificial serum matrix. Samples of blank and 1nM HVB-T concentrations were allowed to hybridize in TE buffers spiked with artificial serum replacement (Figure IV-10) and compared to non-spiked samples (Figure IV-9).Results showed that the serum matrix didn't alter the molecular recognition property between DNA strands as we can still see a clear shift between the blank and the target indicating the occurrence of the hybridization event. This confirms that our system is still efficient even in complex matrices and so it has the potential to be implemented in the point of care settings. However, like the majority of fluorescent sensors, it works better in clean

buffers. The serum matrix has an increased viscosity of the flow sample which induces a lower flow rate of particles and an attenuation of the fluorescence shift and thus a decrease the sensitivity.[50] This could be also accompanied by the non-specific serum protein adsorption onto the PS-Au microbeads surface resulting in lowering the hybridization efficiency between DNA probes and therefore weakening of the fluorescent signal. Furthermore, the population of low fluorescent particles increases because serum contains protein aggregates and cell debris that are non-fluorescent yet may have the same size as the microbeads used.

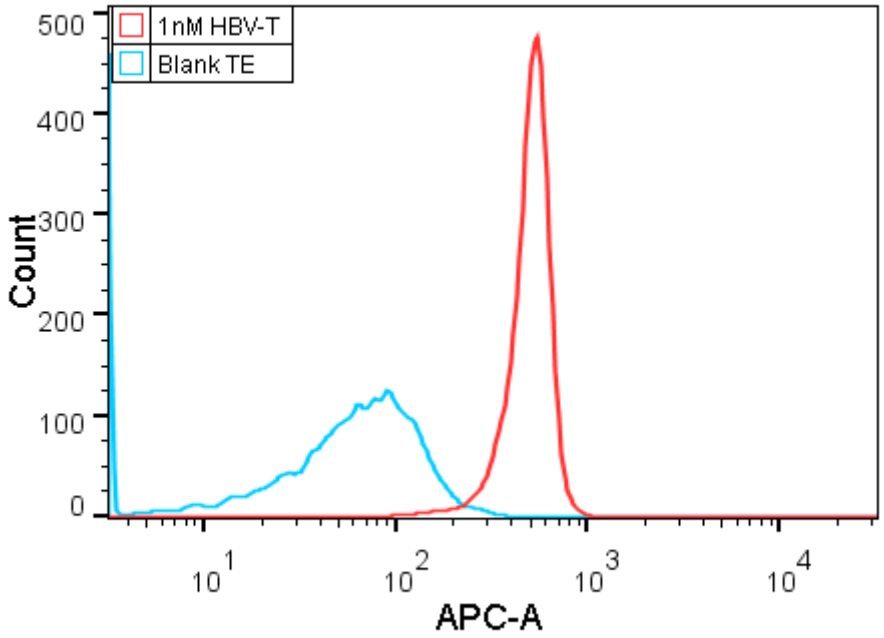

Figure IV-9.Detection of 1 nM target concentration inTE buffer. The experiment was done with10nM HVB-P1 and DiD liposomes (1x) functionalized with 100 nm HVB-P2 in 10 mM PBS buffer (pH = 7.01), 0.6 M NaCl, 3 mM Tris-HCl and 0.6 mM EDTA.

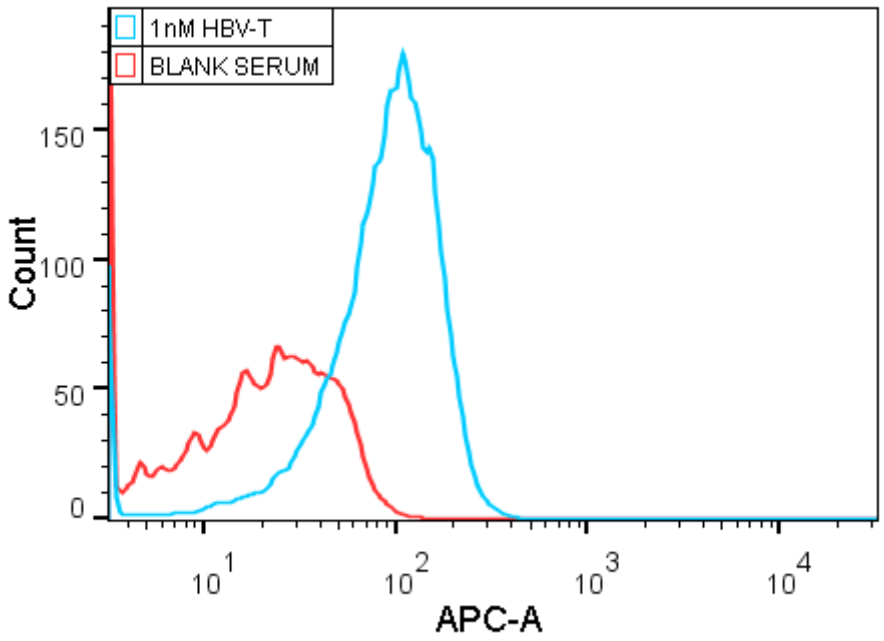

Figure IV-10.Detection of 1 nM target concentration in serum. The experiment was done with10 nM HVB-P1 and DiD liposomes (1x) functionalized with 100 nm HVB-P2 in 10 mM PBS buffer (pH = 7.01), 0.6 M NaCl, 3 mM Tris-HCl and 0.6 mM EDTA, 1x serum replacement

8. Detection Limit Determination and Statistical Analysis

Although in our study we are only interested in developing a yes/no sensing scheme for HVB DNA, we tried determining the detection limit of our sensing strategy. In 3 titration experiments, replicate samples containing different target concentrations (1 pM to 10 nM) were tested separately under the optimized conditions and using the flowcytometer the relative fluorescent intensities were recorded (Figure IV-12, Figure IV-13 and Figure IV-14). Results (Figure IV-15) showed that there was a linear response between 1 and 500 pM concentrations after which we started to see the formation of a plateau indicating fluorescent saturation and complete hybridization of HVB-P2 oligonucloetides. In fact, this plateau can be overcome by increasing the

concentration of HVB-P2.Table IV-1 shows statistical values for the three titration experiments. The Fluorescent intensities are subtracted from the blank intensities which are 69.3, 69.4 and 70.4 for trials 1, 2 and 3 respectively. The limit of detection (LOD) was calculated using the $\frac{3s}{m}$ formula; s is the standard deviation of the 10pM concentration and is equal to 1.54 whereas m is the slope of the calibration curve of equation $y = 1.61x + 18.7$(Figure IV-16). Therefore it was determined as $LOD = \frac{3s}{m} = \frac{3\times1.54}{1.61} = 2.87\ pM$. This DNA detection sensitivity is better than many of the PCR free reported ones (Table IV-2).

Table IV-1.Statistical data of flow cytometry measurments for HBV replicates.

HBV concentration (pM)	**Mean Fluorescent intensities**		
	Trial 1	**Trial 2**	**Trial 3**
1	12	9.3	4.8
5	31.7	38.6	42.6
10	47.7	48.6	45.6
50	95.7	96.6	96.6
100	176.7	173.6	168.6
500	825.7	818.6	831.6
1000	1531.7	1463.6	1474.6
5000	3613.7	3537.6	3487.6
10000	3859.7	3797.6	3891.6

As well, as a proof of concept we carried out steady state fluorescent measurements on the same replicate samples however results (Figure IV-11) showed that the fluorometer was not sensitive enough to sufficiently detect and differentiate

very low concentrations. The signals were mostly noise and there was no significant variation between signals obtained from any sample (1 pM -10 nM concentrations) and the blank and therefore they were all considered as non-signal responses. Nevertheless, the cuvette based measurements required around 1.5 mL sample volume rendering this method not practical for biosensing applications whereby it is desirable to lower the sample volume to the few microliters level (eg. glucose biosensor). As a result, we chose to implement only flow cytometry in any further experiment because it didn't not only require less sample volume but also provided ultimate sensitivity when compared to the fluotometric cuvette based measurements

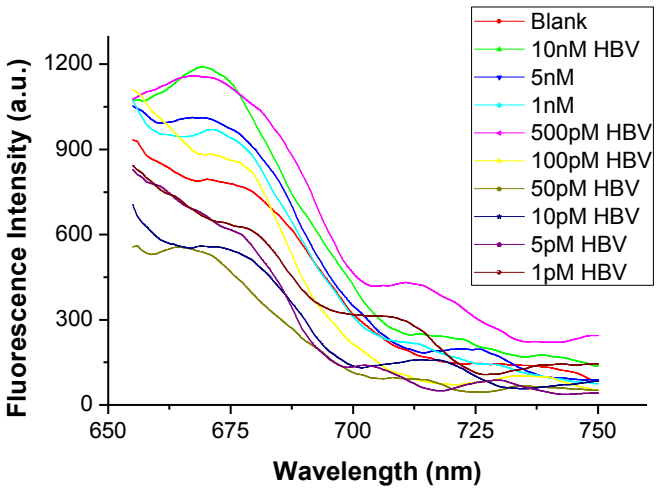

Figure IV-11.Steady state fluorescent measurements with variation in target concentration. All target concentrations were hybridized independently for 30 minutes at room temperature with10 nM HVB-P1 and DiD liposomes (1x) functionalized with 100 nm HVB-P2 in 10 mM PBS buffer (pH = 7.01), 0.6 M NaCl, 3 mM Tris-HCl and 0.6 mM EDTA.

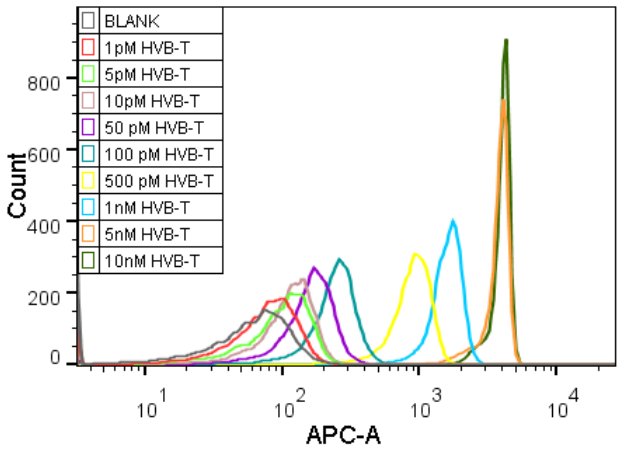

Figure IV-12. Flow cytometry measurements with variation in target concentration. All target concentrations were hybridized independently for 30 minutes at room temperature with 10 nM HVB-P1 and DiD liposomes (1x) functionalized with 100 nm HVB-P2 in 10 mM PBS buffer (pH = 7.01), 0.6 M NaCl, 3 mM Tris-HCl and 0.6 mM EDTA. Trial 1

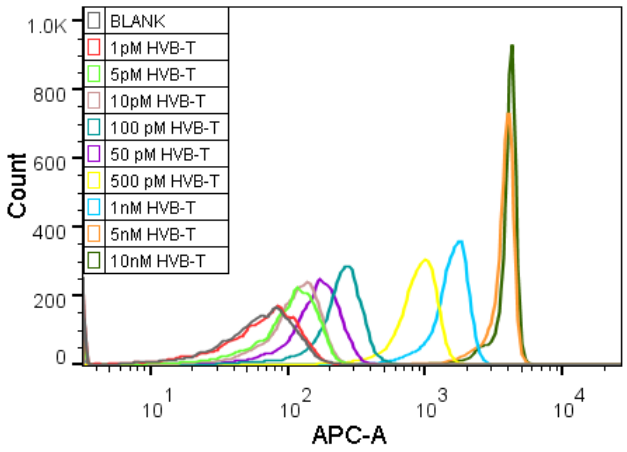

Figure IV-13. Flow cytometry measurements with variation in target concentration. All target concentrations were hybridized independently for 30 minutes at room temperature with 10nM HVB-P1 and DiD liposomes (1x) functionalized with 100nm HVB-P2 in 10mM PBS buffer (pH=7.01), 0.6M NaCl, 3mM Tris-HCl and 0.6mMM EDTA. Trial 2

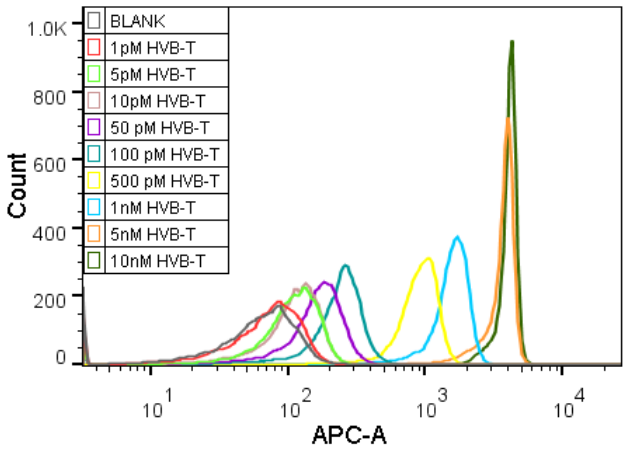

Figure IV-14. Flow cytometry measurements with variation in target concentration. All target concentrations were hybridized independently for 30 minutes at room temperature with 10nM HVB-P1 and DiD liposomes (1x) functionalized with 100nm HVB-P2 in 10mM PBS buffer (pH=7.01), 0.6M NaCl, 3mM Tris-HCl and 0.6mMM EDTA. Trial 3

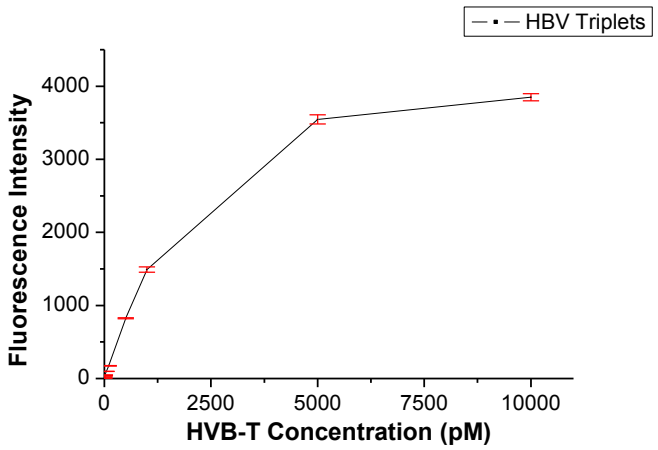

Figure IV-15.Steady state fluorescent measurements as a function of HBV target concentration. The error bars represent the standard deviation of three independent measurements.

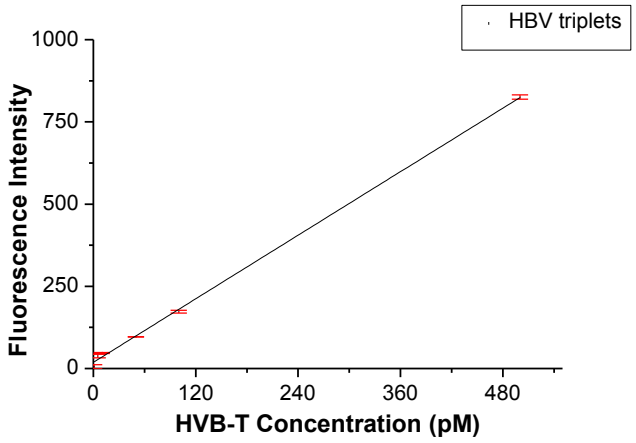

Figure IV-16. Calibration curve of the system measured between 1 and 500 pM HVB-T concentration. The equation of the line is $\boldsymbol{y = 1.61x + 18.7}$ with an r^2 value of 0.998.

Table IV-2. Comparison of the PCR free DNA analysis methods

Method	Detection limit (nM)
Fluorescence Near Gold Nanoparticles for DNA Sensing [106a]	0.1
Molecular beacon-functionalized gold nanoparticles as probes in dry-reagent strip biosensor for DNA analysis [143]	0.05
Graphene Oxide/Nucleic-Acid-Stabilized Silver Nanoclusters: Functional Hybrid Materials for Optical Aptamer Sensing and Multiplexed Analysis of Pathogenic DNAs[144]	1
Fluorescence Resonance Energy Transfer between Quantum Dots and Graphene Oxide for Sensing Biomolecules [145]	12
multi-walled carbon nanotube-based multicolor nanobeacon for Multiplexed analysis of DNA [146]	0.042
DNA-Templated Silver Nanoclusters for Multiplexed Fluorescent DNA Detection[147]	25

9. Multiplexing

In an attempt to sense different targets in the same sample, simultaneous detection of HBV and BA targets was done under optimized conditions (10nM probe1, 100nM probe2,1:1000 DNA :DOPC molar ratio) and by coupling probe 2 of each sequence to a different fluorescent dye (DiD for visualizing HBV and DiA for BA). Results (Figure IV-17) show that it is possible to detect each target without affecting the

sensitivity for the other because no interferences were observed and each target DNA only hybridized with its specific dye labeled probe. When each target is present separately, a dramatic enhancement of the fluorescent signal of its corresponding dye label was only observed accompanied with no increase of that of the other dye. Besides, in the presence of both target, the fluorescent signals overlapped with those obtained from the single target measurements and hence demonstrating the ability to distinguish a specific sequence from the other.

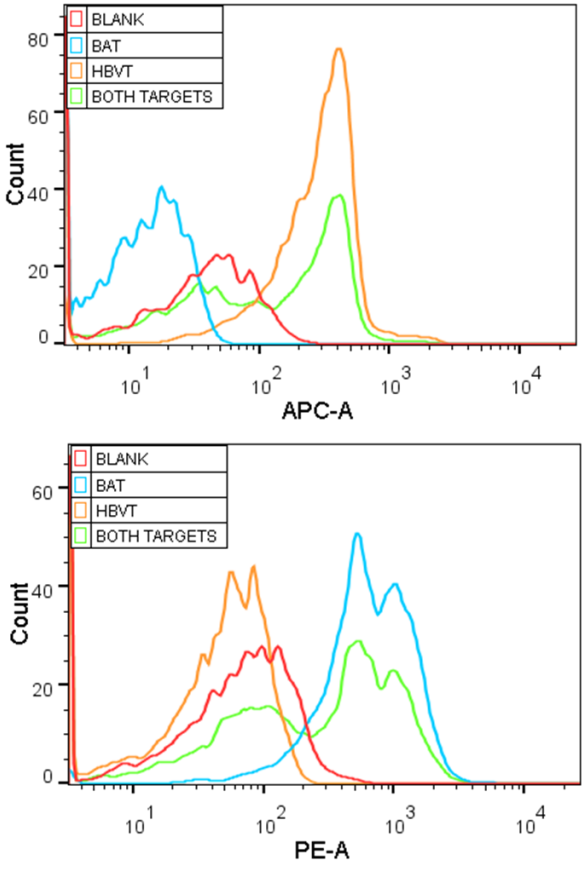

Figure IV-17. Multiplex detection of 1nM target DNA of BA and HBV sequences. The experiment was done at room temperature for 30 minutes with 10nM HVB-P1 and DiD liposomes (1x) functionalized with 100nm HVB-P2 and 10nM BA-P1 and DiA liposomes (1x) functionalized with 100nm BA in 10mM PBS buffer (pH=7.01), 0.6M NaCl, 3mM Tris-HCl and 0.6mMM EDTA.

C. Conclusion

We report a novel and universal sensing method for the detection of oligonucleotide sequences based on the use of liposomes and flow cytometry. The proposed scheme is very good in terms of simplicity, speed and sensitivity (only 5 min is sufficient for sensing the hybridization event with a 2.7 pM limit of detection). This is much better than previously reported fluorescent methods. For instance, Zhang *et al.* reported a detection limit of 25 nM and an incubation time of 24 hours for sensing DNA sequences of H1N1 an H5N1 using silver nanocluster based molecular beacon probes.[147] Liu *et al.* also developed a fluorescent detection method using graphene oxide and silver nanocluster composites with a detection limit of 1 nM and 1 hour hybridization time.[144] On the other hand, there are other methods that may outperform our assay (attomolar range) but these are normally based on PCR which makes them labor demanding, very expensive and prone for easy contamination. [148] Our system is also capable of multiplexing and performing in complex matrices. This is an advantage over colorimetric techniques that can multiplex with high sensitivity as our assay (pM range) but suffer from the applicability for colored and opaque samples. [43] [40, 42a] As such, our proposed scheme offered several improvements over other DNA detection techniques and thus can serve as a promising platform for fast on-site monitoring and easy and reliable routine clinical assessment.

CHAPTER V

CONCLUSION AND FUTURE IMPLICATIONS

In this work, we have successfully developed different platforms for the detection of ultra-trace amounts of protein and DNA biomarkers using electrochemical and fluorescent approaches.

In chapter III, we described a chip-based approach for label-free detection of S100B biomarkers. By tuning the size of the micro-sensors, we achieved high levels of sensitivity. But this method was not valid when used with complex biological fluids. Therefore, we studied the use of fluorescent scheme as an alternative. We presented a sandwich assay that was built on PS-Au microspheres and visualized using flow cytometry. We used three different fluorescent tags to reflect the amount of captured analyte. The coupling of AF 647 or FITC-SNP to the system didn't ensure a high sensitivity whereas the coupling of labeled liposomes enhanced the sensitivity and allowed the detection of low antigen concentrations that are clinically relevant. However, due to the lack of materials we weren't able to perform further optimizations and serum testing. For future directions we can

- Optimize dye concentration inside the liposomes. In this sensing strategy we have used only 24 DiD molecules per liposome. We suspect that by increasing this number, we will get enhanced sensitivities.
- Use PEG-biotin in the preparation of the liposomes. This will make it easier for coupling the liposome to the sandwich assay.

- Replace antibodies by aptamers. Aptamers are synthetic oligonucleotides that can specifically bind to molecular targets just as antibodies do but with higher specificity and selectivity. Aptamers are much easier to obtain as well as they are more stable than antibodies. This makes them a promising tool that could be implemented in immunosensing applications.

In chapter IV, we developed an ultrasensitive universal platform for the detection of oligonucleotide sequences on the basis of our findings in chapter III. The mode of operation is summarized by the immobilization of two DNA strands complementary to the target of interest onto the surface of PS-Au microspheres and dye encapsulated liposomes and then visualization of the hybridization event using flow cytometry. After carrying optimization experiments, the proposed scheme was proven to have an excellent sensitivity (pM range) and alacrity and can be easily modified to detect any sequence of interest. Furthermore, it can perform well in complex matrices which makes it a promising platform for fast multiplexing diagnosis.

As for the future directions we can carry on continued optimization of parameters. These include:

- Use of Backfillers. It is common for thiolated DNA to lay down on the gold surfaces in a disordered array due to nonspecific binding.[149,150] Several studies reported the use of backfillers to improve DNA accessibility by erecting the bounded DNA against the gold surface and preventing nonspecific adsorption.[27,134, 151] Therefore, as a future experiment we can test the sensitivity of the sensing scheme using long chain thiols such as mercaptohexanol or a thiolatedoligoethylene glycol. These molecules were shown to prevent multipoint attachment between nucleobases and protect the

surface from nonspecific adsorption of oligonucleotides [133, 152] and thus they should increase the hybridization efficiency.

- Manipulating the liposome curvature and dye to lipid ratios.
- Investigating the effect of gold nanoparticle sizes on the PS beads.
- Checking the use of lipids with different viscosities.
- Coupling an array of liposomes rather than one.
- Implementing Smart phone based techniques. Inspired by Ozcan *et al.* [48] who reported the use of a smart phone based colorimetric detection for mercury contamination in water, our ultimate objective will be to translate the developed sensing platforms into POC testing using smart phones.

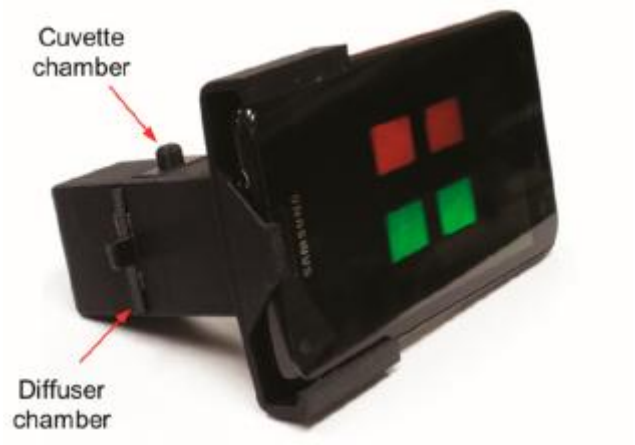

Figure V-1. Smart phone based optical reader. Reprinted with permission from Ozcan *et al.* [48]

In fact, we have currently started exploring some of these experiments and will continue the process in order to apply our systems in laboratory, clinical, and point-of-care settings.

REFERENCES

1. Sin, M. L. Y.; Mach, K. E.; Wong, P. K.; Liao, J. C., Advances and challenges in biosensor-based diagnosis of infectious diseases. *Expert Review of Molecular Diagnostics* **2014,** *14* (2), 225-244.
2. Murugaiyan, S. B.; Ramasamy, R.; Gopal, N.; Kuzhandaivelu, V., Biosensors in clinical chemistry: An overview. *Advanced Biomedical Research* **2014,** *3*, 67.
3. Sethi, S.; Ali, S.; Philip, P. A.; Sarkar, F. H., Clinical Advances in Molecular Biomarkers for Cancer Diagnosis and Therapy. *International Journal of Molecular Sciences* **2013,** *14* (7), 14771-14784.
4. Song, S.; Xu, H.; Fan, C., Potential diagnostic applications of biosensors: current and future directions. *International Journal of Nanomedicine* **2006,** *1* (4), 433-440.
5. Strimbu, K.; Tavel, J. A., What are Biomarkers? *Current opinion in HIV and AIDS* **2010,** *5* (6), 463-466.
6. Lucas, M.; Gaudieri, S., The role of biomarkers in the prevention of globally important diseases. *Biomarkers in Medicine* **2013,** *7* (3), 331-332.
7. Sanjay, S. T.; Fu, G.; Dou, M.; Xu, F.; Liu, R.; Qi, H.; Li, X., Biomarker detection for disease diagnosis using cost-effective microfluidic platforms. *Analyst* **2015,** *140* (21), 7062-7081.
8. (a) You, C.-C.; Miranda, O. R.; Gider, B.; Ghosh, P. S.; Kim, I.-B.; Erdogan, B.; Krovi, S. A.; Bunz, U. H. F.; Rotello, V. M., Detection and identification of proteins using nanoparticle-fluorescent polymer /`chemical nose/' sensors. *Nat Nano* **2007,** *2* (5), 318-323; (b) Bunz, U. H. F.; Rotello, V. M., Gold Nanoparticle–Fluorophore Complexes: Sensitive and Discerning "Noses" for Biosystems Sensing. *Angewandte Chemie International Edition* **2010,** *49* (19), 3268-3279.
9. Caveney, E. J.; Cohen, O. J., Diabetes and Biomarkers. *Journal of Diabetes Science and Technology* **2011,** *5* (1), 192-197.
10. Yu, L.; Boulware, D. C.; Beam, C. A.; Hutton, J. C.; Wenzlau, J. M.; Greenbaum, C. J.; Bingley, P. J.; Krischer, J. P.; Sosenko, J. M.; Skyler, J. S.; Eisenbarth, G. S.; Mahon, J. L.; for the Type 1 Diabetes TrialNet Study, G., Zinc Transporter-8 Autoantibodies Improve Prediction of Type 1 Diabetes in Relatives Positive for the Standard Biochemical Autoantibodies. *Diabetes Care* **2012,** *35* (6), 1213-1218.
11. Meigs, J. B., Multiple Biomarker Prediction of Type 2 Diabetes. *Diabetes Care* **2009,** *32* (7), 1346-1348.
12. Haab, B. B., Applications of antibody array platforms. *Current Opinion in Biotechnology* **2006,** *17* (4), 415-421.
13. (a) Di Battista, A. P.; Rhind, S. G.; Baker, A. J., Application of Blood Based Biomarkers in Human Mild Traumatic Brain Injury. *Frontiers in Neurology* **2013,** *4*; (b) Qian, Z. S.; Shan, X. Y.; Chai, L. J.; Ma, J. J.; Chen, J. R.; Feng, H., A universal fluorescence sensing strategy based on biocompatible graphene quantum dots and graphene oxide for the detection of DNA. *Nanoscale* **2014,** *6* (11), 5671-5674.
14. (a) Vasto, S.; Candore, G.; Duro, G.; Lio, D.; Grimaldi, M. P.; Caruso, C., Alzheimer's disease and genetics of inflammation: a pharmacogenomic vision. *Pharmacogenomics* **2007,** *8*; (b) Racchi, M.; Uberti, D.; Govoni, S.; Memo, M.; Lanni, C.; Vasto, S.; Candore, G.; Caruso, C.; Romeo, L.; Scapagnini, G., Alzheimer's disease: new diagnostic and therapeutic tools. *Immunity & Ageing* **2008,** *5* (1), 1-5.
15. (a) Thal, L. J.; Kantarci, K.; Reiman, E. M.; Klunk, W. E.; Weiner, M. W.; Zetterberg, H.; Galasko, D.; Praticò, D.; Griffin, S.; Schenk, D.; Siemers, E., The Role of Biomarkers in Clinical

Trials for Alzheimer Disease. *Alzheimer disease and associated disorders* **2006,** *20* (1), 6-15; (b) Tobinick, E. L.; Gross, H., Rapid cognitive improvement in Alzheimer's disease following perispinal etanercept administration. *J Neuroinflammation* **2008,** *5*.
16. Vasto, S.; Candore, G.; Listì, F.; Balistreri, C. R.; Colonna-Romano, G.; Malavolta, M.; Lio, D.; Nuzzo, D.; Mocchegiani, E.; Di Bona, D.; Caruso, C., Inflammation, Genes and Zinc in Alzheimer's disease. *Brain Research Review* **2008,** *58*.
17. (a) Uberti, D.; Lanni, C.; Racchi, M.; Govoni, S.; Memo, M., Conformationally altered p53: a putative peripheral marker for Alzheimer's disease. *Neurodegener Dis* **2008,** *5*; (b) Lanni, C.; Uberti, D.; Racchi, M.; Govoni, S.; Memo, M., Unfolded p53: a potential biomarker for Alzheimer's disease. *J Alzheimers Dis* **2007,** *12*; (c) Lanni, C.; Racchi, M.; Mazzini, G.; Ranzenigo, A.; Polotti, R.; Sinforiani, E.; Olivari, L.; Barcikowska, M.; Styczynska, M.; Kuznicki, J.; Szybinska, A.; Govoni, S.; Memo, M.; Uberti, D., Conformationally altered p53: a novel Alzheimer's disease marker? *Mol Psychiatry* **2008,** *13*.
18. (a) Blennow, K.; Hampel, H., CSF markers for incipient Alzheimer's disease. *Lancet Neurol* **2003,** *2*; (b) Blennow, K., Cerebrospinal Fluid Protein Biomarkers for Alzheimer's Disease. *NeuroRx* **2004,** *1* (2), 213-225.
19. (a) Yang, F.; Lim, G. P.; Begum, A. N.; Ubeda, O. J.; Simmons, M. R.; Ambegaokar, S. S.; Chen, P. P.; Kayed, R.; Glabe, C. G.; Frautschy, S. A.; Cole, G. M., Curcumin inhibits formation of amyloid beta oligomers and fibrils, binds plaques, and reduces amyloid in vivo. *J Biol Chem* **2005,** *280*; (b) Scapagnini, G.; Colombrita, C.; Amadio, M.; D'Agata, V.; Arcelli, E.; Sapienza, M.; Quattrone, A.; Calabrese, V., Curcumin activates defensive genes and protects neurons against oxidative stress. *Antioxid Redox Signal* **2006,** *8*; (c) Goel, A.; Kunnumakkara, A. B.; Aggarwal, B. B., Curcumin as "Curecumin": from kitchen to clinic. *Biochem Pharmacol* **2008,** *75*.
20. Mäbert, K.; Cojoc, M.; Peitzsch, C.; Kurth, I.; Souchelnytskyi, S.; Dubrovska, A., Cancer biomarker discovery: Current status and future perspectives. *International Journal of Radiation Biology* **2014,** *90* (8), 659-677.
21. Cho, W. C. S., Contribution of oncoproteomics to cancer biomarker discovery. *Molecular Cancer* **2007,** *6*, 25-25.
22. Henry, N. L.; Hayes, D. F., Cancer biomarkers. *Molecular Oncology* **2012,** *6* (2), 140-146.
23. Jemal, A.; Siegel, R.; Ward, E.; Hao, Y.; Xu, J.; Murray, T.; Thun, M. J., Cancer Statistics, 2008. *CA: A Cancer Journal for Clinicians* **2008,** *58* (2), 71-96.
24. (a) Easton, D. F.; Ford, D.; Bishop, D. T., Breast and ovarian cancer incidence in BRCA1-mutation carriers. Breast Cancer Linkage Consortium. *American Journal of Human Genetics* **1995,** *56* (1), 265-271; (b) Hall, J.; Lee, M.; Newman, B.; Morrow, J.; Anderson, L.; Huey, B.; King, M., Linkage of early-onset familial breast cancer to chromosome 17q21. *Science* **1990,** *250* (4988), 1684-1689.
25. (a) Paik , S.; Shak , S.; Tang , G.; Kim , C.; Baker , J.; Cronin , M.; Baehner , F. L.; Walker , M. G.; Watson , D.; Park , T.; Hiller , W.; Fisher , E. R.; Wickerham , D. L.; Bryant , J.; Wolmark , N., A Multigene Assay to Predict Recurrence of Tamoxifen-Treated, Node-Negative Breast Cancer. *New England Journal of Medicine* **2004,** *351* (27), 2817-2826; (b) Bang, Y.-J.; Van Cutsem, E.; Feyereislova, A.; Chung, H. C.; Shen, L.; Sawaki, A.; Lordick, F.; Ohtsu, A.; Omuro, Y.; Satoh, T.; Aprile, G.; Kulikov, E.; Hill, J.; Lehle, M.; Rüschoff, J.; Kang, Y.-K., Trastuzumab in combination with chemotherapy versus chemotherapy alone for treatment of HER2-positive advanced gastric or gastro-oesophageal junction cancer (ToGA): a phase 3, open-label, randomised controlled trial. *The Lancet 376* (9742), 687-697.
26. Gilligan, T. D.; Seidenfeld, J.; Basch, E. M.; Einhorn, L. H.; Fancher, T.; Smith, D. C.; Stephenson, A. J.; Vaughn, D. J.; Cosby, R.; Hayes, D. F., American Society of Clinical Oncology Clinical Practice Guideline on Uses of Serum Tumor Markers in Adult Males With Germ Cell Tumors. *Journal of Clinical Oncology* **2010,** *28* (20), 3388-3404.

27. Kim, M. J.; Zheng, S.; Kim, T. S.; Kim, S. K., Analysis of DNA coverage using enzymatic cleavage of fluorescent labels. *BioChip Journal* **2011,** *5* (1), 39-46.
28. (a) Lam, B.; Das, J.; Holmes, R. D.; Live, L.; Sage, A.; Sargent, E. H.; Kelley, S. O., Solution-based circuits enable rapid and multiplexed pathogen detection. *Nat Commun* **2013,** *4*; (b) Das, J.; Cederquist, K. B.; Zaragoza, A. A.; Lee, P. E.; Sargent, E. H.; Kelley, S. O., An ultrasensitive universal detector based on neutralizer displacement. *Nat Chem* **2012,** *4* (8), 642-648.
29. (a) Mitchell, P. S.; Parkin, R. K.; Kroh, E. M.; Fritz, B. R.; Wyman, S. K.; Pogosova-Agadjanyan, E. L.; Peterson, A.; Noteboom, J.; O'Briant, K. C.; Allen, A.; Lin, D. W.; Urban, N.; Drescher, C. W.; Knudsen, B. S.; Stirewalt, D. L.; Gentleman, R.; Vessella, R. L.; Nelson, P. S.; Martin, D. B.; Tewari, M., Circulating microRNAs as stable blood-based markers for cancer detection. *Proceedings of the National Academy of Sciences* **2008,** *105* (30), 10513-10518; (b) Porkka, K. P.; Pfeiffer, M. J.; Waltering, K. K.; Vessella, R. L.; Tammela, T. L. J.; Visakorpi, T., MicroRNA Expression Profiling in Prostate Cancer. *Cancer Research* **2007,** *67* (13), 6130-6135.
30. Hu, Z.; Chen, X.; Zhao, Y.; Tian, T.; Jin, G.; Shu, Y.; Chen, Y.; Xu, L.; Zen, K.; Zhang, C.; Shen, H., Serum MicroRNA Signatures Identified in a Genome-Wide Serum MicroRNA Expression Profiling Predict Survival of Non–Small-Cell Lung Cancer. *Journal of Clinical Oncology* **2010,** *28* (10), 1721-1726.
31. Lu, J.; Getz, G.; Miska, E. A.; Alvarez-Saavedra, E.; Lamb, J.; Peck, D.; Sweet-Cordero, A.; Ebert, B. L.; Mak, R. H.; Ferrando, A. A.; Downing, J. R.; Jacks, T.; Horvitz, H. R.; Golub, T. R., MicroRNA expression profiles classify human cancers. *Nature* **2005,** *435* (7043), 834-838.
32. (a) Ono, K.; Kuwabara, Y.; Han, J., MicroRNAs and cardiovascular diseases. *FEBS Journal* **2011,** *278* (10), 1619-1633; (b) Volinia, S.; Calin, G. A.; Liu, C.-G.; Ambs, S.; Cimmino, A.; Petrocca, F.; Visone, R.; Iorio, M.; Roldo, C.; Ferracin, M., A microRNA expression signature of human solid tumors defines cancer gene targets. *Proceedings of the National Academy of Sciences of the United States of America* **2006,** *103* (7), 2257-2261.
33. Silver, C. E.; Beitler, J. J.; Shaha, A. R.; Rinaldo, A.; Ferlito, A., Current trends in initial management of laryngeal cancer: the declining use of open surgery. *European Archives of Oto-Rhino-Laryngology* **2009,** *266* (9), 1333-1352.
34. Tsujiura, M.; Ichikawa, D.; Komatsu, S.; Shiozaki, A.; Takeshita, H.; Kosuga, T.; Konishi, H.; Morimura, R.; Deguchi, K.; Fujiwara, H.; Okamoto, K.; Otsuji, E., Circulating microRNAs in plasma of patients with gastric cancers. *Br J Cancer* **2010,** *102* (7), 1174-1179.
35. Peake, I., The polymerase chain reaction. *Journal of Clinical Pathology* **1989,** *42* (7), 673-676.
36. (a) Socher, E.; Bethge, L.; Knoll, A.; Jungnick, N.; Herrmann, A.; Seitz, O., Low-Noise Stemless PNA Beacons for Sensitive DNA and RNA Detection. *Angewandte Chemie International Edition* **2008,** *47* (49), 9555-9559; (b) Baumstark, D.; Wagenknecht, H.-A., Perylene Bisimide Dimers as Fluorescent “Glue” for DNA and for Base-Mismatch Detection. *Angewandte Chemie International Edition* **2008,** *47* (14), 2612-2614; (c) Grossmann, T. N.; Röglin, L.; Seitz, O., Triplex Molecular Beacons as Modular Probes for DNA Detection. *Angewandte Chemie International Edition* **2007,** *46* (27), 5223-5225.
37. Zanoli, L. M.; D’Agata, R.; Spoto, G., Functionalized gold nanoparticles for ultrasensitive DNA detection. *Analytical and Bioanalytical Chemistry* **2012,** *402* (5), 1759-1771.
38. Yang, Y.; Zhao, L., Sensitive fluorescent sensing for DNA assay. *TrAC Trends in Analytical Chemistry* **2010,** *29* (9), 980-1003.
39. Erdem, A., Nanomaterial-based electrochemical DNA sensing strategies. *Talanta* **2007,** *74* (3), 318-325.
40. Elghanian, R.; Storhoff, J. J.; Mucic, R. C.; Letsinger, R. L.; Mirkin, C. A., Selective Colorimetric Detection of Polynucleotides Based on the Distance-Dependent Optical Properties of Gold Nanoparticles. *Science* **1997,** *277* (5329), 1078-1081.

41. Hong, M.; Zhu, J.; Yin, H.-D., Research Progress in Application of Nanomaterials for Deoxyribonucleic Acid Detection. *Chinese Journal of Analytical Chemistry* **2011,** *39* (1), 146-154.
42. (a) Taton, T. A.; Mirkin, C. A.; Letsinger, R. L., Scanometric DNA Array Detection with Nanoparticle Probes. *Science* **2000,** *289* (5485), 1757-1760; (b) Cao, Y. C.; Jin, R.; Mirkin, C. A., Nanoparticles with Raman Spectroscopic Fingerprints for DNA and RNA Detection. *Science* **2002,** *297* (5586), 1536-1540; (c) Park, S.-J.; Taton, T. A.; Mirkin, C. A., Array-Based Electrical Detection of DNA with Nanoparticle Probes. *Science* **2002,** *295* (5559), 1503-1506.
43. Xia, F.; Zuo, X.; Yang, R.; Xiao, Y.; Kang, D.; Vallée-Bélisle, A.; Gong, X.; Yuen, J. D.; Hsu, B. B. Y.; Heeger, A. J.; Plaxco, K. W., Colorimetric detection of DNA, small molecules, proteins, and ions using unmodified gold nanoparticles and conjugated polyelectrolytes. *Proceedings of the National Academy of Sciences of the United States of America* **2010,** *107* (24), 10837-10841.
44. Wang, J.; Kawde, A.-N.; Musameh, M.; Rivas, G., Dual enzyme electrochemical coding for detecting DNA hybridization. *Analyst* **2002,** *127* (10), 1279-1282.
45. Soleymani, L.; Fang, Z.; Lam, B.; Bin, X.; Vasilyeva, E.; Ross, A. J.; Sargent, E. H.; Kelley, S. O., Hierarchical Nanotextured Microelectrodes Overcome the Molecular Transport Barrier To Achieve Rapid, Direct Bacterial Detection. *ACS Nano* **2011,** *5* (4), 3360-3366.
46. Brockman, J. M.; Frutos, A. G.; Corn, R. M., A Multistep Chemical Modification Procedure To Create DNA Arrays on Gold Surfaces for the Study of Protein−DNA Interactions with Surface Plasmon Resonance Imaging. *Journal of the American Chemical Society* **1999,** *121* (35), 8044-8051.
47. Ostroff, R. M.; Hopkins, D.; Haeberli, A. B.; Baouchi, W.; Polisky, B., Thin Film Biosensor for Rapid Visual Detection of Nucleic Acid Targets. *Clinical Chemistry* **1999,** *45* (9), 1659-1664.
48. Wei, Q.; Nagi, R.; Sadeghi, K.; Feng, S.; Yan, E.; Ki, S. J.; Caire, R.; Tseng, D.; Ozcan, A., Detection and Spatial Mapping of Mercury Contamination in Water Samples Using a Smart-Phone. *ACS Nano* **2014,** *8* (2), 1121-1129.
49. Liu, J.; Cao, Z.; Lu, Y., Functional Nucleic Acid Sensors. *Chemical Reviews* **2009,** *109* (5), 1948-1998.
50. Huang, P.-J. J.; Liu, J., Flow Cytometry-Assisted Detection of Adenosine in Serum with an Immobilized Aptamer Sensor. *Analytical Chemistry* **2010,** *82* (10), 4020-4026.
51. (a) Howarth, M.; Liu, W.; Puthenveetil, S.; Zheng, Y.; Marshall, L. F.; Schmidt, M. M.; Wittrup, K. D.; Bawendi, M. G.; Ting, A. Y., Monovalent, reduced-size quantum dots for imaging receptors on living cells. *Nat Meth* **2008,** *5* (5), 397-399; (b) Michalet, X.; Pinaud, F. F.; Bentolila, L. A.; Tsay, J. M.; Doose, S.; Li, J. J.; Sundaresan, G.; Wu, A. M.; Gambhir, S. S.; Weiss, S., Quantum Dots for Live Cells, in Vivo Imaging, and Diagnostics. *Science* **2005,** *307* (5709), 538-544.
52. Peng, H.; Zhang, L.; Kjällman, T. H. M.; Soeller, C., DNA Hybridization Detection with Blue Luminescent Quantum Dots and Dye-Labeled Single-Stranded DNA. *Journal of the American Chemical Society* **2007,** *129* (11), 3048-3049.
53. (a) Wu, X.; Liu, H.; Liu, J.; Haley, K. N.; Treadway, J. A.; Larson, J. P.; Ge, N.; Peale, F.; Bruchez, M. P., Immunofluorescent labeling of cancer marker Her2 and other cellular targets with semiconductor quantum dots. *Nat Biotech* **2003,** *21* (1), 41-46; (b) Somers, R. C.; Bawendi, M. G.; Nocera, D. G., CdSe nanocrystal based chem-/bio- sensors. *Chemical Society Reviews* **2007,** *36* (4), 579-591.
54. (a) Lin, B.; Liu, D.; Yan, J.; Qiao, Z.; Zhong, Y.; Yan, J.; Zhu, Z.; Ji, T.; Yang, C. J., Enzyme-Encapsulated Liposome-Linked Immunosorbent Assay Enabling Sensitive Personal Glucose Meter Readout for Portable Detection of Disease Biomarkers. *ACS Applied Materials & Interfaces* **2016,** *8* (11), 6890-6897; (b) Torchilin, V. P., Recent advances with liposomes as pharmaceutical carriers. *Nat Rev Drug Discov* **2005,** *4* (2), 145-160.

55. (a) Edwards, K. A.; Baeumner, A. J., Liposomes in analyses. *Talanta* **2006,** *68* (5), 1421-1431; (b) Jesorka, A.; Orwar, O., Liposomes: Technologies and Analytical Applications. *Annual Review of Analytical Chemistry* **2008,** *1* (1), 801-832.
56. (a) Ruktanonchai, U.; Nuchuchua, O.; Charlermroj, R.; Pattarakankul, T.; Karoonuthaisiri, N., Signal amplification of microarray-based immunoassay by optimization of nanoliposome formulations. *Analytical Biochemistry* **2012,** *429* (2), 142-147; (b) Liu, Q.; Boyd, B. J., Liposomes in biosensors. *Analyst* **2013,** *138* (2), 391-409.
57. Nakane, Y.; Ito, M. M.; Kubo, I., Novel Detection Method of Endocrine Disrupting Chemicals Utilizing Liposomes as Cell Membrane Model. *Analytical Letters* **2008,** *41* (16), 2923-2932.
58. (a) Zhang, J.; Sheng, W.; Fan, Z. H., An ensemble of aptamers and antibodies for multivalent capture of cancer cells. *Chemical communications (Cambridge, England)* **2014,** *50* (51), 6722-6725; (b) Cao, X.; Li, S.; Chen, L.; Ding, H.; Xu, H.; Huang, Y.; Li, J.; Liu, N.; Cao, W.; Zhu, Y.; Shen, B.; Shao, N., Combining use of a panel of ssDNA aptamers in the detection of Staphylococcus aureus. *Nucleic Acids Research* **2009,** *37* (14), 4621-4628; (c) Raddatz, M.-S. L.; Dolf, A.; Endl, E.; Knolle, P.; Famulok, M.; Mayer, G., Enrichment of Cell-Targeting and Population-Specific Aptamers by Fluorescence-Activated Cell Sorting. *Angewandte Chemie International Edition* **2008,** *47* (28), 5190-5193.
59. (a) Herr, J. K.; Smith, J. E.; Medley, C. D.; Shangguan, D.; Tan, W., Aptamer-Conjugated Nanoparticles for Selective Collection and Detection of Cancer Cells. *Analytical Chemistry* **2006,** *78* (9), 2918-2924; (b) Xu, Y.; Phillips, J. A.; Yan, J.; Li, Q.; Fan, Z. H.; Tan, W., Aptamer-Based Microfluidic Device for Enrichment, Sorting, and Detection of Multiple Cancer Cells. *Analytical Chemistry* **2009,** *81* (17), 7436-7442.
60. Brown, M.; Wittwer, C., Flow Cytometry: Principles and Clinical Applications in Hematology. *Clinical Chemistry* **2000,** *46* (8), 1221-1229.
61. (a) Taton, T. A.; Lu, G.; Mirkin, C. A., Two-Color Labeling of Oligonucleotide Arrays via Size-Selective Scattering of Nanoparticle Probes. *Journal of the American Chemical Society* **2001,** *123* (21), 5164-5165; (b) Gao, X.; Su, J. Z.; Han, M.; Nie, S., Quantum-dot-tagged microbeads for multiplexed optical coding of biomolecules. *Nature Biotechnology* **2001,** *19* (7), 631-635; (c) Nicewarner-Peña, S. R.; Freeman, R. G.; Reiss, B. D.; He, L.; Peña, D. J.; Walton, I. D.; Cromer, R.; Keating, C. D.; Natan, M. J., Submicrometer Metallic Barcodes. *Science* **2001,** *294* (5540), 137-141; (d) Ferguson, J. A.; Steemers, F. J.; Walt, D. R., High-Density Fiber-Optic DNA Random Microsphere Array. *Analytical Chemistry* **2000,** *72* (22), 5618-5624.
62. (a) Kozak, K. R.; Su, F.; Whitelegge, J. P.; Faull, K.; Reddy, S.; Farias-Eisner, R., Characterization of serum biomarkers for detection of early stage ovarian cancer. *PROTEOMICS* **2005,** *5* (17), 4589-4596; (b) Wei, F.; Patel, P.; Liao, W.; Chaudhry, K.; Zhang, L.; Arellano-Garcia, M.; Hu, S.; Elashoff, D.; Zhou, H.; Shukla, S.; Shah, F.; Ho, C.-M.; Wong, D. T., Electrochemical Sensor for Multiplex Biomarkers Detection. *Clinical Cancer Research* **2009,** *15* (13), 4446-4452.
63. Wang, J.; Liu, G.; Merkoçi, A., Electrochemical Coding Technology for Simultaneous Detection of Multiple DNA Targets. *Journal of the American Chemical Society* **2003,** *125* (11), 3214-3215.
64. Zheng, W.; He, L., Label-Free, Real-Time Multiplexed DNA Detection Using Fluorescent Conjugated Polymers. *Journal of the American Chemical Society* **2009,** *131* (10), 3432-3433.
65. Han, M.; Gao, X.; Su, J. Z.; Nie, S., Quantum-dot-tagged microbeads for multiplexed optical coding of biomolecules. *Nature Biotechnology* **2001,** *19* (7), 631-5.
66. (a) Zetterberg, H.; Smith, D. H.; Blennow, K., Biomarkers of mild traumatic brain injury in cerebrospinal fluid and blood. *Nat Rev Neurol* **2013,** *9* (4), 201-210; (b) Hergenroeder, G. W.; Redell, J. B.; Moore, A. N.; Dash, P. K., Biomarkers in the Clinical Diagnosis and Management of Traumatic Brain Injury. *Molecular Diagnosis & Therapy* **2008,** *12* (6), 345-358.

67. (a) Zetterberg, H.; Smith, D. H.; Blennow, K., Biomarkers of mild traumatic brain injury in cerebrospinal fluid and blood. *Nature reviews. Neurology* **2013,** *9* (4), 201-210; (b) Jeter, C. B.; Hergenroeder, G. W.; Hylin, M. J.; Redell, J. B.; Moore, A. N.; Dash, P. K., Biomarkers for the Diagnosis and Prognosis of Mild Traumatic Brain Injury/Concussion. *Journal of Neurotrauma* **2012,** *30* (8), 657-670.
68. Buonora, J. E.; Yarnell, A. M.; Lazarus, R. C.; Mousseau, M.; Latour, L. L.; Rizoli, S. B.; Baker, A. J.; Rhind, S. G.; Diaz-Arrastia, R.; Mueller, G. P., Multivariate Analysis of Traumatic Brain Injury: Development of an Assessment Score. *Frontiers in Neurology* **2015,** *6*, 68.
69. (a) Kelly, J. C.; Amerson, E. H.; Barth, J. T., Mild Traumatic Brain Injury: Lessons Learned from Clinical, Sports, and Combat Concussions. *Rehabilitation Research and Practice* **2012,** *2012*, 371970; (b) Barlow, K. M., Chapter 95 - Traumatic brain injury. In *Handbook of Clinical Neurology*, Olivier Dulac, M. L.; Harvey, B. S., Eds. Elsevier: 2013; Vol. Volume 112, pp 891-904.
70. (a) Di Battista, A. P.; Rhind, S. G.; Baker, A. J., Application of Blood-Based Biomarkers in Human Mild Traumatic Brain Injury. *Frontiers in Neurology* **2013,** *4*, 44; (b) Risdall, J. E.; Menon, D. K., Traumatic brain injury. *Philosophical Transactions of the Royal Society B: Biological Sciences* **2011,** *366* (1562), 241-250.
71. Teasdale, G.; Jennett, B., Originally published as Volume 2, Issue 7872ASSESSMENT OF COMA AND IMPAIRED CONSCIOUSNESS. *The Lancet* **1974,** *304* (7872), 81-84.
72. Berger, R. P.; Beers, S. R.; Richichi, R.; Wiesman, D.; Adelson, P. D., Serum Biomarker Concentrations and Outcome after Pediatric Traumatic Brain Injury. *Journal of Neurotrauma* **2007,** *24* (12), 1793-1801.
73. Shenton, M. E.; Hamoda, H. M.; Schneiderman, J. S.; Bouix, S.; Pasternak, O.; Rathi, Y.; M-A, V.; Purohit, M. P.; Helmer, K.; Koerte, I.; Lin, A. P.; C-F, W.; Kikinis, R.; Kubicki, M.; Stern, R. A.; Zafonte, R., A Review of Magnetic Resonance Imaging and Diffusion Tensor Imaging Findings in Mild Traumatic Brain Injury. *Brain imaging and behavior* **2012,** *6* (2), 137-192.
74. Žurek, J.; Fedora, M., The usefulness of S100B, NSE, GFAP, NF-H, secretagogin and Hsp70 as a predictive biomarker of outcome in children with traumatic brain injury. *Acta Neurochirurgica* **2012,** *154* (1), 93-103.
75. Giacoppo, S.; Bramanti, P.; Barresi, M.; Celi, D.; Foti Cuzzola, V.; Palella, E.; Marino, S., Predictive Biomarkers of Recovery in Traumatic Brain Injury. *Neurocritical Care* **2012,** *16* (3), 470-477.
76. Hulsebosch, C. E., Gliopathy Ensures Persistent Inflammation and Chronic Pain after Spinal Cord Injury. *Experimental neurology* **2008,** *214* (1), 6-9.
77. Berger, R. P.; Bazaco, M. C.; Wagner, A. K.; Kochanek, P. M.; Fabio, A., Trajectory Analysis of Serum Biomarker Concentrations Facilitates Outcome Prediction after Pediatric Traumatic and Hypoxemic Brain Injury. *Developmental Neuroscience* **2011,** *32* (5-6), 396-405.
78. (a) Harald Wolf; Sophie Frantal; Gholam S. Pajenda; Olivia Salameh; Harald Widhalm; Stefan Hajdu; Kambiz Sarahrudi, Predictive value of neuromarkers supported by a set of clinical criteria in patients with mild traumatic brain injury: S100B protein and neuron-specific enolase on trial. *Journal of Neurosurgery* **2013,** *118* (6), 1298-1303; (b) Rodríguez-Rodríguez, A.; Egea-Guerrero, J. J.; León-Justel, A.; Gordillo-Escobar, E.; Revuelto-Rey, J.; Vilches-Arenas, Á.; Carrillo-Vico, A.; Domínguez-Roldán, J. M.; Murillo-Cabezas, F.; Guerrero, J. M., Role of S100B protein in urine and serum as an early predictor of mortality after severe traumatic brain injury in adults. *Clinica Chimica Acta* **2012,** *414*, 228-233; (c) Goyal, A.; Failla, M. D.; Niyonkuru, C.; Amin, K.; Fabio, A.; Berger, R. P.; Wagner, A. K., S100b as a Prognostic Biomarker in Outcome Prediction for Patients with Severe Traumatic Brain Injury. *Journal of Neurotrauma* **2013,** *30* (11), 946-957.
79. Korfias, S.; Stranjalis, G.; Boviatsis, E.; Psachoulia, C.; Jullien, G.; Gregson, B.; Mendelow, A. D.; Sakas, D. E., Serum S-100B protein monitoring in patients with severe traumatic brain injury. *Intensive Care Medicine* **2007,** *33* (2), 255-260.

80. Di Battista, A. P.; Buonora, J. E.; Rhind, S. G.; Hutchison, M. G.; Baker, A. J.; Rizoli, S. B.; Diaz-Arrastia, R.; Mueller, G. P., Blood Biomarkers in Moderate-To-Severe Traumatic Brain Injury: Potential Utility of a Multi-Marker Approach in Characterizing Outcome. *Frontiers in Neurology* **2015,** *6*, 110.
81. (a) Pai, N. P.; Vadnais, C.; Denkinger, C.; Engel, N.; Pai, M., Point-of-Care Testing for Infectious Diseases: Diversity, Complexity, and Barriers in Low- And Middle-Income Countries. *PLoS Med* **2012,** *9* (9), e1001306; (b) Singh, R.; Mukherjee, M. D.; Sumana, G.; Gupta, R. K.; Sood, S.; Malhotra, B. D., Biosensors for pathogen detection: A smart approach towards clinical diagnosis. *Sensors and Actuators B: Chemical* **2014,** *197*, 385-404; (c) Niemz, A.; Ferguson, T. M.; Boyle, D. S., Point-of-care nucleic acid testing for infectious diseases. *Trends in biotechnology* **2011,** *29* (5), 240-250.
82. Lozano, R.; Naghavi, M.; Foreman, K.; Lim, S.; Shibuya, K.; Aboyans, V.; Abraham, J.; Adair, T.; Aggarwal, R.; Ahn, S. Y.; AlMazroa, M. A.; Alvarado, M.; Anderson, H. R.; Anderson, L. M.; Andrews, K. G.; Atkinson, C.; Baddour, L. M.; Barker-Collo, S.; Bartels, D. H.; Bell, M. L.; Benjamin, E. J.; Bennett, D.; Bhalla, K.; Bikbov, B.; Abdulhak, A. B.; Birbeck, G.; Blyth, F.; Bolliger, I.; Boufous, S.; Bucello, C.; Burch, M.; Burney, P.; Carapetis, J.; Chen, H.; Chou, D.; Chugh, S. S.; Coffeng, L. E.; Colan, S. D.; Colquhoun, S.; Colson, K. E.; Condon, J.; Connor, M. D.; Cooper, L. T.; Corriere, M.; Cortinovis, M.; de Vaccaro, K. C.; Couser, W.; Cowie, B. C.; Criqui, M. H.; Cross, M.; Dabhadkar, K. C.; Dahodwala, N.; De Leo, D.; Degenhardt, L.; Delossantos, A.; Denenberg, J.; Des Jarlais, D. C.; Dharmaratne, S. D.; Dorsey, E. R.; Driscoll, T.; Duber, H.; Ebel, B.; Erwin, P. J.; Espindola, P.; Ezzati, M.; Feigin, V.; Flaxman, A. D.; Forouzanfar, M. H.; Fowkes, F. G. R.; Franklin, R.; Fransen, M.; Freeman, M. K.; Gabriel, S. E.; Gakidou, E.; Gaspari, F.; Gillum, R. F.; Gonzalez-Medina, D.; Halasa, Y. A.; Haring, D.; Harrison, J. E.; Havmoeller, R.; Hay, R. J.; Hoen, B.; Hotez, P. J.; Hoy, D.; Jacobsen, K. H.; James, S. L.; Jasrasaria, R.; Jayaraman, S.; Johns, N.; Karthikeyan, G.; Kassebaum, N.; Keren, A.; Khoo, J.-P.; Knowlton, L. M.; Kobusingye, O.; Koranteng, A.; Krishnamurthi, R.; Lipnick, M.; Lipshultz, S. E.; Ohno, S. L.; Mabweijano, J.; MacIntyre, M. F.; Mallinger, L.; March, L.; Marks, G. B.; Marks, R.; Matsumori, A.; Matzopoulos, R.; Mayosi, B. M.; McAnulty, J. H.; McDermott, M. M.; McGrath, J.; Memish, Z. A.; Mensah, G. A.; Merriman, T. R.; Michaud, C.; Miller, M.; Miller, T. R.; Mock, C.; Mocumbi, A. O.; Mokdad, A. A.; Moran, A.; Mulholland, K.; Nair, M. N.; Naldi, L.; Narayan, K. M. V.; Nasseri, K.; Norman, P.; O'Donnell, M.; Omer, S. B.; Ortblad, K.; Osborne, R.; Ozgediz, D.; Pahari, B.; Pandian, J. D.; Rivero, A. P.; Padilla, R. P.; Perez-Ruiz, F.; Perico, N.; Phillips, D.; Pierce, K.; Pope Iii, C. A.; Porrini, E.; Pourmalek, F.; Raju, M.; Ranganathan, D.; Rehm, J. T.; Rein, D. B.; Remuzzi, G.; Rivara, F. P.; Roberts, T.; De León, F. R.; Rosenfeld, L. C.; Rushton, L.; Sacco, R. L.; Salomon, J. A.; Sampson, U.; Sanman, E.; Schwebel, D. C.; Segui-Gomez, M.; Shepard, D. S.; Singh, D.; Singleton, J.; Sliwa, K.; Smith, E.; Steer, A.; Taylor, J. A.; Thomas, B.; Tleyjeh, I. M.; Towbin, J. A.; Truelsen, T.; Undurraga, E. A.; Venketasubramanian, N.; Vijayakumar, L.; Vos, T.; Wagner, G. R.; Wang, M.; Wang, W.; Watt, K.; Weinstock, M. A.; Weintraub, R.; Wilkinson, J. D.; Woolf, A. D.; Wulf, S.; Yeh, P.-H.; Yip, P.; Zabetian, A.; Zheng, Z.-J.; Lopez, A. D.; Murray, C. J. L., Global and regional mortality from 235 causes of death for 20 age groups in 1990 and 2010: a systematic analysis for the Global Burden of Disease Study 2010. *The Lancet* **2012,** *380* (9859), 2095-2128.
83. Yager, P.; Domingo, G. J.; Gerdes, J., Point-of-Care Diagnostics for Global Health. *Annual Review of Biomedical Engineering* **2008,** *10* (1), 107-144.
84. (a) Yao, C.-Y.; Fu, W.-L., Biosensors for hepatitis B virus detection. *World Journal of Gastroenterology : WJG* **2014,** *20* (35), 12485-12492; (b) Cha, B. H.; Lee, S.-M.; Park, J. C.; Hwang, K. S.; Kim, S. K.; Lee, Y.-S.; Ju, B.-K.; Kim, T. S., Detection of Hepatitis B Virus (HBV) DNA at femtomolar concentrations using a silica nanoparticle-enhanced microcantilever sensor. *Biosensors and Bioelectronics* **2009,** *25* (1), 130-135.
85. (a) Lee, C. Z.; Huang, G. T.; Yang, P. M.; Sheu, J. C.; Lai, M. Y.; Chen, D. S., Correlation of HBV DNA levels in serum and liver of chronic hepatitis B patients with cirrhosis. *Liver* **2002,** *22*

(2), 130-135; (b) Iloeje, U. H.; Yang, H. I.; Su, J.; Jen, C. L.; You, S. L.; Chen, C. J., Predicting Cirrhosis Risk Based on the Level of Circulating Hepatitis B Viral Load. *Gastroenterology* **2006,** *130* (3), 678-686.

86. Liang, T. J., Hepatitis B: The virus and disease. *Hepatology* **2009,** *49* (S5), S13-S21.

87. (a) Bansal, J.; Singh, I.; Bhatnagar, P. K.; Mathur, P. C., DNA sequence detection based on Raman spectroscopy using single walled carbon nanotube. *Journal of Bioscience and Bioengineering* **2013,** *115* (4), 438-441; (b) Irenge, L. M.; Gala, J.-L., Rapid detection methods for Bacillus anthracis in environmental samples: a review. *Applied Microbiology and Biotechnology* **2012,** *93* (4), 1411-1422; (c) Levine, S. M.; Tang, Y.-W.; Pei, Z., Recent advances in the rapid detection of Bacillus anthracis. *Reviews in Medical Microbiology* **2005,** *16* (4), 125-133.

88. Amoako, K. K.; Janzen, T. W.; Shields, M. J.; Hahn, K. R.; Thomas, M. C.; Goji, N., Rapid detection and identification of Bacillus anthracis in food using pyrosequencing technology. *International Journal of Food Microbiology* **2013,** *165* (3), 319-325.

89. Be, N. A.; Thissen, J. B.; Gardner, S. N.; McLoughlin, K. S.; Fofanov, V. Y.; Koshinsky, H.; Ellingson, S. R.; Brettin, T. S.; Jackson, P. J.; Jaing, C. J., Detection of Bacillus anthracis DNA in Complex Soil and Air Samples Using Next-Generation Sequencing. *PLoS ONE* **2013,** *8* (9), e73455.

90. Nozawa, K.; Gailhanou, H.; Raison, L.; Panizza, P.; Ushiki, H.; Sellier, E.; Delville, J. P.; Delville, M. H., Smart Control of Monodisperse Stöber Silica Particles: Effect of Reactant Addition Rate on Growth Process. *Langmuir* **2005,** *21* (4), 1516-1523.

91. Kotsuchibashi, Y.; Zhang, Y.; Ahmed, M.; Ebara, M.; Aoyagi, T.; Narain, R., Fabrication of FITC-doped silica nanoparticles and study of their cellular uptake in the presence of lectins. *Journal of Biomedical Materials Research Part A* **2013,** *101A* (7), 2090-2096.

92. Derivatized silica spheres as immunospecific markers for high resolution labeling in electron microscopy. *The Journal of Cell Biology* **1978,** *78* (2), 309-318.

93. Olariu, C. I.; Yiu, H. H. P.; Bouffier, L.; Nedjadi, T.; Costello, E.; Williams, S. R.; Halloran, C. M.; Rosseinsky, M. J., Multifunctional Fe3O4 nanoparticles for targeted bi-modal imaging of pancreatic cancer. *Journal of Materials Chemistry* **2011,** *21* (34), 12650-12659.

94. Nakajima, N.; Ikada, Y., Mechanism of Amide Formation by Carbodiimide for Bioconjugation in Aqueous Media. *Bioconjugate Chemistry* **1995,** *6* (1), 123-130.

95. (a) Grieshaber, D.; MacKenzie, R.; Voeroes, J.; Reimhult, E., Electrochemical biosensors-Sensor principles and architectures. *Sensors* **2008,** *8* (3), 1400-1458; (b) Hrapovic, S.; Liu, Y. L.; Male, K. B.; Luong, J. H. T., Electrochemical biosensing platforms using platinum nanoparticles and carbon nanotubes. *Anal. Chem.* **2004,** *76* (4), 1083-1088; (c) Katz, E.; Willner, I., Probing biomolecular interactions at conductive and semiconductive surfaces by impedance spectroscopy: Routes to impedimetric immunosensors, DNA-Sensors, and enzyme biosensors. *Electroanalysis* **2003,** *15* (11), 913-947; (d) Katz, E.; Willner, I.; Wang, J., Electroanalytical and bioelectroanalytical systems based on metal and semiconductor nanoparticles. *Electroanalysis* **2004,** *16* (1-2), 19-44.

96. (a) Engvall, E.; Perlmann, P., ENZYME-LINKED IMMUNOSORBENT ASSAY, ELISA .3. QUANTITATION OF SPECIFIC ANTIBODIES BY ENZYME-LABELED ANTI-IMMUNOGLOBULIN IN ANTIGEN-COATED TUBES. *J. Immunol.* **1972,** *109* (1), 129-&; (b) Engvall, E.; Perlmann, P., ENZYME-LINKED IMMUNOSORBENT ASSAY (ELISA) QUANTITATIVE ASSAY OF IMMUNOGLOBULIN-G. *Immunochemistry* **1971,** *8* (9), 871-&; (c) Voller, A.; Bartlett, A.; Bidwell, D. E., ENZYME IMMUNOASSAYS WITH SPECIAL REFERENCE TO ELISA TECHNIQUES. *J. Clin. Pathol.* **1978,** *31* (6), 507-520.

97. Rowe, A. A.; Bonham, A. J.; White, R. J.; Zimmer, M. P.; Yadgar, R. J.; Hobza, T. M.; Honea, J. W.; Ben-Yaacov, I.; Plaxco, K. W., CheapStat: an open-source,"Do-It-Yourself" potentiostat for analytical and educational applications. *PloS one* **2011,** *6* (9), e23783.

98. Das, J.; Kelley, S. O., Protein Detection Using Arrayed Microsensor Chips: Tuning Sensor Footprint to Achieve Ultrasensitive Readout of CA-125 in Serum and Whole Blood. *Analytical Chemistry* **2011,** *83* (4), 1167-1172.
99. Sage, A. T.; Besant, J. D.; Lam, B.; Sargent, E. H.; Kelley, S. O., Ultrasensitive Electrochemical Biomolecular Detection Using Nanostructured Microelectrodes. *Accounts of chemical research* **2014,** *47* (8), 2417-2425.
100. (a) Paine, A. J.; Luymes, W.; McNulty, J., Dispersion polymerization of styrene in polar solvents. 6. Influence of reaction parameters on particle size and molecular weight in poly(N-vinylpyrrolidone)-stabilized reactions. *Macromolecules* **1990,** *23* (12), 3104-3109; (b) Jinhua, L.; Guangyuan, Z., Polystyrene Microbeads by Dispersion Polymerization: Effect of Solvent on Particle Morphology. *International Journal of Polymer Science* **2014,** *2014*, 4; (c) Bamnolker, H.; Margel, S., Dispersion polymerization of styrene in polar solvents: Effect of reaction parameters on microsphere surface composition and surface properties, size and size distribution, and molecular weight. *Journal of Polymer Science Part A: Polymer Chemistry* **1996,** *34* (10), 1857-1871.
101. Li, Y.; Pan, Y.; Zhu, L.; Wang, Z.; Su, D.; Xue, G., Facile and Controlled Fabrication of Functional Gold Nanoparticle-coated Polystyrene Composite Particle. *Macromolecular Rapid Communications* **2011,** *32* (21), 1741-1747.
102. (a) Fritze, A.; Hens, F.; Kimpfler, A.; Schubert, R.; Peschka-Süss, R., Remote loading of doxorubicin into liposomes driven by a transmembrane phosphate gradient. *Biochimica et Biophysica Acta (BBA) - Biomembranes* **2006,** *1758* (10), 1633-1640; (b) Chen, Z.; Deng, J.; Zhao, Y.; Tao, T., Cyclic RGD peptide-modified liposomal drug delivery system: enhanced cellular uptake in vitro and improved pharmacokinetics in rats. *International Journal of Nanomedicine* **2012,** *7*, 3803-3811.
103. Ngo, A. T.; Karam, P.; Fuller, E.; Burger, M.; Cosa, G., Liposome Encapsulation of Conjugated Polyelectrolytes: Toward a Liposome Beacon. *Journal of the American Chemical Society* **2008,** *130* (2), 457-459.
104. Poger, D.; Mark, A. E., On the Validation of Molecular Dynamics Simulations of Saturated and cis-Monounsaturated Phosphatidylcholine Lipid Bilayers: A Comparison with Experiment. *Journal of Chemical Theory and Computation* **2010,** *6* (1), 325-336.
105. Hurst, S. J.; Lytton-Jean, A. K. R.; Mirkin, C. A., Maximizing DNA Loading on a Range of Gold Nanoparticle Sizes. *Analytical Chemistry* **2006,** *78* (24), 8313-8318.
106. (a) Cheng, Y.; Stakenborg, T.; Van Dorpe, P.; Lagae, L.; Wang, M.; Chen, H.; Borghs, G., Fluorescence Near Gold Nanoparticles for DNA Sensing. *Analytical Chemistry* **2011,** *83* (4), 1307-1314; (b) Yagi, N.; Satonaka, K.; Horio, M.; Shimogaki, H.; Tokuda, Y.; Maeda, S., The Role of DNase and EDTA on DNA Degradation in Formaldehyde Fixed Tissues. *Biotechnic & Histochemistry* **1996,** *71* (3), 123-129.
107. (a) Thurman, D. J.; Alverson, C.; Dunn, K. A.; Guerrero, J.; Sniezek, J. E., Traumatic brain injury in the United States: A public health perspective. *The Journal of head trauma rehabilitation* **1999,** *14* (6), 602-15; (b) Sauber-Schatz, E. K.; Mack, K. A.; Diekman, S. T.; Paulozzi, L. J., Associations between pain clinic density and distributions of opioid pain relievers, drug-related deaths, hospitalizations, emergency department visits, and neonatal abstinence syndrome in Florida. *Drug and alcohol dependence* **2013,** *133* (1), 161-6.
108. Humphreys, I.; Wood, R. L.; Phillips, C. J.; Macey, S., The costs of traumatic brain injury: a literature review. *ClinicoEconomics and outcomes research : CEOR* **2013,** *5*, 281-7.
109. Mondello, S.; Muller, U.; Jeromin, A.; Streeter, J.; Hayes, R. L.; Wang, K. K., Blood-based diagnostics of traumatic brain injuries. *Expert review of molecular diagnostics* **2011,** *11* (1), 65-78.
110. (a) Waggener, J. D., The neuropathology of head trauma. *Arizona medicine* **1968,** *25* (2), 163-9; (b) Schoch, K. M.; von Reyn, C. R.; Bian, J.; Telling, G. C.; Meaney, D. F.; Saatman, K.

E., Brain injury-induced proteolysis is reduced in a novel calpastatin-overexpressing transgenic mouse. *Journal of neurochemistry* **2013,** *125* (6), 909-20; (c) Hunt, R. F.; Boychuk, J. A.; Smith, B. N., Neural circuit mechanisms of post-traumatic epilepsy. *Frontiers in cellular neuroscience* **2013,** *7*, 89.
111. (a) Vaca, L., Point-of-care diagnostic tools to detect circulating microRNAS as biomarkers of disease. *Sensors* **2014,** *14* (5), 9117-31; (b) Hu, J.; Wang, S.; Wang, L.; Li, F.; Pingguan-Murphy, B.; Lu, T. J.; Xu, F., Advances in paper-based point-of-care diagnostics. *Biosensors & bioelectronics* **2014,** *54*, 585-97.
112. Dijksma, M.; Boukamp, B. A.; Kamp, B.; van Bennekom, W. P., Effect of Hexacyanoferrate(II/III) on Self-Assembled Monolayers of Thioctic Acid and 11-Mercaptoundecanoic Acid on Gold. *Langmuir* **2002,** *18* (8), 3105-3112.
113. Turková, J., Oriented immobilization of biologically active proteins as a tool for revealing protein interactions and function. *Journal of Chromatography B: Biomedical Sciences and Applications* **1999,** *722* (1–2), 11-31.
114. Lu, B.; Smyth, M. R.; O'Kennedy, R., Tutorial review. Oriented immobilization of antibodies and its applications in immunoassays and immunosensors. *Analyst* **1996,** *121* (3), 29R-32R.
115. Wink, T.; J. van Zuilen, S.; Bult, A.; P. van Bennekom, W., Self-assembled Monolayers for Biosensors. *Analyst* **1997,** *122* (4), 43R-50R.
116. Malem, F.; Mandler, D., Self-assembled monolayers in electroanalytical chemistry: application of .omega.-mercapto carboxylic acid monolayers for the electrochemical detection of dopamine in the presence of a high concentration of ascorbic acid. *Analytical Chemistry* **1993,** *65* (1), 37-41.
117. Arya, S. K.; Chornokur, G.; Venugopal, M.; Bhansali, S., Dithiobis(succinimidyl propionate) modified gold microarray electrode based electrochemical immunosensor for ultrasensitive detection of cortisol. *Biosensors and Bioelectronics* **2010,** *25* (10), 2296-2301.
118. Cabrita, J. F.; Abrantes, L. M.; Viana, A. S., N-Hydroxysuccinimide-terminated self-assembled monolayers on gold for biomolecules immobilisation. *Electrochimica Acta* **2005,** *50* (10), 2117-2124.
119. Tulip, F. S.; Eteshola, E.; Desai, S.; Mostafa, S.; Roopa, S.; Evans, B.; Islam, S. K., Direct Label-Free Electrical Immunodetection of Transplant Rejection Protein Biomarker in Physiological Buffer Using Floating Gate AlGaN/GaN High Electron Mobility Transistors. *IEEE Transactions on NanoBioscience* **2014,** *13* (2), 138-145.
120. Quan, D.; Shin, W., Modification of electrode surface for covalent immobilization of laccase. *Materials Science and Engineering: C* **2004,** *24* (1–2), 113-115.
121. Wagner, P.; Hegner, M.; Kernen, P.; Zaugg, F.; Semenza, G., Covalent immobilization of native biomolecules onto Au(111) via N-hydroxysuccinimide ester functionalized self-assembled monolayers for scanning probe microscopy. *Biophysical Journal* **1996,** *70* (5), 2052-2066.
122. Jeong, Y.; Lee, K. H.; Park, H.; Choi, J., Enhanced detection of single-cell-secreted proteins using a fluorescent immunoassay on the protein-G-terminated glass substrate. *International Journal of Nanomedicine* **2015,** *10*, 7197-7205.
123. Kumar, S.; Aaron, J.; Sokolov, K., Directional conjugation of antibodies to nanoparticles for synthesis of multiplexed optical contrast agents with both delivery and targeting moieties. *Nat. Protocols* **2008,** *3* (2), 314-320.
124. Bard, A.; Faulkner, L., *Electrochemical Methods: Fundamentals and Applications*. John Wiley & Sons, Inc: 2001.
125. Schulte, S.; Podlog, L. W.; Hamson-Utley, J. J.; Strathmann, F. G.; Strüder, H. K., A Systematic Review of the Biomarker S100B: Implications for Sport-Related Concussion Management. *Journal of Athletic Training* **2014,** *49* (6), 830-850.

126. Kragstrup, T. W.; Vorup-Jensen, T.; Deleuran, B.; Hvid, M., A simple set of validation steps identifies and removes false results in a sandwich enzyme-linked immunosorbent assay caused by anti-animal IgG antibodies in plasma from arthritis patients. *SpringerPlus* **2013,** *2* (1), 1-10.
127. Schmidt, S. D.; Mazzella, M. J.; Nixon, R. A.; Mathews, P. M., Aβ Measurement by Enzyme-Linked Immunosorbent Assay. In *Amyloid Proteins: Methods and Protocols*, Sigurdsson, M. E.; Calero, M.; Gasset, M., Eds. Humana Press: Totowa, NJ, 2012; pp 507-527.
128. Anderson, G. P.; Nerurkar, N. L., Improved fluoroimmunoassays using the dye Alexa Fluor 647 with the RAPTOR, a fiber optic biosensor. *Journal of Immunological Methods* **2002,** *271* (1–2), 17-24.
129. Rodríguez-Sáinz, C.; Valor, L.; Hernández, D. C.; Gil, J.; Carbone, J.; Pascual-Bernaldez, M.; Rodríguez-Alcántara, F.; Martínez, I.; Vicario, J. L.; Mallal, S.; Fernández-Cruz, E., Flow Cytometry Analysis with a New FITC-Conjugated Monoclonal Antibody-3E12 for HLA-B*57:01 Rapid Screening in Prevention of Abacavir Hypersensitivity in HIV-1–Infected Patients. *HIV Clinical Trials* **2013,** *14* (4), 160-164.
130. Suzuki, Y.; Yokoyama, K., Development of Functional Fluorescent Molecular Probes for the Detection of Biological Substances. *Biosensors* **2015,** *5* (2), 337-363.
131. Gervais, L.; Delamarche, E., Toward one-step point-of-care immunodiagnostics using capillary-driven microfluidics and PDMS substrates. *Lab on a Chip* **2009,** *9* (23), 3330-3337.
132. Stålnacke, B.-M.; Sojka, P., Repeatedly Heading a Soccer Ball Does Not Increase Serum Levels of S-100B, a Biochemical Marker of Brain Tissue Damage: an Experimental Study. *Biomarker Insights* **2008,** *3*, 87-91.
133. Peterson, A. W.; Heaton, R. J.; Georgiadis, R. M., The effect of surface probe density on DNA hybridization. *Nucleic Acids Research* **2001,** *29* (24), 5163-5168.
134. Huang, E.; Satjapipat, M.; Han, S.; Zhou, F., Surface Structure and Coverage of an Oligonucleotide Probe Tethered onto a Gold Substrate and Its Hybridization Efficiency for a Polynucleotide Target. *Langmuir* **2001,** *17* (4), 1215-1224.
135. Cardullo, R. A.; Agrawal, S.; Flores, C.; Zamecnik, P. C.; Wolf, D. E., Detection of nucleic acid hybridization by nonradiative fluorescence resonance energy transfer. *Proceedings of the National Academy of Sciences of the United States of America* **1988,** *85* (23), 8790-8794.
136. Didenko, V. V., DNA Probes Using Fluorescence Resonance Energy Transfer (FRET): Designs and Applications. *BioTechniques* **2001,** *31* (5), 1106-1121.
137. Nguyen, T.; Brunson, D.; Crespi, C. L.; Penman, B. W.; Wishnok, J. S.; Tannenbaum, S. R., DNA damage and mutation in human cells exposed to nitric oxide in vitro. *Proceedings of the National Academy of Sciences of the United States of America* **1992,** *89* (7), 3030-3034.
138. Owczarzy, R.; Moreira, B. G.; You, Y.; Behlke, M. A.; Walder, J. A., Predicting Stability of DNA Duplexes in Solutions Containing Magnesium and Monovalent Cations. *Biochemistry* **2008,** *47* (19), 5336-5353.
139. Calzuola, I.; Gianfranceschi, G. L.; Marsili, V., Binding citrate/DNA in presence of divalent cations - Potential mimicry of acidic peptides/DNA interactions. *Molecular Biology Reports* **2001,** *28* (1), 43-6.
140. Špringer, T.; Šípová, H.; Vaisocherová, H.; Štěpánek, J.; Homola, J., Shielding effect of monovalent and divalent cations on solid-phase DNA hybridization: surface plasmon resonance biosensor study. *Nucleic Acids Research* **2010,** *38* (20), 7343-7351.
141. Qureshi, A.; Niazi, J. H.; Kallempudi, S.; Gurbuz, Y., Label-free capacitive biosensor for sensitive detection of multiple biomarkers using gold interdigitated capacitor arrays. *Biosensors and Bioelectronics* **2010,** *25* (10), 2318-2323.
142. Quershi, A.; Gurbuz, Y.; Kang, W. P.; Davidson, J. L., A novel interdigitated capacitor based biosensor for detection of cardiovascular risk marker. *Biosensors and Bioelectronics* **2009,** *25* (4), 877-882.

143. Mao, X.; Xu, H.; Zeng, Q.; Zeng, L.; Liu, G., Molecular beacon-functionalized gold nanoparticles as probes in dry-reagent strip biosensor for DNA analysis. *Chemical Communications* **2009,** (21), 3065-3067.
144. Liu, X.; Wang, F.; Aizen, R.; Yehezkeli, O.; Willner, I., Graphene Oxide/Nucleic-Acid-Stabilized Silver Nanoclusters: Functional Hybrid Materials for Optical Aptamer Sensing and Multiplexed Analysis of Pathogenic DNAs. *Journal of the American Chemical Society* **2013,** *135* (32), 11832-11839.
145. Dong, H.; Gao, W.; Yan, F.; Ji, H.; Ju, H., Fluorescence Resonance Energy Transfer between Quantum Dots and Graphene Oxide for Sensing Biomolecules. *Analytical Chemistry* **2010,** *82* (13), 5511-5517.
146. Chen, J.; Huang, Y.; Shi, M.; Zhao, S.; Zhao, Y., Highly sensitive multiplexed DNA detection using multi-walled carbon nanotube-based multicolor nanobeacon. *Talanta* **2013,** *109*, 160-166.
147. Zhang, Y.; Zhu, C.; Zhang, L.; Tan, C.; Yang, J.; Chen, B.; Wang, L.; Zhang, H., DNA-Templated Silver Nanoclusters for Multiplexed Fluorescent DNA Detection. *Small* **2015,** *11* (12), 1385-1389.
148. (a) Chen, C.; Ridzon, D. A.; Broomer, A. J.; Zhou, Z.; Lee, D. H.; Nguyen, J. T.; Barbisin, M.; Xu, N. L.; Mahuvakar, V. R.; Andersen, M. R.; Lao, K. Q.; Livak, K. J.; Guegler, K. J., Real-time quantification of microRNAs by stem–loop RT–PCR. *Nucleic Acids Res.* **2005,** *33* (20), e179; (b) RAYMOND, C. K.; ROBERTS, B. S.; GARRETT-ENGELE, P.; LIM, L. P.; JOHNSON, J. M., Simple, quantitative primer-extension PCR assay for direct monitoring of microRNAs and short-interfering RNAs. *RNA* **2005,** *11* (11), 1737-1744.
149. Sandström, P.; Boncheva, M.; Åkerman, B., Nonspecific and Thiol-Specific Binding of DNA to Gold Nanoparticles. *Langmuir* **2003,** *19* (18), 7537-7543.
150. Kimura-Suda, H.; Petrovykh, D. Y.; Tarlov, M. J.; Whitman, L. J., Base-Dependent Competitive Adsorption of Single-Stranded DNA on Gold. *Journal of the American Chemical Society* **2003,** *125* (30), 9014-9015.
151. Peeters, S.; Stakenborg, T.; Reekmans, G.; Laureyn, W.; Lagae, L.; Van Aerschot, A.; Van Ranst, M., Impact of spacers on the hybridization efficiency of mixed self-assembled DNA/alkanethiol films. *Biosensors and Bioelectronics* **2008,** *24* (1), 72-77.
152. Cederquist, K. B.; Keating, C. D., Hybridization Efficiency of Molecular Beacons Bound to Gold Nanowires: Effect of Surface Coverage and Target Length. *Langmuir* **2010,** *26* (23), 18273-18280.